East African Journal of Biophysical and Computational Sciences

(E A J B C S)

ISSN (Online): 2789-3618 and ISSN (Print): 2789-360X

COLLEGE OF NATURAL AND COMPUTATIONAL SCIENCES,
HAWASSA UNIVERSITY

Volume 7 Issue 1 June, 2026

East African Journal of Biophysical and Computational Sciences
ISSN (Online): 2789-3618 and ISSN (Print): 2789-360X

East African Journal of Biophysical and Computational Sciences (EAJBCS)

ISSN (Online): 2789-3618 and ISSN (Print): 2789-360X

Volume 7 Issue 1

College of Natural and Computational Sciences
Hawassa University

June, 2026

Table of Contents

S.No	Title	First Author	Page range
1S	Bifurcation Analysis of Eco-Epidemiological Mathematical Model with Saturated Incidence Rate and General Holling Type Response Function	Solomon Molla Alemu	1-17
2S	Computational Study of MHD Blood Flow through Bifurcated Artery Using Caputo-Fabrizio Fractional Derivative, Thermal Radiation, and Magnetic Field for Tumor Therapies	Isah Abdullahi	18-26
3S	Prevalence and Determinant Factors of Malaria Infection among Patients Attending Gimbichu Primary Hospital, Soro District, Central Ethiopia, Ethiopia	Melese Birmeka	27-33
4S	Feeding Habits and Trace Metal Concentrations in Organs of the Nile Catfish, *Synodontis schall* (Bloch & Schneider) (Pisces: Mochokidae), in Lake Abaya, Ethiopia	Elias Dadebo	34-42
5S	Intuitionistic Fuzzy Multi-objective Optimization Method for Determination of Optimal Cropping Pattern	Habtamu Tsegaye Teferi	43-63

East African Journal of Biophysical and Computational Sciences (EAJBCS)

East African Journal of Biophysical and Computational Sciences (EAJBCS) whose ISSN (Online): 2789-3618 and ISSN (Print): 2789-360X is a double-blind peer-reviewed open-access journal published by Hawassa University, College of Natural & Computational Sciences. This Journal is a multi and interdisciplinary journal that is devoted to attracting high-quality, latest, and valuable advancements in the fields of natural sciences. The Journal invites publications from different geographical contexts and disciplines to advance the depths of knowledge related to physics, chemistry, geology, biology, & veterinary medicine. The manuscript originated from other sciences such as biotechnology, sport science, statistics, and mathematics can also be accepted based on their adjunct nature. The Journal encourages publications of both scholarly and industrial papers on various themes with the aim of giving innovative solutions to natural sciences. It encourages the publishing of open access academic journals on a regular basis (presumably biannual). The Journal publishes original research articles, critical reviews, mini-reviews, short communications, case reports related to the specific theme & a variety of special issues in English. The Journal, published under the Creative Commons open access license (CC BY-NC-ND), doesn't charge fees for publishing an article and hence offers an opportunity to all social classes regardless of their economic statuses. This helps to promote academic research published by resource-poor researchers as a mechanism to give back to society.

The journal is already indexed on known databases like AJOL, DOAJ and CABI ABSTRACTS

Editorial Team

East African Journal of Biophysical and Computational Sciences
ISSN (Online): 2789-3618 and ISSN (Print): 2789-360X

ARTICLE

ARTICLE INFO
Volume 7(1), 2026
https://dx.doi.org/10.4314/eajbcs.v7i1.1S

ARTICLE HISTORY
Received: 16 November, 2025
Accepted: 30 April, 2026
Published Online: 10 June, 2026

CITATION
Alemu et.al (2026) Bifurcation Analysis of Eco-Epidemiological Mathematical Model with Saturated Incidence Rate and General Holling Type Response Function. *East African Journal of Biophysical and Computational Sciences* Volume 7(1), 2026. .https://dx.doi.org/10.4314/eajbcs.v7i1.1S.1-17

East African Journal of Biophysical and Computational Sciences (EAJBCS) is already indexed on known databases like AJOL, DOAJ, CABI ABSTRACTS and FAO AGRIS.

Bifurcation Analysis of Eco-Epidemiological Mathematical Model with Saturated Incidence Rate and General Holling Type Response Function

Solomon Molla Alemu[1], Tesfaye Tefera Mamo[2], Mohammed Yiha Dawed[3,*]

[1]Addis Ababa Science and Technology University, Department of Mathematics, Addis Ababa, Ethiopia,
[2]Debre Berhan University, Department of Mathematics, Debre Berhan, Ethiopia,
[3]Hawassa University, Department of Mathematics, Hawassa, Ethiopia

*Corresponding author: mohammedyiha@hu.edu.et

Abstract

This paper presents a bifurcation analysis of an Eco-epidemiological model with saturated incidence rate and general Holling-Type functional responses. The model describes a predator–prey system in which the prey population is infected by a communicable disease, and the predator feeds on both susceptible and infected individuals. Fundamental properties of the system, including existence and uniqueness, positivity, and boundedness of solutions, are established to ensure biological feasibility. Equilibrium points are identified and their stability is examined. The basic reproduction number R_0 is derived to determine threshold conditions for disease persistence. Using Sotomayor's theorem, transcritical and Hopf bifurcations are rigorously verified. The results indicate that increasing the inhibition rate stabilizes the system and promotes coexistence, whereas higher transmission rates destabilize equilibria and generate sustained oscillations. Numerical simulations and bifurcation diagrams validate the analytical findings, demonstrating transitions between stable steady states and periodic dynamics.

Keywords: Eco-epidemiology, Saturated incidence rate, Bifurcation, General Holling Type, Emergent carrying capacity

1 Introduction

In applied mathematics, mathematical modeling serves as an essential tool for investigating real-world problems across diverse disciplines, including biology, epidemiology, and ecology (Bezabih et al., 2021). Numerous researchers have demonstrated that the dynamic interactions between predator and prey populations can be effectively analyzed using the tools of mathematical ecology (Das, 2016; Demir, 2019). Building upon the foundational works of Lotka (1925) and Volterra (1927), various sophisticated predator–prey models have been developed to describe complex ecological interactions under different realistic scenarios (Ghanbari, 2021; Sieber et al., 2014). Furthermore, Anderson and May (1986) established a pioneering framework that integrates the epidemiological models of Kermack and McKendrick (Brauer, 2005) with classical Lotka–Volterra predator–prey dynamics. As a result, recent decades have been marked by a growing body of research devoted to analyzing the dynamical behavior of eco-epidemiological models (Biswas et al., 2015). Since conducting experiments is often impractical or unethical, mathematical modeling has become an essential approach for investigating and understanding the transmission and control of infectious diseases. Numerous researchers (e.g., Hugo and Simanjilo (2019) and Sieber et al. (2014)) have explored predator–prey models incorporating disease dynamics, highlighting how infections within the prey and/or predator populations can significantly influence the ecological interactions and system stability. The primary focus of eco-epidemiological models revolves around how infections impact species mortality, decrease reproduction rates, the nature of contamination, changes in population size, the eradication or control of epidemic outbreaks, the persistence and the overarching dynamics of the diseased species (Sieber et al., 2014). Saifuddin et al. (2016) demonstrated that, under an explicit carrying capacity, susceptible and infected prey exhibit identical competitive abilities, whereas under an emergent carrying capacity, infected prey compete less effectively than susceptible ones in the presence of disease. Biswas et al. (2015) examined a modified Lotka-Volterra system that incorporates the prey infection propagation term based on the mass action law, while Haldar et al. (2021) focused on standard incidence within predator-prey interactions. Liu et al. (1987) proposed an epidemiological model characterized by a nonlinear incidence rate. Gumel and Moghadas (2003) formulated

a tritrophic dynamics that incorporating a distinct saturating incidence term to more accurately capture complex transmission dynamics, while Ruan and Wang (2003) extended this line of research by examining an epidemic model that integrates essential system with a saturating incidence term to investigate the overall system behavior. Their approach is deemed more justifiable because it considers behavioral changes and the crowding effect among infected individuals, thus preventing the contact rate from becoming unbounded by selecting appropriate parameters (Maiti et al., 2019). Hu et al. (2017) analyzed a discrete-time eco-epidemiological framework, focusing on the system dynamic behavior under a Holling type-II incidence function in place of the bilinear incidence rate. Following these influential studies have incorporated disease transmission into prey and/or predator populations under various incidence mechanisms, including mass action, standard incidence, and nonlinear forms. Among these, saturated incidence rates have attracted considerable attention because they incorporate behavioral changes and crowding effects, thereby preventing unrealistic unbounded transmission when the infected population becomes large. Such formulations provide a more biologically realistic representation of disease spread.

From an ecological perspective, predator–prey dynamics are strongly influenced by the prey's response to predation, while the predator population, in turn, directly or indirectly regulates the prey population (Panja, 2020). In order to accurately characterize the responsiveness of predation rates to variations in prey biomass across different population densities, ecologically realistic functional responses have been formulated that explicitly incorporate prey behavioral patterns. The following functional responses are developed: Beddington-DeAngelis (Li & Takeuchi, 2011), Crowley-Martin (Maiti et al., 2019), General Holling type (Dawed et al., 2020), Michaelis-Menten type (HT-II), Holling type III, Holling type IV (which came later) (Holling, 1959). Holling responses are commonly categorized into specific forms (Type I–IV), each with distinct ecological characteristics. However, in this study, the use of the term "General Holling-Type functional responses" is intentionally and methodologically justified. We mean either of these forms or combinations of them:

$$f(x) = ax, \quad g(x) = \frac{ax}{b+x}, \quad h(x) = \frac{ax^2}{b+x^2}, \quad r(x) = \frac{ax}{1+bx+cx^2},$$

where, a is attack rate, b is a half saturation constant and c is the measure of the predator tolerance to the prey to attack. Haque and Venturino (2007) studied an eco-epidemic model in which the predator population is infected and predation follows a ratio-dependent functional response. Moreover, Kooi et al. (2011) also have discussed on tritrophics food web eco-epidemiological system with predator infection, where the infection transmitted among predators follow a hybrid response function as Holling type-IV functional response and Beddington–DeAngelis type functional response (Li & Takeuchi, 2011). Capasso and Serio (1978) introduced an interaction term to account for the saturation effect in large infectious populations. Consequently, incorporating saturation in disease transmission (Cai & Li, 2010) becomes particularly relevant in eco-epidemiological models when the number of infectives is high. Real-world predation involves complex mechanisms (Wayesa et al., 2024, 2025) such as prey refuge, handling time, predator interference, and adaptive feeding, which can be captured using general Holling-type functional responses. However, most eco-epidemiological models rely on simplified predation terms and standard disease transmission functions, with limited attention given to combining generalized predation dynamics and saturated incidence. Key research gaps include:

- Lack of systematic analysis of the combined effects of saturated disease transmission and general Holling-type responses on system stability.
- Limited exploration of how these nonlinear mechanisms drive qualitative changes such as transcritical and Hopf bifurcations.
- Few models incorporating emergent carrying capacity with unequal competition between susceptible and infected prey.
- The absence of a rigorous analytical framework linking the basic reproduction number, stability switching, and bifurcation dynamics Wang et al. (2016) under such generalized conditions.

To address these gaps, the study proposes a novel eco-epidemiological model integrating saturated incidence, generalized Holling-type predation on susceptible and infected prey, and an emergent carrying capacity framework with distinct competition effects. This integrated approach strengthens theoretical understanding of system stability, persistence, and complex population oscillations.

The remainder of this paper is organized as follows: Section 2 presents the mathematical formulation of the model; Section 3 establishes fundamental dynamical properties; Section 4 is devoted to stability and bifurcation analysis; Section 5 provides numerical simulations that support the analytical findings; Finally, the concluding section summarizes the main results and discusses their ecological implications.

2 Mathematical Model

In this section, we investigate the eco-epidemiological dynamics to explore the influence of a saturated incidence function on the sustainable coexistence of two interacting species within the same ecosystem. Let $A(t)$ and $B(t)$ denote the prey and predator densities at time t, respectively. The model is formulated based on the following biological assumptions:

The total prey population is divided into two compartments

$$A(t) = A_1(t) + A_2(t)$$

where $A_1(t)$ and $A_2(t)$ represent the susceptible and infected prey populations, respectively.

The researchers assume that the lifespan of infected prey is shorter than that of susceptible prey (Haldar et al., 2021). The susceptible prey population $A_1(t)$ follows logistic growth in the absence of predation and disease. Furthermore, both susceptible and infected prey share limited environmental resources. However, they do not possess identical competitive abilities. To capture this ecological feature, we incorporate distinct competition coefficients representing emergent carrying capacity: b_1 denotes intra-specific competition among susceptible prey, while b_2 represents inter-specific competition between susceptible and infected prey (Ghanbari, 2021; Sieber et al., 2014). Thus, the logistic growth of susceptible prey is given by

$$\frac{dA_1}{dt} = r_{A_1} A_1 \left(1 - b_1 A_1 - b_2 A_2\right).$$

The disease spreads among prey solely through direct contact. Infected prey do not recover or acquire immunity; instead, they are removed from the system through predation, disease-induced mortality at rate δ, and natural death at rate α_1.

We assume that susceptible prey become infected according to a nonlinear saturated incidence function

$$\frac{\beta A_1 A_2}{1 + sA_2}$$

as proposed in Maiti et al. (2019). Here, βA_2 represents the force of infection rate, while $\frac{1}{1+sA_2}$ accounts for behavioral changes and crowding effects among infected individuals. This formulation prevents the transmission rate from becoming unbounded for large infected populations (Ruan & Wang, 2003).

Ecologically, infected prey is generally more vulnerable to predation due to its weakened physiological condition. To capture this phenomenon, we incorporate distinct general Holling-Type functional responses, $\Phi_{A_1}(A_1)$ and $\Phi_{A_2}(A_2)$, which represent the predator's consumption of susceptible and infected prey biomass, respectively.

Accordingly, the susceptible prey dynamics are given by

$$\frac{dA_1}{dt} = r_{A_1} A_1 \left(1 - b_1 A_1 - b_2 A_2\right) - \frac{\beta A_1 A_2}{1 + sA_2} - \Phi_{A_1}(A_1) B,$$

while the infected prey dynamics are described by

$$\frac{dA_2}{dt} = \frac{\beta A_1 A_2}{1+sA_2} - (\alpha_1+\delta)A_2 - \Phi_{A_2}(A_2)B.$$

The model assumes a specialist predator population $B(t)$ that feeds on both susceptible and infected prey, with predation governed by general Holling-type functional responses. Accordingly, the predator's population dynamics are formulated based on these generalized predation interactions.

$$\frac{dB}{dt} = C_1\Phi_{A_1}(A_1)B + C_2\Phi_{A_2}(A_2)B - \alpha_2 B,$$

where C_1 and C_2 denote the conversion efficiencies of susceptible and infected prey into predator biomass, respectively, and α_2 represents the natural mortality rate of the predator.

The descriptions of state variables and parameters are provided in Table 1. All parameters are assumed to be positive. Hence, based on the above assumptions, the governing eco-epidemiological model takes the form

$$\begin{cases} \dfrac{dA_1}{dt} = r_{A_1}A_1\Big(1-b_1A_1-b_2A_2\Big) - \dfrac{\beta A_1A_2}{1+sA_2} - \Phi_{A_1}(A_1)B, \\ \dfrac{dA_2}{dt} = \dfrac{\beta A_1A_2}{1+sA_2} - (\alpha_1+\delta)A_2 - \Phi_{A_2}(A_2)B, \\ \dfrac{dB}{dt} = C_1\Phi_{A_1}(A_1)B + C_2\Phi_{A_2}(A_2)B - \alpha_2 B, \end{cases} \tag{1}$$

with initial conditions

$$A_1(0) = A_1^0 > 0, \quad A_2(0) = A_2^0 \geq 0, \quad B(0) = B^0 > 0. \tag{2}$$

2.1 Non-Dimensionalization

Non-Dimensionalization simplify and make the equations easier to interpret. The transformation equations could be:
$A_1 = \frac{1}{b_1}S, A_2 = \frac{1}{b_1}I, B = \frac{s}{b_1}P, t = \frac{1}{r_{A_1}}T, \Phi_{A_1}$
$(A_1) = \frac{r_{A_1}}{C_1}\psi_S(S)$, and $\Phi_{A_2}(A_2) = \frac{r_{A_1}}{C_2}\psi_I(I)$.

Thus, the scaled form of the dynamical system is

$$\begin{cases} \dfrac{dS}{dT} = S\Big(1-S-\kappa I\Big) - \dfrac{\gamma SI}{1+\eta I} - \theta_1\psi_S(S)P, \\ \dfrac{dI}{dT} = \dfrac{\gamma SI}{1+\eta I} - \zeta I - \theta_2\psi_I(I)P, \\ \dfrac{dP}{dT} = \psi_S(S)P + \psi_I(I)P - \xi P, \end{cases} \tag{3}$$

where $\kappa = \frac{b_2}{b_1}$, $\theta_1 = \frac{s}{C_1}$, $\theta_2 = \frac{s}{C_2}$, $\gamma = \frac{\beta}{b_1 r_{A_1}}$, $\eta = \frac{s}{b_1}$, $\zeta = \frac{\alpha_1+\delta}{r_{A_1}}$, $\xi = \frac{\alpha_2}{r_{A_1}}$, and

$$S(0) = S_0 > 0, I(0) = I_0 \geq 0, P(0) = P_0 > 0. \tag{4}$$

3 Mathematical Model Analysis

The analysis of mathematical models in eco-epidemiology provides valuable insights into disease transmission dynamics, host–pathogen interactions, and the ecological feedback mechanisms within the system. Such analysis helps to explore system behavior, identify critical parameters, and examine aspects like stability, bifurcation, and possible outcomes, including disease outbreaks. Furthermore, properties such as the existence and uniqueness of solutions, positivity, boundedness, as well as permanence, persistence, and numerical simulations of the model system 3, will be studied.

3.1 Positivity of the solution

Let us denote $\mathbb{R}^3_+ = \{(S,I,P) \in \mathbb{R}^3 : S > 0, I \geq 0, P > 0\}$, the positive octants of the solution of our model system (3).

Theorem 1. *The non-negative octant in $\mathbb{R}^3$ is remain positive under the dynamics for the model (3).*

Proof. We want to verify

$$S(T) > 0, \qquad I(T) > 0, \qquad P(T) > 0, \qquad \text{for all }, T \geq 0,$$

Rewrite the system (3) in the form

$$\begin{aligned} \frac{dS}{dT} &= S\Big(1-S-\kappa I - \frac{\gamma I}{1+\eta I} - \frac{\theta_1\psi_S(S)P}{S}\Big) = SQ_1(S,I,P), \\ \frac{dI}{dT} &= I\left(\frac{\gamma S}{1+\eta I} - \zeta - \frac{\theta_2\psi_I(I)P}{I}\right) = IQ_2(S,I,P), \\ \frac{dP}{dT} &= P\left(\psi_S(S) + \psi_I(I) - \xi\right) = PQ_3(S,I,P). \end{aligned}$$

From the above expression and the initial conditions (4), we have:

$$\begin{aligned} S(T) &= S_0 \exp\left(\int_0^T Q_1(S,I,P)du\right), \\ I(T) &= I_0 \exp\left(\int_0^T Q_2(S,I,P)du\right), \\ P(T) &= P_0 \exp\left(\int_0^T Q_3(S,I,P)du\right). \end{aligned}$$

As, the initial conditions (4) and the exponential form are positive, thus, all the state variables $S(T)$, $I(T)$ and $P(T)$ are positive $\forall T \geq 0$. Therefore, every solutions of the mathematical model 3 are positive. □

3.2 Bounded behavior of trajectories

Theorem 2. *All possible solution of the dynamical system (3) are consistently bounded in $\mathbb{R}^3_+$ and enter in the invariant zone*

$$\Sigma = \left\{\Big(S(T),I(T),P(T)\Big) \in \mathbb{R}^3_+ : 0 < S \leq \max\{S_0,1\}, \right. \\ \left. 0 < \nu \leq \max\left\{\frac{(1+\xi-m)^2}{4(\xi-m)}, \nu_0\right\}\right\} \tag{5}$$

where $\nu(T) = S(T) + I(T) + \theta_1 P(T)$, $0 < \psi_I(I) \leq m$.

Proof. As established in Proposition (1), the solutions $S(T)$, $I(T)$, and $P(T)$ of system (3) remain positive for all $T \geq 0$. Considering the first equation of the model (3), it follows that

$$\frac{dS}{dT} = S\Big(1-S-\kappa I\Big) - \frac{\gamma SI}{1+\eta I} - \theta_1\psi_S(S)P \leq S(1-S)$$

This directly leads to

$$S(T) \leq \left[1 + \Big(\frac{1}{S_0} - 1\Big)e^{-T}\right]^{-1} = \frac{S_0}{S_0 + (1-S_0)e^{-T}}.$$

Therefore,

$$\lim_{T\to\infty} \sup S(T) \leq \max\{S_0, 1\}.$$

Table 1: The state variables and parameters description

Variables/Parameters	Ecological Meaning	Dimension
A_1	Susceptible prey density	Per Area
A_2	Infected prey density	Per Area
B	Predator density	Per Area
Φ_{A_1} (resp.Φ_{A_2})	Response functions	Per time
r_{A_1}	Natural propagation rate of susceptible prey	Per time
b_1	Intra-specific competition coefficient among susceptible prey	Area
b_2	Inter-specific competition coefficient between susceptible and infected prey	Area
β	Transmission rate	Per time
s	Inhibition rate	Area coverage
C_1	Proportion of susceptible prey into predator	No unit
C_2	Proportion of infected prey into predator	No unit
α_1/α_2	Natural death rates of infected prey/predator	Per time
δ	Disease induced mortality rate	Per time

Thus, $S(t)$ is bounded. To show other state variables $I(T)$ and $P(T)$ are bounded we consider

$$v = S + I + \theta_1 P$$

By differentiating v with respect to time T, we obtain

$$\begin{aligned}
\frac{dv}{dT} &= \frac{dS}{dT} + \frac{dI}{dT} + \theta_1 \frac{dP}{dT} \\
&= S\Big(1 - S - \kappa I\Big) - \frac{\gamma SI}{1+\eta I} - \theta_1 \psi_S(S)P \\
&\quad + \left(\frac{\gamma_2 SI}{1+\eta I} - \zeta I - \theta_2 \psi_I(I)P\right) \\
&\quad + \theta_1 \left(\psi_S(S)P + \psi_I(I)P - \xi P\right) \\
&= S\Big(1 - S\Big) - \kappa SI - \zeta I - \theta_2 \psi_I(I)P + \theta_1 \psi_I(I)P - \theta_1 \xi P \\
&\leq S\Big(1 - S\Big) - \kappa SI - \zeta I + \theta_1 \psi_I(I)P - \theta_1 \xi P \\
&= (1+\xi)S - S^2 - \kappa SI - (\zeta - \xi)I + \theta_1 \psi_I(I)P - \xi(S + I + \theta_1 P) \\
&\leq (1+\xi)S - S^2 + \theta_1 \psi_I(I)P - \xi v
\end{aligned}$$

The general Holling Type response function $\psi_I(I)$ is bounded, say, $\psi_I(I) \leq m$, $0 < m < \xi \leq \zeta$. Then after simplification we arrive

$$\frac{dv}{dT} \leq (1 + \xi - m)S - S^2 - (\xi - m)v \leq \frac{(1+\xi-m)^2}{4} - (\xi - m)v.$$

We can thus conclude that

$$v(T) \leq \frac{(1+\xi-m)^2}{4(\xi-m)} - \left(\frac{(1+\xi-m)^2}{4(\xi-m)} - v_0\right) e^{-(\xi-m)T}.$$

As a result, we find that

$$\lim_{T\to\infty} \sup v(T) \leq \max\left\{\frac{(1+\xi-m)^2}{4(\xi-m)}, v_0\right\}.$$

Hence, $v(T)$ remains bounded for all $T \geq 0$, which implies that the other state variables are also bounded. Consequently, all solutions of system (3) are uniformly bounded on $[0, \infty)$. □

3.3 Existence & Uniqueness

Theorem 3. *Let $F = (f_1, f_2, f_3)$. If F satisfies the Lipschitz condition and has continuous first partial derivatives with respect to x in a domain D, then $F(T, x)$ is locally Lipschitz in x. Consequently, for any initial point $(T_0, x_0) \in D$, there exists a unique solution $x(T, T_0, x_0)$ of the system*

$$\frac{dx}{dT} = F(T, x), \quad x(T_0) = x_0,$$

which passes through (T_0, x_0).

Proof. Let the right parts of the dynamical system (3) be denoted by $F = (f_1, f_2, f_3)$. Since f_1, f_2 and f_3 are continuous function, $F = (f_1, f_2, f_3)$ is continuous function in several variables, that is, $F \in C^1(\mathbb{R}^3_+)$. Thus, F satisfy the Lipschitz condition with respect to x in D. Hence, the solution of system (3) exists. The locally Lipschitz condition of F is verified using $\frac{\partial f_i}{\partial x_j}$, $i, j = 1, 2, 3$ to be continuously bounded within the domain D (Bezabih et al., 2021). We note that $F \in C^1(\mathbb{R}^3_+, Lip)$ in D and $f_1 = \frac{dS}{dT}$, $f_2 = \frac{dI}{dT}$ and $f_3 = \frac{dP}{dT}$. To show $\frac{\partial f_i}{\partial x_j}$, $i, j = 1, 2, 3$ to be continuously bounded. Now we get

$$\begin{aligned}
&\frac{\partial f_1}{\partial S} = (1 - 2S - \kappa I) - \frac{\gamma I}{1+\eta I} - \theta_1 \psi_S'(S)P \leq 1, \\
&\frac{\partial f_1}{\partial I} = -\kappa S - \frac{\gamma S}{(1+\eta I)^2} = -S\left(\kappa + \frac{\gamma S}{(1+\eta I)^2}\right), \\
&\text{This implies } \left|\frac{df_1}{dI}\right| = S\left(\kappa + \frac{\gamma S}{(1+\eta I)^2}\right) < \infty, \text{ as } S \text{ and } I \text{ are bounded,} \\
&\frac{df_1}{dP} = -\theta_1 \psi_S(S) \text{ implies } \left|\frac{df_1}{dP}\right| = \left|-\theta_1 \psi_S(S)\right| = \theta_1 \psi_S(S) < \theta_1 N_1, \\
&\qquad \text{as } \psi_S(S) \leq N_1 \in \mathbb{R}, \\
&\frac{\partial f_2}{\partial S} = \frac{\gamma I}{1+\eta I} \leq \frac{\gamma}{\eta}, \\
&\frac{\partial f_2}{\partial I} = \frac{\gamma S}{(1+\eta I)^2} - \zeta - \theta_2 \psi_I'(I)P \leq \frac{\gamma S}{(1+\eta I)^2} < \infty, \\
&\qquad \text{as } S \text{ and } I \text{ are bounded,} \\
&\frac{df_2}{dP} = -\theta_2 \psi_I(I) \implies \left|\frac{df_2}{dP}\right| = \left|-\theta_2 \psi_I(I)\right| = \theta_2 \psi_I(I) < \theta_2 N_2, \\
&\qquad \text{as } \psi_I(I) \leq N_2 \in \mathbb{R}, \\
&\frac{\partial f_3}{\partial S} = \psi_S'(S)P < \infty, \\
&\frac{\partial f_3}{\partial I} = \psi_I'(I)P < \infty, \\
&\frac{\partial f_3}{\partial P} = \psi_S(S) + \psi_I(I) - \xi < \psi_S(S) + \psi_I(I) \leq N_1 + N_2 < \infty.
\end{aligned}$$

As these all are continuous and bounded, F satisfy the locally Lipschitz condition. Therefore, the unique solution of the system (3) is verified as it is explained in Allen et al. (2007) and Hale (2009). □

3.4 Equilibrium points

The fixed points of the dynamical system (3) are the roots of a nonlinear system of equations.

$$S\Big(1 - S - \kappa I\Big) - \frac{\gamma SI}{1+\eta I} - \theta_1 \psi_S(S)P = 0, \tag{6}$$

$$\frac{\gamma SI}{1+\eta I} - \zeta I - \theta_2 \psi_I(I)P = 0, \tag{7}$$

$$\psi_S(S)P + \psi_I(I)P - \xi P = 0. \tag{8}$$

Hence, the extinction fixed point is $E^0(0,0,0)$, the axial fixed point is $E^1(1,0,0)$.
The predator free equilibrium point E^2 is obtained by the intersection point of the zero growth isocline of susceptible $\left(\frac{dS}{dT}=0\right)$ and the zero growth isocline of infected species $\left(\frac{dI}{dT}=0\right)$ where $P=0$. That is,

$$S^*\left(1 - S^* - \kappa I^*\right) - \frac{\gamma S^* I^*}{1+\eta I^*} = 0, \tag{9}$$

$$\frac{\gamma S^* I^*}{1+\eta I^*} - \zeta I^* = 0, \tag{10}$$

From equation (10), we get

$$S^* = \frac{\zeta}{\gamma} + \frac{\zeta\eta}{\gamma} I^*$$

Substitute this equation in (9), after simplification we arrived

$$\Delta_1 I^{*2} + \Delta_2 I^* + \Delta_3 = 0, \tag{11}$$

where $\Delta_1 = \eta\left(\kappa + \frac{\zeta\eta}{\gamma}\right) > 0$, $\Delta_2 = \frac{2\eta\zeta}{\gamma} + \gamma + \kappa - \eta$ and $\Delta_3 = \frac{\zeta}{\gamma} - 1$.
The positive roots I^* in the quadratic equation above is possible provided that the discriminant of an equation is positive, that is, $\Delta_2^2 - 4\Delta_1\Delta_2 > 0$ and follow from Descartes' rule of sign. We have the following results:

- If $\zeta > \gamma$ (i.e., $\Delta_3 > 0$) and $\frac{2\eta\zeta}{\gamma} + \gamma + \kappa > \eta$ (i.e $\Delta_2 > 0$), then (11) has no positive root meaning that there is no feasible equilibrium point E^2.

- If $\zeta < \gamma$ (i.e., $\Delta_3 < 0$), then there exists a unique equilibrium point E^2.

- If $\zeta > \gamma$ (i.e., $\Delta_3 > 0$) and $\frac{2\eta\zeta}{\gamma} + \gamma + \kappa < \eta$ (i.e., $\Delta_2 < 0$), then equation (11) has two positive roots, consequently two equilibrium points E_1^2, and E_2^2.

Disease free equilibrium point

The infection free fixed point of the form $E^3(S^*, 0, P^*)$ is solution of non-linear system

$$S^*\left(1 - S^*\right) - \theta_1 \psi_S(S^*)P^* = 0 \text{ and } \psi_S(S^*)P^* - \xi P^* = 0.$$

This gives $\psi_S(S^*) = \xi$ and $P^* = \dfrac{S^*\left(1-S^*\right)}{\xi\theta_1}$.

Table 2 provides an explanation of the illness free equilibrium point's existence criteria. where h is half saturation constant and w denote predator attack rate.

Table 2: Existence conditions of the disease free fixed point.

HT	HT-I	HT-II	HT-III	HT-IV
S^*	$\frac{\xi}{\omega}$	$\frac{h\xi}{\omega-\xi}$	$\sqrt{\frac{h^2\xi}{\omega-\xi}}$	$\frac{e(\omega-\xi)+\sqrt{e^2(\xi-\omega)^2-4\xi he}}{2\xi}$
Conditions	$\xi < \omega$	$h\xi < \omega - \xi$ and $\omega > \xi$	$h^2\xi < \omega - \xi$ and $\omega > \xi$	$(\xi-\omega)e > 2\sqrt{\xi h}$

The basic reproduction number, R_0

According to Layek (2015), the basic reproduction number is the average number of new infections from a single sick individual in a community that is completely susceptible over the course of the infectious period. It is used to predict whether the epidemic will spread or die out (Omar et al., 2024). To compute the basic reproduction number, we consider only the infected compartment of system (3)

$$\frac{dI}{dT} = \frac{\gamma SI}{1+\eta I} - \zeta I - \theta_2 \psi_I(I)P. \tag{12}$$

Following the next-generation matrix approach, we write

$$\frac{dI}{dT} = \mathcal{F}(I) - \mathcal{V}(I),$$

where the new infection and the transition (removal) terms represent

$$\mathcal{F}(I) = \frac{\gamma SI}{1+\eta I}, \text{ and } \mathcal{V}(I) = \zeta I + \theta_2 \psi_I(I)P.$$

Since R_0 measures the invasion of infection when I is small, we linearize the system around $I=0$. Using Taylor expansion,

$$\frac{\gamma SI}{1+\eta I} = \gamma SI(1 - \eta I + O(I^2)).$$

keeping only first-order terms gives $\mathcal{F}(I) \approx \gamma SI$. Similarly, expanding $\psi_I(I)$ near $I=0$, $\psi_I(I) \approx \psi_I'(0)I$.

Thus,

$$\mathcal{V}(I) \approx \zeta I + \theta_2 \psi_I'(0)P^* I.$$

The linearized equation becomes

$$\frac{dI}{dT} = \left[\gamma S^* - \left(\zeta + \theta_2 \psi_I'(0)P^*\right)\right] I.$$

Hence, the new infection rate is

$$F = \gamma S^*,$$

and the total removal rate is

$$V = \zeta + \theta_2 \psi_I'(0)P^*.$$

By the next-generation method,

$$R_0 = FV^{-1}.$$

Therefore,

$$R_0 = \frac{\gamma S^*}{\zeta + \theta_2 \psi_I'(0)P^*}. \tag{13}$$

Coexistence Equilibrium Point

Theorem 4. *The system admits a coexistence equilibrium $E^*(S^*, I^*, P^*)$ if the following conditions hold:*

$$S^* + \kappa I^* < 1, \quad \frac{\gamma S^*}{1+\eta I^*} > \zeta, \quad \psi_S(S^*) + \psi_I(I^*) = \xi, \quad R_0 > 1$$

.

Proof. To determine the coexistence equilibrium point $E^*(S^*, I^*, P^*)$, we set

$$\frac{dS}{dT} = 0, \qquad \frac{dI}{dT} = 0, \qquad \frac{dP}{dT} = 0.$$

Thus the equilibrium point satisfies the algebraic equations

$$S^*(1 - S^* - \kappa I^*) - \frac{\gamma S^* I^*}{1+\eta I^*} - \theta_1 \psi_S(S^*) P^* = 0, \tag{3.9}$$

$$\frac{\gamma S^* I^*}{1+\eta I^*} - \zeta I^* - \theta_2 \psi_I(I^*) P^* = 0, \tag{3.10}$$

$$\psi_S(S^*) P^* + \psi_I(I^*) P^* - \xi P^* = 0. \tag{3.11}$$

From the first, second and third equations we have $S^* + \kappa I^* < 1$, $\frac{\gamma S^*}{1+\eta I^*} > \zeta$, and $\psi_S(S^*) + \psi_I(I^*) = \xi$, respectively.
Note that

$$R_0 = \frac{\xi \theta_1 \gamma \psi_S^{-1}(\xi)}{\zeta \xi \theta_1 + \theta_2 \psi_I'(0) \psi_S^{-1}(\xi)\left(1 - \psi_S^{-1}(\xi)\right)}.$$

$$\frac{\gamma S^*}{1+\eta I^*} > \zeta \iff \frac{\gamma S^*}{\zeta(1+\eta I^*)} > 1.$$

At equilibrium (using $S^* = \psi_S^{-1}(\xi)$ we obtain

$$\frac{\gamma S^*}{\zeta(1+\eta I^*)} = R_0.$$

$$\frac{\gamma S^*}{1+\eta I^*} > \zeta \iff R_0 > 1.$$

□

4 Stability and Bifurcation Analysis

By examining sign of the derivative matrix's eigenvalues, we can determine the stability of a fixed points as in Dawed et al. (2020). The system (3) has a stable fixed point $E^*(S^*, I^*, P^*)$ if all characteristic roots of the Jacobian matrix, $J(E^*)$,

$$J(E^*) = \begin{pmatrix} J_{11} & J_{12} & J_{13} \\ J_{21} & J_{22} & J_{23} \\ J_{31} & J_{32} & J_{33} \end{pmatrix} \tag{14}$$

have negative real part where
$J_{11} = 1 - 2S^* - \kappa I^* - \frac{\gamma I^*}{1+\eta I^*} - \theta_1 \psi_S'(S^*) P^*$, $J_{12} = -\kappa S^* - \frac{\gamma S^*}{(1+\eta I^*)^2}$,
$J_{13} = -\theta_1 \psi_S(S^*)$, $J_{21} = \frac{\gamma I^*}{1+\eta I^*}$, $J_{22} = \frac{\gamma S^*}{(1+\eta I^*)^2} - \zeta - \theta_2 \psi_I'(I^*) P^*$,
$J_{23} = -\theta_2 \psi_I(I^*)$, $J_{31} = \psi_S'(S^*) P^*$, $J_{32} = \psi_I'(I^*) P^*$, and $J_{33} = \psi_S(S^*) + \psi_I(I^*) - \xi$.

The corresponding characteristic equation is $\det(J(E^*) - \lambda I_3) = 0$, that is

$$\begin{vmatrix} J_{11} - \lambda & J_{12} & J_{13} \\ J_{21} & J_{22} - \lambda & J_{23} \\ J_{31} & J_{32} & J_{33} - \lambda \end{vmatrix} = 0 \tag{15}$$

4.1 Local stability analysis

4.1.1 Stability nature near $E^0(0,0,0)$

$$J(E^0) = \begin{pmatrix} 1 & 0 & 0 \\ 0 & -\zeta & 0 \\ 0 & 0 & -\xi \end{pmatrix}$$

Thus, $\lambda_1 = 1 > 0$, $\lambda_2 = -\zeta < 0$, and $\lambda_3 = -\xi < 0$. Hence, the trivial fixed point E^0 is unstable. Biologically, this indicates that total extinction of the populations is impossible.

4.1.2 System behavior near $E^1(1,0,0)$

$$J(E^1) = \begin{pmatrix} -1 & -\kappa - \gamma & -\theta_1 \psi_S(1) \\ 0 & \gamma - \zeta & 0 \\ 0 & 0 & \psi_S(1) - \xi \end{pmatrix}$$

The eigenvalues are $\lambda_1 = -1$, $\lambda_2 = \gamma - \zeta$, and $\lambda_3 = \psi_S(1) - \xi$. Thus, the axial fixed point is locally asymptotically stable whenever $\gamma < \zeta$ and $\psi_S(1) < \xi$. This has a biological implication that susceptible prey population survive alone whenever no disease in the environment and without predator whenever the conditions holds.

4.1.3 System behavior near consumer free fixed point $E^2(S^*, I^*, 0)$

Theorem 5. *The consumer-free fixed point $E^2(S^*, I^*, 0)$ is locally asymptotically stable if the following conditions hold*

$$\begin{aligned} &(i) \quad \psi_S(S^*) + \psi_I(I^*) < \xi, \\ &(ii) \quad \zeta + 2S^* + \kappa I^* + \frac{\gamma I^*}{1+\eta I^*} < 1 + \frac{\gamma S^*}{(1+\eta I^*)^2}, \\ &(iii) \quad \left(1 - 2S^* - \kappa I^* - \frac{\gamma I^*}{1+\eta I^*}\right) \\ &\qquad \times \left(\frac{\gamma S^*}{(1+\eta I^*)^2} - \zeta\right) \\ &\qquad + \left(\kappa S^* + \frac{\gamma S^*}{(1+\eta I^*)^2}\right) \frac{\gamma I^*}{1+\eta I^*} > 0. \end{aligned}$$

Proof. The community matrix of the model (3) at E^2 is given by

$$J(E^2) = \begin{pmatrix} 1 - 2S^* - \kappa I^* - \frac{\gamma I^*}{1+\eta I^*} & -\kappa S^* - \frac{\gamma S^*}{(1+\eta I^*)^2} & -\theta_1 \psi_S(S^*) \\ \frac{\gamma I^*}{1+\eta I^*} & \frac{\gamma S^*}{(1+\eta I^*)^2} - \zeta & -\theta_2 \psi_I(I^*) \\ 0 & 0 & \psi_S(S^*) + \psi_I(I^*) - \xi \end{pmatrix}$$

The associated auxiliary equation is $det(J(E^2) - \lambda I_3) = 0$, that is

$$\begin{vmatrix} \sigma_1 - \lambda & \pi_1 & -\theta_1 \psi_S(S^*) \\ \pi_2 & \sigma_2 - \lambda & -\theta_2 \psi_I(I^*) \\ 0 & 0 & \sigma_3 - \lambda \end{vmatrix} = 0,$$

where, $\sigma_1 = 1 - 2S^* - \kappa I^* - \frac{\gamma I^*}{1+\eta I^*}$, $\sigma_2 = \frac{\gamma S^*}{(1+\eta I^*)^2} - \zeta$, $\sigma_3 = \psi_S(S^*) + \psi_I(I^*) - \xi$, $\pi_1 = -\kappa S^* - \frac{\gamma S^*}{(1+\eta I^*)^2} < 0$ and $\pi_2 = \frac{\gamma I^*}{1+\eta I^*} > 0$. Thus, one eigenvalue at $E^2(S^*, I^*, 0)$ is $\lambda_1 = \sigma_3 = \psi_S(S^*) + \psi_I(I^*) - \xi$. Now, λ_1 is negative if $\psi_S(S^*) + \psi_I(I^*) < \xi$. The rest two eigenvalues are found from the matrix

$$\bar{J}(E^2) = \begin{pmatrix} 1 - 2S^* - \kappa I^* - \frac{\gamma I^*}{1+\eta I^*} & -\kappa S^* - \frac{\gamma S^*}{(1+\eta I^*)^2} \\ \frac{\gamma I^*}{1+\eta I^*} & \frac{\gamma S^*}{(1+\eta I^*)^2} - \zeta \end{pmatrix}.$$

Using the Routh–Hurwitz criterion, the two eigenvalues of $\bar{J}$ are negative in their real parts provided that

$$\zeta + 2S^* + \kappa I^* + \frac{\gamma I^*}{1+\eta I^*} < 1 + \frac{\gamma S^*}{(1+\eta I^*)^2} \text{ and}$$
$$\left(1 - 2S^* - \kappa I^* - \frac{\gamma I^*}{1+\eta I^*}\right)\left(\frac{\gamma S^*}{(1+\eta I^*)^2} - \zeta\right) +$$
$$\left(\kappa S^* + \frac{\gamma S^*}{(1+\eta I^*)^2}\right)\frac{\gamma I^*}{1+\eta I^*} > 0.$$

Therefore, we infer that the model system (3) is locally asymptotically stable at the predator free equilibrium point E^2 as long as the conditions (i), (ii), and (iii) hold. □

4.1.4 Local Stability Near the Disease-Free Equilibrium Point

Theorem 6. *Local asymptotic stability of the infection-free fixed point $E^3(S^*, 0, P^*)$ of system (3) is ensured if the following criteria are satisfied:*

1. $R_0 < 1$,
2. $\psi_S'(S^*) > 0$,
3. $\psi_S'(S^*)(S^*)^2 - \left(2\xi + \psi_S'(S^*)\right)S^* + \xi < 0$.

Proof.

$$J(E^3) = \begin{pmatrix} \nabla_1 & -\kappa S^* - \gamma S^* & -\theta_1 \psi_S(S^*) \\ 0 & \nabla_2 & 0 \\ \psi_S'(S^*)P^* & \psi_I'(0)P^* & \nabla_3 \end{pmatrix} \quad (16)$$

where, $\nabla_1 = 1 - 2S^* - \theta_1 \psi_S'(S^*)P^*$, $\nabla_2 = \gamma S^* - \zeta - \theta_2 \psi_I'(0)P^*$ and $\nabla_3 = \psi_S(S^*) - \xi = 0$.

The associated auxiliary equation of $J(E^3)$ is

$$\begin{vmatrix} \nabla_1 - \lambda & -\kappa S^* - \gamma S^* & -\theta_1 \psi_S(S^*) \\ 0 & \nabla_2 - \lambda & 0 \\ \psi_S'(S^*)P^* & \psi_I'(0)P^* & \nabla_3 - \lambda \end{vmatrix} = 0$$

Since the matrix is block triangular with respect to the infected variable, one eigenvalue is

$$\lambda_1 = \nabla_2 = \gamma S^* - \zeta - \theta_2 \psi_I'(0)P^*.$$

Using the basic reproduction number

$$R_0 = \frac{\gamma S^*}{\zeta + \theta_2 \psi_I'(0)P^*},$$

we write

$$\lambda_1 = (\zeta + \theta_2 \psi_I'(0)P^*)(R_0 - 1).$$

Thus, if $R_0 < 1$, then $\lambda_1 < 0$ and the infection cannot invade. The others two eigenvalues are computed from the matrix

$$J = \begin{pmatrix} 1 - 2S^* - \theta_1 \psi_S'(S^*)P^* & -\theta_1 \psi_S(S^*) \\ \psi_S'(S^*)P^* & 0 \end{pmatrix}$$

By the Routh-Hurwitz stability rule, the two eigenvalues of J possess negative real parts provided that $\theta_1 \xi \psi_S'(S^*)P^* > 0$ (i.e., $\psi_S'(S^*) > 0$) and $\psi_S'(S^*)S^{*2} - (2\xi + \psi_S'(S^*))S^* + \xi < 0$. Thus, if conditions (1)–(3) are satisfied, we conclude that the model system (3) is locally asymptotically stable at the disease-free fixed point E^3. The predator eating efficiency is so high whenever conditions (1)–(3) are satisfied. The predator will only eat healthy prey because there is no infected prey present.

□

4.1.5 Global stability analysis using the Bendixson-Dulac theorem

Theorem 7. *If the Infection Free Equilibrium point $(S^*, 0, P^*)$ is locally asymptotically stable in the positive SP - plane region, then it is also globally asymptotically stable in the same region if $\frac{\psi_S(S)}{S} \geq \frac{\psi_S(S^*)}{S^*}$.*

Proof. Consequently, the system can be reduced to the following two-dimensional subsystem

$$\frac{dS}{dT} = S(1 - S) - \theta_1 \psi_S(S)P, \quad (17)$$
$$\frac{dP}{dT} = \psi_S(S)P - \xi P. \quad (18)$$

Consider $h(S, P) = \frac{1}{SP}$ as a Dulac positive function in the positive quadrant. Also, define the following functions

$$h_1(S, P) = S(1 - S) - \theta_1 \psi_S(S)P, \quad (19)$$
$$h_2(S, P) = \psi_S(S)P - \xi P. \quad (20)$$

Then,

$$\phi(S, P) = \frac{\partial}{\partial S}(h\, h_1) + \frac{\partial}{\partial P}(h\, h_2) = -\left(\frac{1}{P} + \theta_1 \frac{S\psi_S'(S) - \psi_S(S)}{S^2}\right).$$

Hence, $\phi(S, P)$ is a negative function of its arguments if $S\psi_S'(S) - \psi_S(S) \geq 0$. Note that by mean value thorem $S\psi_S'(S) - \psi_S(S) \geq 0$ and $\frac{\psi_S(S)}{S} \geq \frac{\psi_S(S^*)}{S^*}$ are equivalent. Since $\phi(S, P)$ does not change sign and is not identically zero in the positive quadrant of the SP-plane, by the Bendixson - Dulac criterion the infection free equilibrium point is globally asymptotically stable in the region

$$D = \left\{(S, P) \in R_+^2 : \frac{\psi_S(S)}{S} \geq \frac{\psi_S(S^*)}{S^*}, P > 0\right\}.$$

Moreover, the system has no limit cycle in the region. □

4.1.6 System stability conditions near endemic equilibrium point

Theorem 8. *Local asymptotic stability of the endemic equilibrium point $E^*(S^*, I^*, P^*)$ holds provided that the following conditions are met:*

(i) $D + G < 0$,
(ii) $q_1q_4 - Eq_5 + Gq_2 + Dq_3 < 0$,
(iii) $(D + G)(DG + q_2 + q_3 + Eq_4) + q_1q_4 - Eq_5 + Gq_2 + Dq_3 > 0$,

where the parameters D, E, F, and G are defined in the proof.

Proof. The positive fixed point $E^*(S^*, I^*, P^*)$ of the dynamics (3) is locally asymptotically stable if all the characteristic roots of the Jacobian matrix, J, has negative real parts, where

$$J(E^*) = \begin{pmatrix} D & -\kappa S^* - \gamma S^* F^2 & -\theta_1 \psi_S(S^*) \\ E & G & -\theta_2 \psi_I(I^*) \\ \psi_S'(S^*)P^* & \psi_I'(I^*)P^* & 0 \end{pmatrix}.$$

where, $D = 1 - 2S^* - \kappa I^* - \gamma I^* F - \theta_1 \psi_S'(S^*)P^*$, $E = \gamma I^* F$, $F = \dfrac{1}{1+\eta I^*}$ and $G = \gamma S^* F^2 - \zeta - \theta_2 \psi_I'(I^*)P^*$.

The characteristic equation is

$$\begin{vmatrix} D - \lambda & -\kappa S^* - \gamma S^* F^2 & -\theta_1 \psi_S(S^*) \\ E & G - \lambda & -\theta_2 \psi_I(I^*) \\ \psi_S'(S^*)P^* & \psi_I'(I^*)P^* & -\lambda \end{vmatrix} = 0$$

This implies

$$\lambda^3 + k_1\lambda^2 + k_2\lambda + k_3 = 0 \tag{21}$$

where, $k_1 = -(D + G)$, $k_2 = DG + q_2 + q_3 + Eq_4$, $k_3 = -(q_1q_4 - Eq_5 + Gq_2 + Dq_3)$, $q_1 = \theta_2\psi_I(I^*)\psi_S'(S^*)P^*$, $q_2 = \theta_1\psi_S(S^*)\psi_S'(S^*)P^*$, $q_3 = \theta_2\psi_I(I^*)\psi_I'(I^*)P^*$, $q_4 = \kappa S^* + \gamma S^* F^2$ and $q_5 = \theta_1\psi_S(S^*)\psi_I'(I^*)P^*$. Consequentially, if $D+G < 0$, then $k_1 > 0$. If $q_1q_4 - Eq_5 + Gq_2 + Dq_3 < 0$, then $k_3 > 0$. Moreover, $k_1k_2 - k_3 > 0$ if $(D + G)(DG + q_2 + q_3 + Eq_4) + q_1q_4 - Eq_5 + Gq_2 + Dq_3 > 0$. According to the Routh–Hurwitz criterion, the model system 3 is locally asymptotically stable at the endemic fixed point $E^* = (S^*, I^*, P^*)$ if the corresponding conditions are satisfied. □

4.2 Local bifurcation analysis

Bifurcations analysis helps to predict and understand transitions in the behavior of dynamical system as parameters value change. Local bifurcation refers, change in the qualitative behavior of dynamical system near fixed point as a system's parameters are varied.

Theorem 9. *(Transcritical Bifurcation)*

1. *The diseased model (3) demonstrate a transcritical bifurcation at parameter values $\zeta = \zeta^{[1]} = \gamma$ or $\xi = \xi^{[2]} = \psi_S(1)$ in the neighborhood of the equilibrium point $E^1(1, 0, 0)$.*

2. *When the parameter ξ attains the bifurcation threshold $\hat{\xi} = \psi_S(S^*) + \psi_I(I^*)$, the system (3) near the equilibrium $E^2(S^*, I^*, 0)$ exhibits*

   (i). No saddle-node bifurcation occurs but

   (ii). A transcritical bifurcation is observed.

Proof. (1). Consider the community matrix of model (3) evaluated at $E^1(1, 0, 0)$:

$$J(E^1) = \begin{pmatrix} -1 & -(\kappa + \gamma) & -\theta_1\psi_S(1) \\ 0 & \gamma - \zeta & 0 \\ 0 & 0 & \psi_S(1) - \xi \end{pmatrix}.$$

The eigenvalues of $J(E^1)$ are $\lambda_1 = -1 < 0$, $\lambda_2 = \gamma - \zeta$, and $\lambda_3 = \psi_S(1) - \xi$. Therefore, E^1 is locally asymptotically stable provided that $\gamma < \zeta$ and $\psi_S(1) < \xi$ hold. Substituting either $\zeta = \gamma$ or $\xi = \psi_S(1)$ into $J(E^1)$ yields a zero eigenvalue in the characteristic equation.

With $\zeta = \zeta^{[1]}$, the eigenvectors V and W, associated with the zero eigenvalue of the Jacobian $J^{[1]}(E^1, \zeta^{[1]})$ and its transpose, respectively, are

$$V = \begin{pmatrix} -(\kappa + \gamma)a \\ a \\ 0 \end{pmatrix}, \quad W = \begin{pmatrix} 0 \\ b \\ 0 \end{pmatrix},$$

where $a, b \neq 0$. The derivative of the vector field $F(S, I, P) = (F_1, F_2, F_3)^T$ with respect to ζ is

$$F_\zeta(X, \zeta) = \begin{pmatrix} 0 \\ -I \\ 0 \end{pmatrix}, \quad F_\zeta(E^1, \zeta^{[1]}) = \begin{pmatrix} 0 \\ 0 \\ 0 \end{pmatrix},$$

implying

$$W^T F_\zeta(E^1, \zeta^{[1]}) = 0.$$

Hence, the first condition of Sotomayor's theorem Pirayesh et al., 2016 for a transcritical bifurcation is met.

Next, we compute

$$DF_\zeta(E^1, \zeta^{[1]}) = \begin{pmatrix} 0 & 0 & 0 \\ 0 & -1 & 0 \\ 0 & 0 & 0 \end{pmatrix}, \quad DF_\zeta(E^1, \zeta^{[1]})V = \begin{pmatrix} 0 \\ -a \\ 0 \end{pmatrix},$$

so that

$$W^T[DF_\zeta(E^1, \zeta^{[1]})V] = -ab \neq 0.$$

Finally, the second derivative of F along V is

$$D^2F(E^1, \zeta^{[1]})(V, V) = \begin{pmatrix} -2v_1^2 + 2\gamma\eta v_2^2 + 2(-\kappa - \gamma)v_1v_2 \\ -2\gamma\eta v_2^2 + 2\gamma v_1 v_2 \\ 0 \end{pmatrix},$$

giving

$$W^T[D^2F(E^1, \zeta^{[1]})(V, V)] = -2b\zeta(\eta v_2^2 - v_1v_2) \neq 0 \quad \text{whenever } \eta v_2 \neq v_1.$$

Therefore, by Sotomayor's theorem Pirayesh et al., 2016; Yu et al., 2020, the model (3) demonstrate transcritical bifurcation at $\zeta = \zeta^{[1]}$ near the axial fixed point $E^1(1, 0, 0)$ provided that $\eta v_2 \neq v_1$.

Now, let us examine the bifurcation at $\xi = \xi^{[2]} = \psi_S(1)$. The eigenvectors V and W, associated to the zero eigenvalues of the matrices $J^{[2]}(E^1, \xi^{[2]})$ and its transpose respectively, can be written as

$$V = (v_1 \quad v_2 \quad v_3)^T = (-\theta_1\psi_S(1) \quad 0 \quad c)^T \text{ and } W = (0 \quad 0 \quad d)^T$$

where c and d are nonzero real numbers. It follows that

$$F_\xi(X, \xi) = \begin{pmatrix} 0 \\ 0 \\ -P \end{pmatrix}, \quad F_\zeta(E^1, \xi^{[2]}) = \begin{pmatrix} 0 \\ 0 \\ 0 \end{pmatrix}.$$

This implies that, $W^T F_\xi(E^1, \xi^{[2]}) = 0$. Moreover,

$$DF_\xi(E^1, \xi^{[2]}) = \begin{pmatrix} 0 & 0 & 0 \\ 0 & 0 & 0 \\ 0 & 0 & -1 \end{pmatrix},$$

$$\mathrm{DF}_\xi(E^1, \xi^{[2]})V = \begin{pmatrix} 0 & 0 & 0 \\ 0 & 0 & 0 \\ 0 & 0 & -1 \end{pmatrix}\begin{pmatrix} -\theta_1\psi_S(1)c \\ 0 \\ c \end{pmatrix} = \begin{pmatrix} 0 \\ 0 \\ -c \end{pmatrix}.$$

Hence, $W^T[DF_\xi(E^1,\xi^{[2]})V] = -cd \neq 0$. Furthermore,

$$D^2F(E^1,\xi^{[2]})(V,V) = \begin{pmatrix} -2v_1^2 - 2\theta_1\psi_S'(1)v_1v_3 \\ 0 \\ 2\psi_S'(1)v_1v_3 \end{pmatrix}$$

which implies that,

$$W^T[D^2F(E^1,\xi^{[2]})(V,V)] = 2\psi_S'(1)v_1v_3 = -2dc^2\theta_1\xi\psi_S'(1) \neq 0.$$

Hence, based on the Sotomayor's theorem as in Pirayesh et al. (2016) and Yu et al. (2020) the model exhibit transcritical bifurcation at $\xi = \xi^{[2]} = \psi_S(1)$ near to the axial equilibria $E^1(1,0,0)$.
See the proof of (2) in the appendix A. □

Theorem 10 (Hopf Bifurcation). *The system undergoes a Hopf bifurcation near to the equilibrium point $E^2(S^*,I^*,0)$ at the parameter value $\eta = \eta^*$, provided the following criteria are hold:*

1. *At $\eta = \eta^*$, we have $D_1 = 0$ and $D_2 > 0$, which guarantees the existence of a pair of purely imaginary eigenvalues, and*
2. *The transversality condition is satisfied, i.e.,*

$$\Re\left(\frac{d\lambda_j}{d\eta}\right)_{\eta=\eta^*} \neq 0, \quad j = 2,3,$$

where λ_j denote the eigenvalues of the auxiliary equation

$$\lambda^2 + D_1\lambda + D_2 = 0$$

associated with E^2. Here, $D_1 = -(\sigma_1+\sigma_2)$ and $D_2 = \sigma_1\sigma_2 - \pi_1\pi_2$, with σ_i and π_i $(i = 1,2)$ defined in the proof part.

Proof. The auxiliary equation of the model (3) at E^2 is

$$\begin{vmatrix} \sigma_1 - \lambda & \pi_1 & -\theta_1\psi_S(S^*) \\ \pi_2 & \sigma_2 - \lambda & -\theta_2\psi_I(I^*) \\ 0 & 0 & \sigma_3 - \lambda \end{vmatrix} = 0,$$

where, $\sigma_1 = 1 - 2S^* - \kappa I^* - \frac{\gamma I^*}{1+\eta I^*}$, $\sigma_2 = \frac{\gamma S^*}{(1+\eta I^*)^2} - \zeta$, $\sigma_3 = \psi_S(S^*) + \psi_I(I^*) - \xi$, $\pi_1 = -\kappa S^* - \frac{\gamma S^*}{(1+\eta I^*)^2} < 0$ and $\pi_2 = \frac{\gamma I^*}{1+\eta I^*} > 0$. After simplification

$$(\sigma_3 - \lambda)(\lambda^2 + D_1\lambda + D_2) = 0 \tag{22}$$

where

$$D_1 = -(\sigma_1+\sigma_2) = -\left(1 - 2S^* - \kappa I^* - \frac{\gamma I^*}{1+\eta I^*} + \frac{\gamma S^*}{(1+\eta I^*)^2} - \zeta\right),$$

$$D_2 = \sigma_1\sigma_2 - \pi_1\pi_2 = \left(1 - 2S^* - \kappa I^* - \frac{\gamma I^*}{1+\eta I^*}\right)\left(\frac{\gamma S^*}{(1+\eta I^*)^2} - \zeta\right) + \left(\kappa S^* + \frac{\gamma S^*}{(1+\eta I^*)^2}\right)\frac{\gamma I^*}{1+\eta I^*}.$$

Eq'n (22) has pure imaginary roots if $D_1 = 0$ and $D_2 > 0$ from which the threshold value $\eta = \eta^*$. Thus, when $\eta = \eta^*$, $\lambda_1 = \sigma_3$, $\lambda_2 = i\sqrt{D_2}$, and $\lambda_3 = -i\sqrt{D_2}$. Differentiating equation (22) with respect to η, we have

$$2\lambda\frac{d\lambda}{d\eta} + \lambda\frac{dD_1}{d\eta} + D_1\frac{d\lambda}{d\eta} + \frac{dD_2}{d\eta} = 0.$$

This implies that, $\frac{d\lambda}{d\eta} = -\frac{\dot{D}_2 + \lambda\dot{D}_1}{D_1 + 2\lambda}$. Thus, at $\eta = \eta^*$ it is reduced to

$$\left[\frac{d\lambda}{d\eta}\right]_{\eta=\eta^*} = -\left[\frac{\dot{D}_2 + \lambda\dot{D}_1}{D_1 + 2\lambda}\right]_{\lambda=i\sqrt{D_2}} = \frac{-\dot{D}_1\sqrt{D_2}}{2D_2} + i\frac{\dot{D}_2\sqrt{D_2}}{2D_2}.$$

Hence, $Re\left[\frac{d\lambda_j}{d\eta}\right]_{\eta=\eta^*} = -\frac{\dot{D}_1\sqrt{D_2}}{2D_2} \neq 0$.
Hence, the transversality condition

$$\Re\left(\frac{d\lambda_j}{d\eta}\right)_{\eta=\eta^*} \neq 0, \quad j = 2,3,$$

is satisfied, which confirms the occurrence of a Hopf bifurcation at $\eta = \eta^*$. Furthermore, it can be demonstrated that there exists a threshold value of the parameter γ at which the present model also demonstrate a stability switch via Hopf bifurcation.

□

Theorem 11. *If the bifurcation parameter is given by*

$$\zeta^{[0]} = \frac{\theta_1\xi\gamma_2 S - \theta_2\psi_I'(0)S(1-S)}{\theta_1\xi},$$

then the model system (3) at the infection-free fixed point $E^3(S^*,0,P^*)$ does not exhibit a saddle-node bifurcation. Instead, the transcritical bifurcation of the system is observed. See the proof in the appendix B.

5 Computational Analysis

In order to validate the theoretical results, the researchers numerically explore the dynamic behavior of their model using the `ode45` solver in MATLAB. Owing to the unavailability of empirical data, a biologically feasible and representative set of parameter values is adopted for the purpose of numerical simulations. $X = \{\alpha_1 = 0.001, \alpha_2 = 0.007, \gamma = 2.5, \theta_1 = 0.04, \theta_2 = 0.02, \zeta = 0.04, \kappa = 1.3, \xi = 0.01, \eta = 0.03, h = 0.064,$ and $e = 0.05\}$. Moreover, for simulation purposes, we consider four representative models selected from the sixteen possible combinations of Holling-type functional responses. Specifically:

- **Model 1:** Represents the disease model with(HT-I–HT-II).
- **Model 2:** Corresponds to the combination (HT-II–HT-III).
- **Model 3:** Defined by the combination (HT-III–HT-II).
- **Model 4:** Represents the combination (HT-IV–HT-III).

These four sample models are selected as representative cases among the sixteen Holling-type response function combinations to capture different nonlinear interaction mechanisms and to compare their qualitative impacts on the disease transmission dynamics. When the consumer species is absent in the dynamics 3, then the model is dominated by prey population. The time-series plots in Figure (1) show that both $S(t)$ and $I(t)$ converge smoothly to their fixed point values $E^2(S^*,I^*,0)$, indicating local asymptotic stability. The infected prey population increases initially due to infection transmission, then stabilizes at a moderate level, while the susceptible population decreases and reaches a steady state.

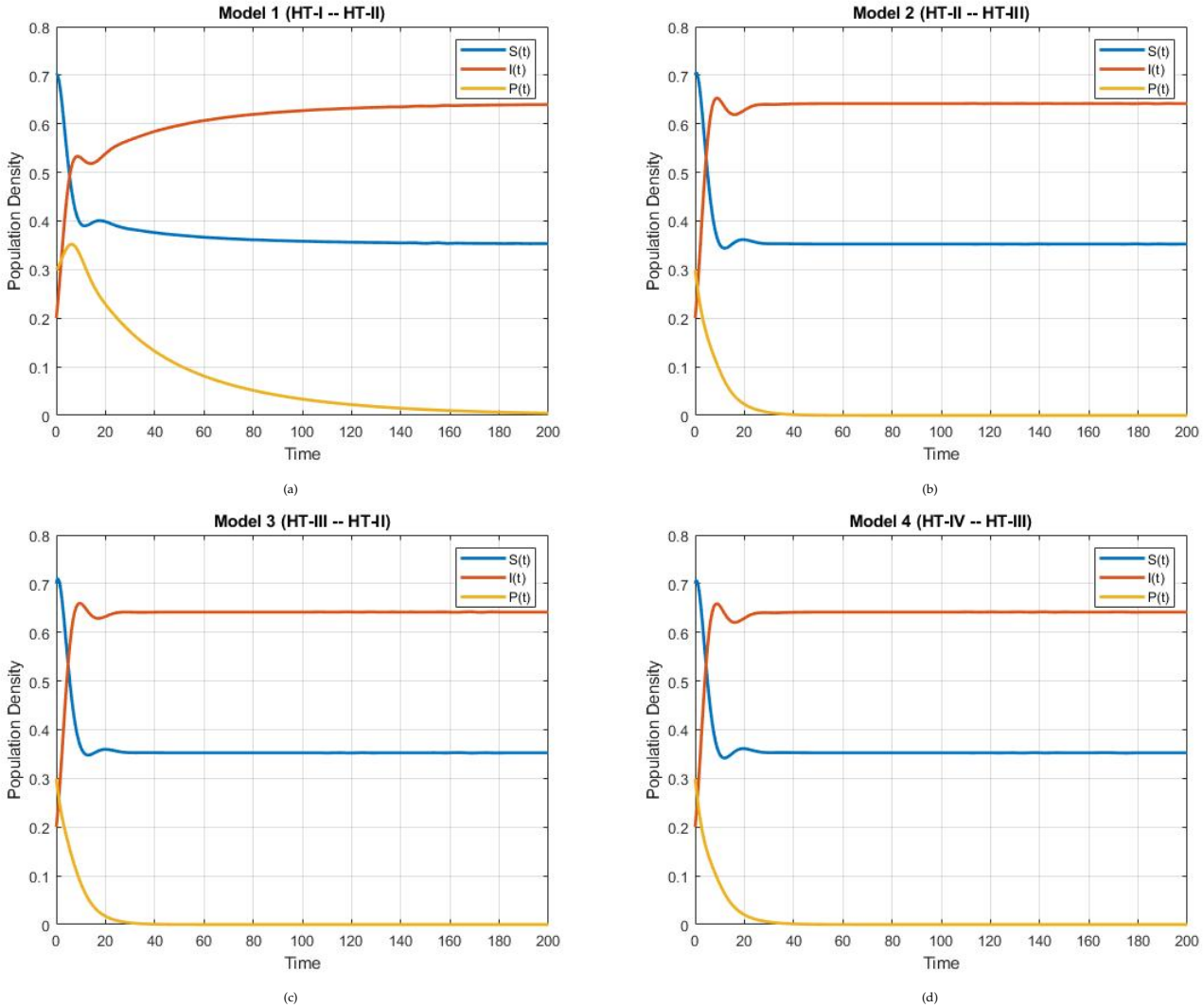

Figure 1: Time series plot of the system (3), where the parametric values $\kappa = 0.3$; $\gamma = 0.8$; $\eta = 0.2$; $\theta_1 = 0.4$; $\theta_2 = 0.3$; $\zeta = 0.25$; $xi = 0.5$; $a_1 = 0.6$; $a_2 = 0.5$; $b_1 = 0.4$; $b_2 = 0.3$; $c_1 = 0.2$; and initial condition $(0.70,\ 0.120,\ 0.3)$.

When host is absent in the model system (3), the dynamics reduce to a predator-prey subsystem involving S and P. In Figure (2) the time series plots show both populations converging to the host-free fixed point $E^3(S^*, 0, P^*)$. Consumers grow up initially fueled by prey availability, then stabilize as prey density decreases. Additionally, the phase diagrams confirm that trajectories approach the subspace $I = 0$. The infection-free fixed point is locally asymptotically stable under the parameter sets considered, consistent with Theorem 6.

Figure 3 shows the system dynamics begin with periodic oscillation and through time it goes to a locally asymptotically stable endemic fixed point, where the computational laboratory is performed for some possible Holling Type response function combinations of the mathematical Eco-Epidemiology model for the diseased-model (3).

Overall, the simulations show that both predator-free and disease-free equilibria are stable, while nonlinear functional responses mainly affect the rate and amplitude of transient dynamics rather than the final steady state. These results emphasize the regulatory roles of infection and predation in prey dynamics and the stabilizing influence of functional response saturation.

The bifurcation diagrams in Figures 4 confirm the predicted transcritical bifurcations in system (3) (Theorem 9). As the parameter ζ cross its thresholds, equilibria exchange stability, with the infected equilibrium I^* smoothly transitioning from stable to unstable.

Ecologically, small changes in disease-induced mortality ζ can shift the system between disease-free and infected states, or from predator extinction to coexistence, reflecting the influence of nonlinear functional responses ψ_S and ψ_I.

Models 1 and 2 show bifurcations at lower thresholds, indicating higher sensitivity and faster infection spread under simpler responses. In contrast, Models 3 and 4, show stronger saturation or complex predation terms, display delayed transitions, highlighting greater ecological resilience.

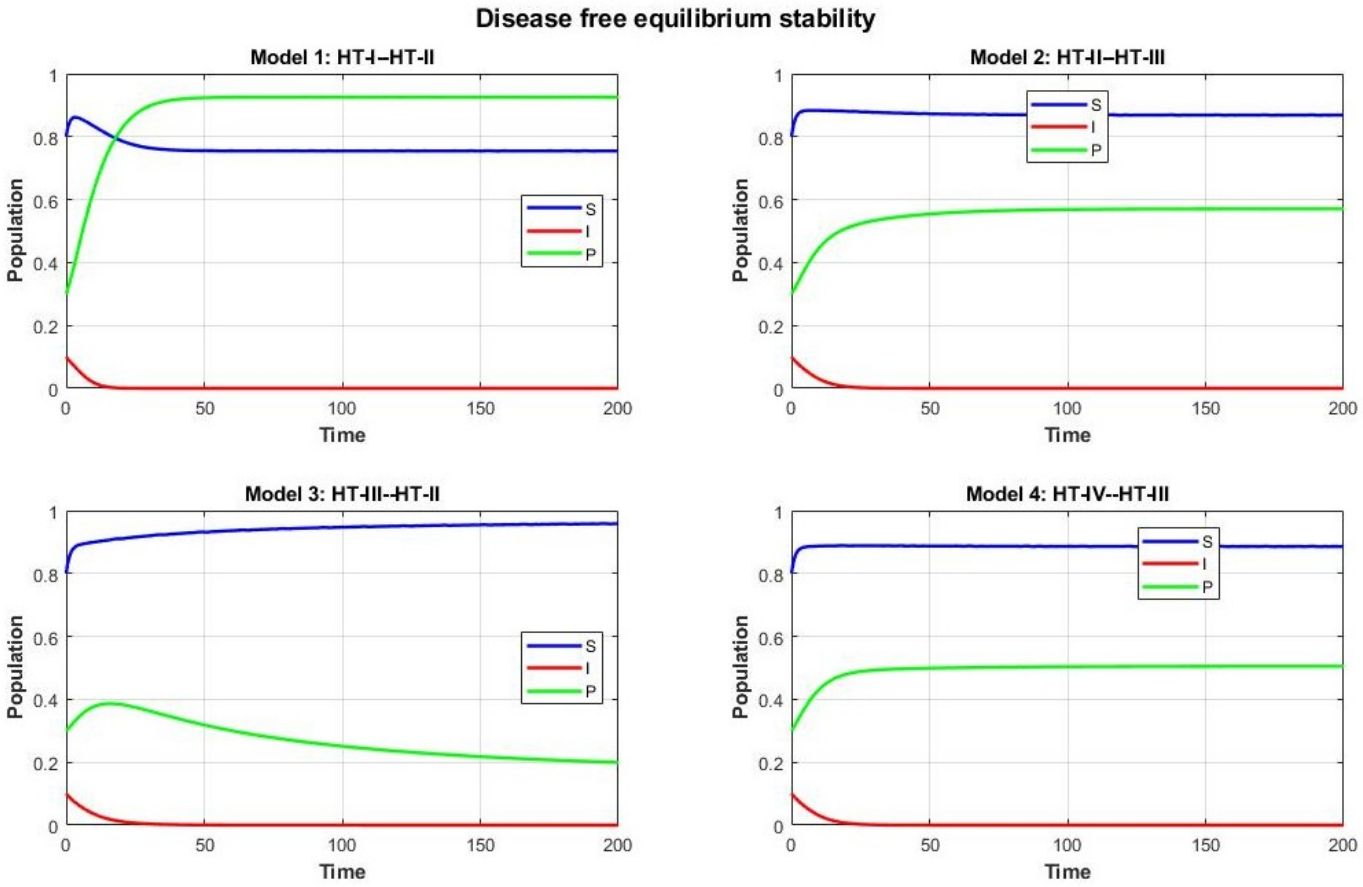

Figure 2: Time series plot of the system (3), where the parametric values $\kappa = 0.10$; $\gamma = 0.4$; $\eta = 0.10$; $\zeta = 0.30$; $\theta_1 = 0.50$; $\theta_2 = 0.70$; $\xi = 0.40$; $a = 0.65$; $b = 0.3$; $h = 0.20$; $h_1 = 0.30$; $h_2 = 0.25$; and initial condition $(0.80,\ 0.1,\ 0.3)$.

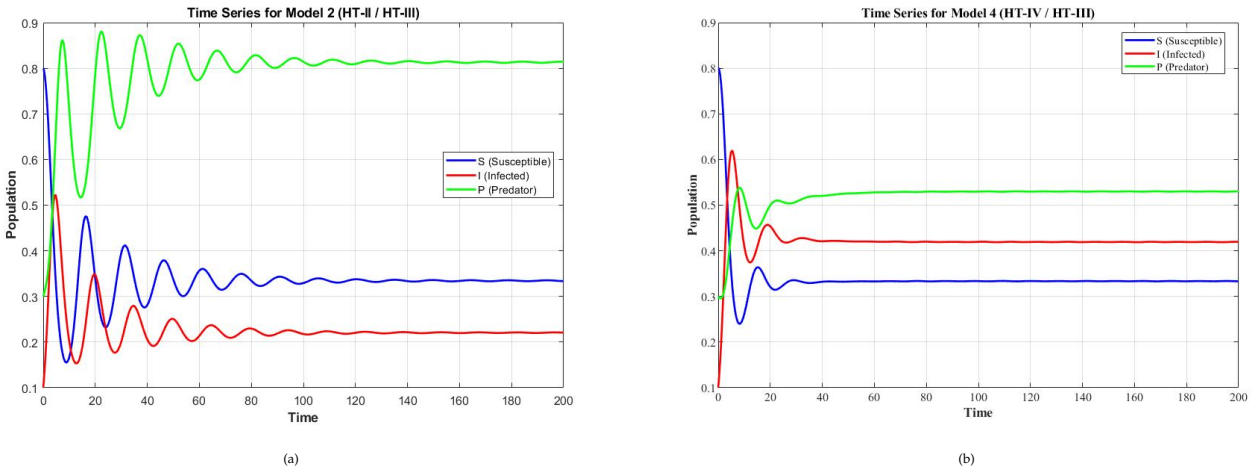

(a) (b)

Figure 3: Time seires plot of the model system 3, where the parameter values $\gamma = 1.2$, $\theta_1 = 0.5$, $\theta_2 = 0.3$, $\zeta = 0.3$, $\kappa = 0.1$, $\xi = 0.4$, $a = 0.6$, $b = 0.3$, $c = 0.2$, $\eta = 0.03$, $h_1 = 0.3$, $h_2 = 0.25$ and for the, initial condition $(0.8, 0.1, 0.3)$.

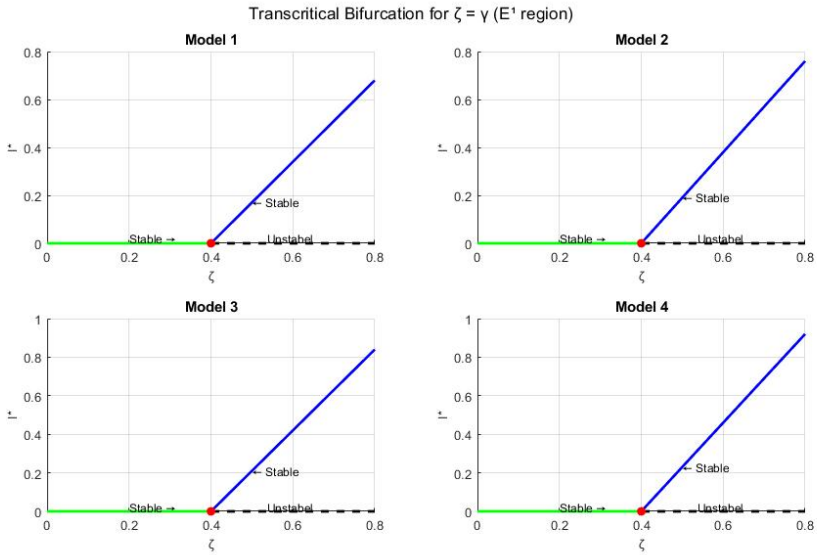

Figure 4: Bifurcation diagrams for Models 1–4 with respect to $\zeta = \gamma$ near the equilibrium $E^1(1, 0, 0)$. The horizontal axis represents the bifurcation parameter ζ, and the vertical axis represents the infected equilibrium I^*. Solid lines denote stable equilibria, while dashed lines denote unstable equilibria and the bifurication value is $\zeta = 0.4$.

5.1 Impact of the inhibition rate, η

The inhibition rate η appears in the infection term which regulates the rate at which susceptible prey become infected. From Figure(5), the parameter η controls the saturation level of the infection process for small values of η, the incidence rate is almost linear in I, leading to rapid spread of infection; for large η, the infection saturates quickly, representing inhibitory effects such as crowding, limited contact, or behavioral avoidance. Ecologically, η represents density-dependent inhibition in the infection process due to immunity, crowding, or behavioural avoidance among prey. As η increases, the effective contact rate between susceptible and infected prey decreases, reducing infection pressure. This reduction weakens the oscillatory feedback between prey and predator populations, thereby promoting stability in the coexistence equilibrium.

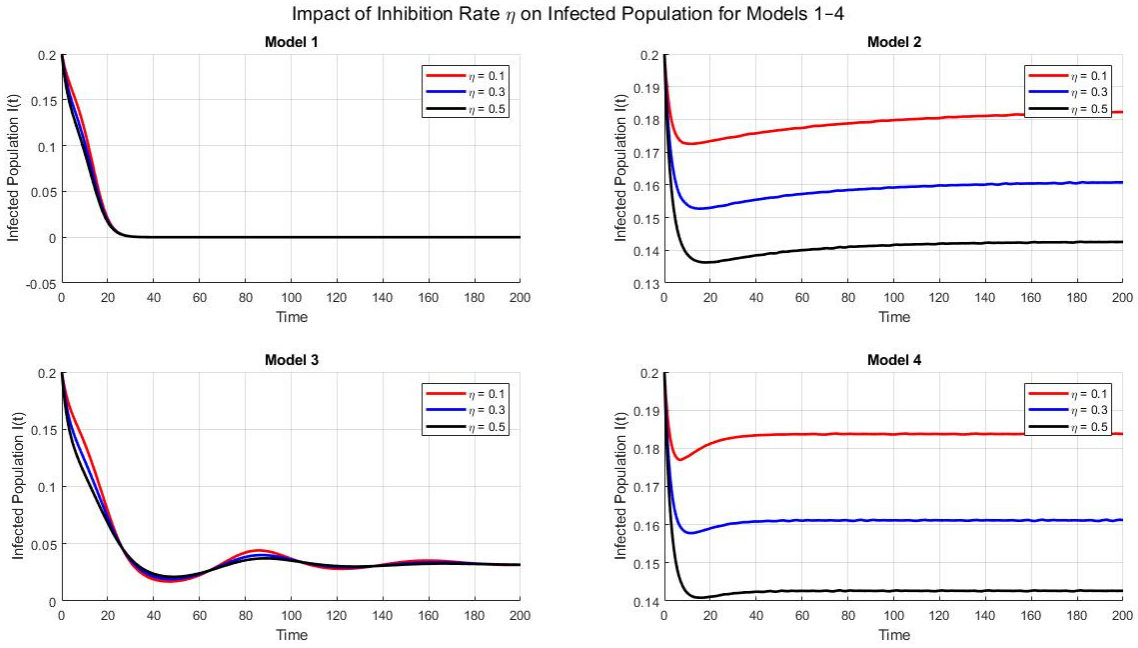

Figure 5: Time series showing the impact of the inhibition rate η on system stability for HT-II–HT-III, where parameters value $\eta = 0.1,\ 0.3,\ 0.5, \kappa = 0.5; \gamma = 0.8; \theta_1 = 0.2;$ $\theta_2 = 0.15; \zeta = 0.6; \xi = 0.5; a = 0.6; b = 0.3; c = 0.2;$ and initial condition $(0.7,\ 0.2,\ 0.1)$.

5.2 Impact of the transmission rate, γ

As illustrated in Figure 6, the transmission parameter γ has also have a signification effect on the dynamical behaviour of population I , and as transmission rates γ increasing the infected prey population rise up, and making the nature of stability of the coexistence equilibrium is becomes more periodic and take long time to stable. Moreover, for different Holling Type response functions combination, the patterns of stability of endemic equilibrium point are identical.

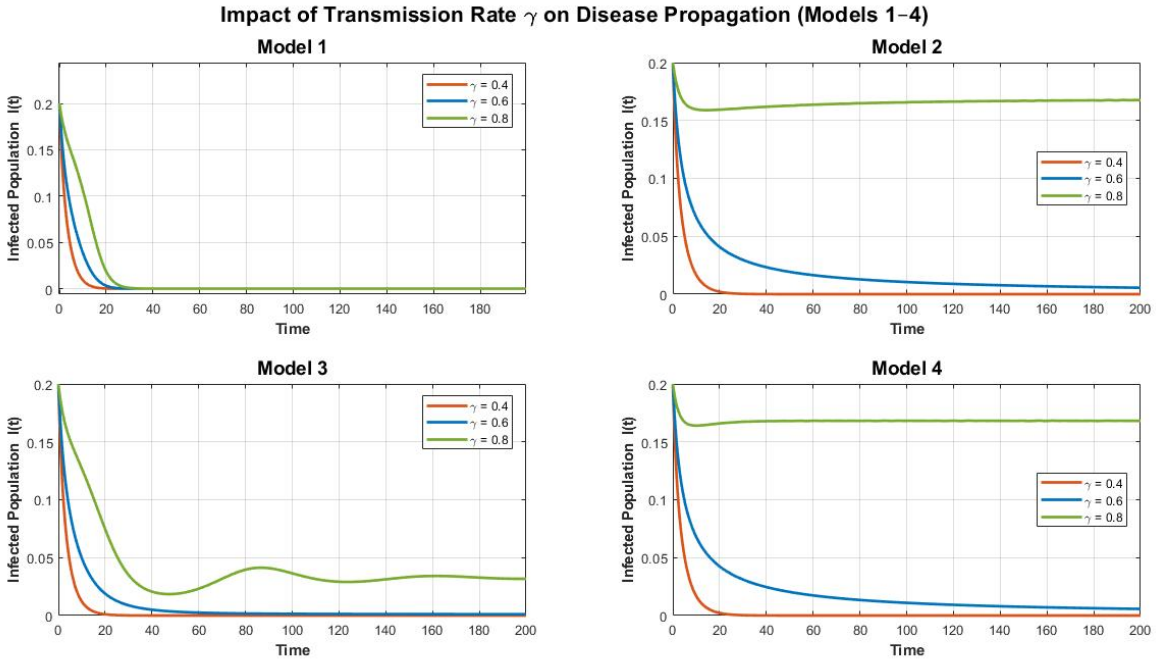

Figure 6: Time series plot of the dynamical system (3) for different values of transmission rate $\gamma = 0.4,\ 0.6,\ 0.8$ for Mode 1-4, where other parameter values $\kappa = 0.5$, $\eta = 0.3$, $\theta_1 = 0.2$, $\theta_2 = 0.15$, $\zeta = 0.6$, $\xi = 0.5$; $a = 0.6$; $b = 0.3$; $c = 0.2$ and initial condition $(0.7,\ 0.2,\ 0.1)$.

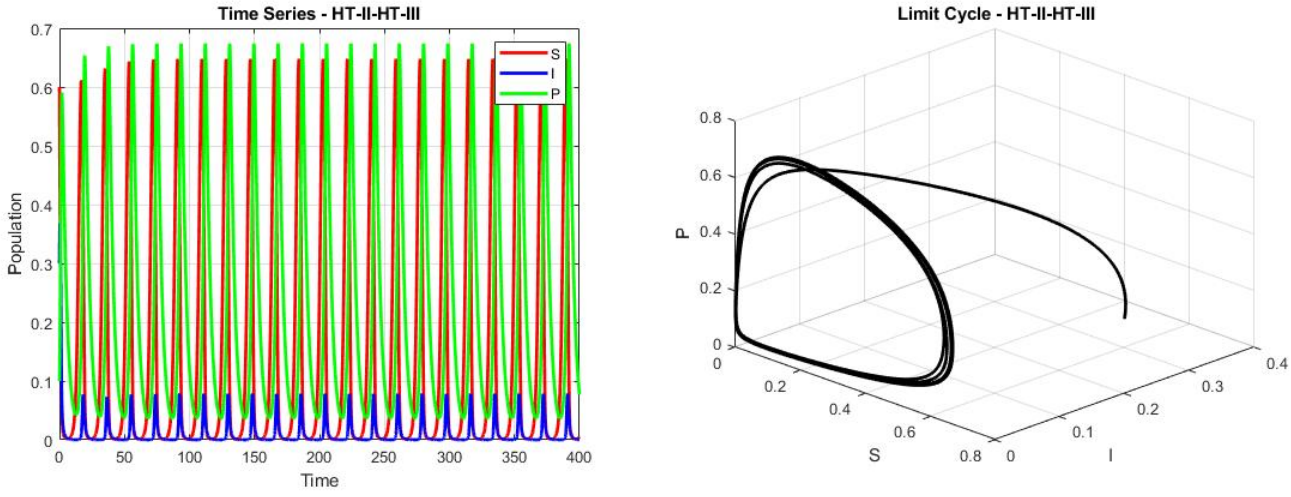

(a) (b)

Figure 7: Time series plot(periodic solution) and phase diagram (limit cycle) of the model system HT-II–HT-III, where the parameter values $\kappa = 0.4$, $\gamma = 5.0$, $\zeta = 0.6$, $\theta_1 = 1.2$, $\theta_2 = 1.0$, $a_1 = 1.5$, $a_2 = 1.3$, $b = 0.4$, $h = 0.2$, $\xi = 0.3$, $\eta = 2.0$, and initial condition (0.6, 0.3, 0.1).

Figure 7 indicates existence of Hopf bifurcation which verifies Theorem 4.6. Ecologically, η measures the strength of inhibitory (saturation) effects regulating predation or disease transmission. For $\eta < \eta^*$, the populations coexist at a stable steady state. When $\eta > \eta^*$, the equilibrium loses stability and sustained oscillations emerge due to feedback between infection spread and predation pressure. Increased infection enhances predator growth, which subsequently suppresses the host population, leading to predator decline and eventual host recovery. This recurring mechanism generates persistent population cycles, reflecting realistic eco-epidemiological fluctuations observed in natural ecosystems.

6 Result

In this section, we concisely summarize the main analytical and numerical findings obtained in Sections 4 and 5 for the eco-epidemiological model (3). The local and global stability conditions of all equilibrium points, corresponding to different combinations of Holling-Type functional responses, are presented in Table (3). These results establish the parametric regimes under which the system exhibits disease-free, endemic, predator-free, or coexistence states.

The bifurcation analysis results of the eco-epidemiological dynamics 3 near equilibrium points are summarized in table (4).

Table 3: Stability analysis result of Equilibrium points of the model system 3: Note; LAS ≡ locally asymptotically stable, GAS ≡ globally asymptotically stable

Equilibria	Stability conditions	Stability status
E^0	Always	Unstable
E^1	$\gamma < \zeta$ and $\psi_S(1) = \zeta$	LAS
E^2	Conditions stated in Theorem (5) (i)–(iii)	LAS
E^3	Conditions stated in Theorem (6) (1)–(3)	LAS
E^3	$\psi_S(S) \geq \exp \int_0^T \frac{du}{S}$	GAS
E^*	Conditions stated in Theorem (8)(i)–(iii)	LAS

The collective results depicted in Figures 4 clearly demonstrate how variations in the key bifurcation parameter ζ regulate the coexistence and persistence of prey, infected prey, and predator populations. The transcritical bifurcation marks a critical threshold where the system shifts from a disease-free to an endemic equilibrium, reflecting a change in ecological stability and disease prevalence.

From an ecological perspective, increasing the recovery rate (ξ) helps drive the system toward a disease-free state. Comparing Models 1–4, introducing nonlinear saturation in infection and predation stabilizes the system by postponing bifurcations. This highlights the importance of using realistic functional responses in eco-epidemiological models to capture key biological feedbacks and better understand ecosystem resilience under disease pressure.

Table 4: Local bifurcation analysis result of Equilibrium points of the model 3: TB ≡ Transcritical bifurcation, HB ≡ Hopf bifurcation

E.P	**Threshold value**	**Stability condition**	**Bifurcation**
E^1	$\gamma = \zeta$	$\eta v_2 \neq v_1$	TB
E^1	$\psi_S(1) = \xi$	always	TB
E^2	$\hat{\xi} = \psi_S(S^*) + \psi_I(I^*)$	$\psi_S'(S^*)V_1 + \psi_I'(I^*)V_2 \neq 0$	TB
E^2	$\eta = \eta^*$	$D_1 = 0, D_2 > 0$ and $Re\left[\frac{d\lambda_j}{d\eta}\right]_{\eta=\eta^*} \neq 0$	HB
E^3	$\zeta^{[0]} = \frac{\theta_1\xi\gamma_2 S - \theta_2\psi_I'(0)S(1-S)}{\theta_1\xi}$	$-(2\gamma\eta S^* + \theta_2\psi_I''(0)P^*)V_2^2\Upsilon + 2(\gamma V_1 V_2\Upsilon - \theta_2\psi_I'(0)V_2V_3)\Upsilon \neq 0$	TB

The inhibition (saturation) parameter η plays a critical regulatory role. When η is below the critical threshold ($\eta^* = 2$), the system settles into a stable coexistence of susceptible prey, infected prey, and predators. However, once η exceeds this value, a Hopf bifurcation occurs: the equilibrium becomes unstable and a stable limit cycle emerges. Biologically, this leads to recurring oscillations driven by feedback between disease transmission and predation. Increased susceptible prey boosts infection and predator growth; predators then reduce prey populations, which in turn lowers predator numbers, allowing prey to recover and restarting the cycle.

Overall, the Hopf bifurcation shows how changes in inhibitory effects can shift the ecosystem from stable coexistence to sustained oscillations, underscoring the delicate balance between disease dynamics and predator–prey interactions.

7 Conclusion

In this study, the researchers have investigated an eco-epidemiological mathematical model in which a prey population is infected by microparasites, while predators feed on both susceptible and infected prey following a general Holling-type functional response. The model was developed to explore how disease transmission and predation efficiency affect the overall community structure and population dynamics. An emergent carrying capacity was introduced to reflect the fact that infected prey, having reduced fitness, are more easily captured by predators. The stability and bifurcation conditions were derived for different equilibrium points, including trivial, axial, predator-free, disease-free, and endemic states. Analytical and numerical analyses showed strong agreement between theoretical predictions and simulation results.

The system exhibits oscillatory behavior for lower values of the inhibition rate (η), whereas higher inhibition rates promote stability. Hopf bifurcation analysis, taking η as the bifurcation parameter, revealed that increasing inhibition enhances system stability. Furthermore, when the predation rates (ω_1, ω_2) exceed a critical threshold, the predator-free equilibrium becomes unstable, and a stable disease-free coexistence of prey and predator emerges. The bifurcation analysis indicates that disease transmission and predator–prey interactions jointly determine ecosystem stability. Managing infection parameters such as the transmission rate can prevent oscillatory outbreaks and species extinction. Hence, controlling ecological feedbacks through parameter tuning plays a crucial role in maintaining biodiversity and long-term coexistence within predator–prey systems. Overall, the theoretical and numerical investigations are carried out under saturating incidence rates demonstrate the biological consistency of the proposed model. The results provide valuable insights into the interplay between infection, predation efficiency, and population stability in eco-epidemiological systems. The primary contribution of this work lies in providing a comprehensive bifurcation analysis under these combined nonlinear mechanisms. We rigorously establish threshold dynamics through the basic reproduction number and employ bifurcation theory to demonstrate the occurrence of transcritical and Hopf bifurcations. The results reveal how inhibition and transmission parameters govern transitions between disease-free equilibria, endemic coexistence, and sustained oscillatory outbreaks.

Future studies can extend this work by incorporating time delays representing disease incubation or predator gestation periods, which may lead to more complex dynamical behaviors such as chaos or multiple attractors. Furthermore, integrating stochastic effects, seasonal

variations, or optimal control strategies may enhance the model applicability to real-world ecological management and conservation policies.

Data Availability Statement

The data supporting the findings of this study are available from the authors upon reasonable request.

Conflicts of interest

The authors declare that they have no conflicts of interest relevant to this study.

Author Contributions

All have equal contribution.

Funding

This research received no specific grant from any funding agency.

References

Allen, L. J., Bolker, B. M., Lou, Y., & Nevai, A. L. (2007). Asymptotic profiles of the steady states for an sis epidemic patch model. *SIAM Journal on Applied Mathematics*, *67*(5), 1283–1309.

Anderson, R. M., & May, R. M. (1986). The invasion, persistence and spread of infectious diseases within animal and plant communities. *Philosophical Transactions of the Royal Society of London. B, Biological Sciences*, *314*(1167), 533–570.

Bezabih, A. F., Edessa, G. K., & Rao, K. P. (2021). Mathematical modeling the impact of infectious diseases in prey-predator interactions.

Biswas, S., Samanta, S., & Chattopadhyay, J. (2015). A model based theoretical study on cannibalistic prey–predator system with disease in both populations. *Differential Equations and Dynamical Systems*, *23*, 327–370.

Brauer, F. (2005). The kermack–mckendrick epidemic model revisited. *Mathematical biosciences*, *198*(2), 119–131.

Cai, L. M., & Li, X. Z. (2010). Global analysis of a vector-host epidemic model with nonlinear incidences. *Applied Mathematics and Computation*, *217*(7), 3531–3541.

Capasso, V., & Serio, G. (1978). A generalization of the kermack-mckendrick deterministic epidemic model. *Mathematical biosciences*, *42*(1-2), 43–61.

Das, K. P. (2016). A study of harvesting in a predator–prey model with disease in both populations. *Mathematical Methods in the Applied Sciences*, *39*(11), 2853–2870.

Dawed, M. Y., Tchepmo Djomegni, P. M., & Krogstad, H. E. (2020). Complex dynamics in a tritrophic food chain model with general functional response. *Natural Resource Modeling*, *33*(2), e12260.

Demir, M. (2019). Optimal control strategies in ecosystem-based fishery models.

Ghanbari, B. (2021). On the modeling of an eco-epidemiological model using a new fractional operator. *Results in physics*, *21*, 103799.

Gumel, A. B., & Moghadas, S. M. (2003). A qualitative study of a vaccination model with non-linear incidence. *Applied mathematics and computation*, *143*(2-3), 409–419.

Haldar, S., Khatua, A., Das, K., & Kar, T. K. (2021). Modeling and analysis of a predator–prey type eco-epidemic system with time delay. *Modeling Earth Systems and Environment*, *7*, 1753–1768.

Hale, J. K. (2009). *Ordinary differential equations*. Courier Corporation.

Haque, M., & Venturino, E. (2007). An ecoepidemiological model with disease in predator: The ratio-dependent case. *Mathematical methods in the Applied Sciences*, *30*(14), 1791–1809.

Holling, C. S. (1959). The components of predation as revealed by a study of small-mammal predation of the european pine sawfly1. *The canadian entomologist*, *91*(5), 293–320.

Hu, Z., Teng, Z., Zhang, T., Zhou, Q., & Chen, X. (2017). Globally asymptotically stable analysis in a discrete time eco-epidemiological system. *Chaos, Solitons & Fractals*, *99*, 20–31.

Hugo, A., & Simanjilo, E. (2019). Analysis of an eco-epidemiological model under optimal control measures for infected prey. *Applications and Applied Mathematics: An International Journal (AAM)*, *14*(1), 8.

Kooi, B. W., van Voorn, G. A., & pada Das, K. (2011). Stabilization and complex dynamics in a predator–prey model with predator suffering from an infectious disease. *Ecological Complexity*, *8*(1), 113–122.

Layek, G. C. (2015). *An introduction to dynamical systems and chaos* (Vol. 449). Springer.

Li, H., & Takeuchi, Y. (2011). Dynamics of the density dependent predator–prey system with beddington–deangelis functional response. *Journal of Mathematical Analysis and Applications*, *374*(2), 644–654.

Liu, W. M., Hethcote, H. W., & Levin, S. A. (1987). Dynamical behavior of epidemiological models with nonlinear incidence rates. *Journal of mathematical biology*, *25*, 359–380.

Lotka, A. J. (1925). *Elements of physical biology*. Williams; Wilkins.

Maiti, A. P., Jana, C., & Maiti, D. K. (2019). A delayed eco-epidemiological model with nonlinear incidence rate and crowley–martin functional response for infected prey and predator. *Nonlinear Dynamics*, *98*, 1137–1167.

Omar, F. M., Sohaly, M. A., & El-Metwally, H. (2024). Lyapunov functions and global stability analysis for epidemic model with n-infectious. *Indian Journal of Physics*, *98*(5), 1913–1922.

Panja, P. (2020). Prey–predator–scavenger model with monod–haldane type functional response. *Rendiconti del Circolo Matematico di Palermo Series 2*, *69*(3), 1205–1219.

Pirayesh, B., Pazirandeh, A., & Akbari, M. (2016). Local bifurcation analysis in nuclear reactor dynamics by sotomayor's theorem. *Annals of Nuclear Energy*, *94*, 716–731.

Ruan, S., & Wang, W. (2003). Dynamical behavior of an epidemic model with a nonlinear incidence rate. *Journal of differential equations*, *188*(1), 135–163.

Saifuddin, M., Biswas, S., Samanta, S., Sarkar, S., & Chattopadhyay, J. (2016). Complex dynamics of an eco-epidemiological model with different competition coefficients and weak allee in the predator. *Chaos, Solitons & Fractals*, *91*, 270–285.

Sieber, M., Malchow, H., & Hilker, F. M. (2014). Disease-induced modification of prey competition in eco-epidemiological models. *Ecological complexity*, *18*, 74–82.

Volterra, V. (1927). Fluctuations in the abundance of a species considered mathematically. *Nature*, *119*(2983), 12–13.

Wang, N., Zhao, M., Yu, H., Dai, C., Wang, B., & Wang, P. (2016). Bifurcation behavior analysis in a predator-prey model. *Discrete Dynamics in Nature and Society*, *2016*(1), 3565316.

Wayesa, N. N., Obsu, L. L., & Dawed, M. Y. (2024). Analysis of predator–prey model with inclusion of temperature variability in prey refugees. *Journal of Applied Mathematics*, *2024*(1), 5138320.

Wayesa, N. N., Obsu, L. L., & Dawed, M. Y. (2025). Predator–prey population dynamics with time delay and prey refuge effects. *Modeling Earth Systems and Environment*, *11*(2), 142.

Yu, X., Zhu, Z., Lai, L., & Chen, F. (2020). Stability and bifurcation analysis in a single-species stage structure system with michaelis–menten-type harvesting. *Advances in Difference Equations*, *2020*, 1–18.

Appendix A

let the Jacobian matrix the model(3) at the predator free equilibrium point $E^2(S^*, I^*, 0)$ denote by $J(E^2) = (\hat{A_{ij}})_{3\times3}$

$$J(E^2) = \begin{pmatrix} 1 - 2S^* - \kappa I^* - \dfrac{\gamma I^*}{1+\eta I^*} & -\kappa S^* - \dfrac{\gamma S^*}{(1+\eta I^*)^2} & -\theta_1\psi_S(S^*) \\ \dfrac{\gamma I^*}{1+\eta I^*} & \dfrac{\gamma S^*}{(1+\eta I^*)^2} - \zeta & -\theta_2\psi_I(I^*) \\ 0 & 0 & \psi_S(S^*) + \psi_I(I^*) - \xi \end{pmatrix}.$$

From the condition at which $J(E^2)$ has zero eigenvalue, that is, $\lambda_1 = \sigma_3 = \psi_S(S^*) + \psi_I(I^*) - \xi = 0$ the bifurcation value is

$$\hat{\xi} = \psi_S(S^*) + \psi_I(I^*).$$

Now we compute the Jacobian matrix $\hat{J}(E^2) = (\hat{A_{ij}})_{3\times3}$ at $\xi = \hat{\xi}$ which is same as above $J(E^2)$ except $\hat{A_{33}} = 0$. The eigenvectors of $\hat{J}(E^2, \hat{\xi})$ and $\hat{J}^T(E^2, \hat{\xi})$, corresponding to the zero eigenvalue are, respectively

$$V = \begin{pmatrix} \Psi_1\mathbf{e} \\ \mathbf{e} \\ \Psi_2\mathbf{e} \end{pmatrix} = \begin{pmatrix} V_1 \\ V_2 \\ V_3 \end{pmatrix} \text{ and } W = \begin{pmatrix} 0 \\ 0 \\ \mathbf{f} \end{pmatrix}$$

where, $\Psi_1 = \dfrac{\hat{A_{12}}\hat{A_{23}} - \hat{A_{22}}\hat{A_{13}}}{\hat{A_{21}}\hat{A_{13}} - \hat{A_{11}}\hat{A_{23}}}$, $\Psi_2 = \dfrac{\hat{A_{11}}\hat{A_{22}} - \hat{A_{12}}\hat{A_{21}}}{\hat{A_{21}}\hat{A_{13}} - \hat{A_{11}}\hat{A_{23}}}$, moreover $\mathbf{e}$ and $\mathbf{f}$ are nonzero real numbers. From our model system (3), we have:

$$F_\xi(X, \xi) = \begin{pmatrix} 0 \\ 0 \\ -P \end{pmatrix} \Longrightarrow F_\xi(E^2, \hat{\xi}) = \begin{pmatrix} 0 \\ 0 \\ 0 \end{pmatrix}$$

Thus, $W^T F_\xi(E^2, \hat{\xi}) = 0$. Applying Sotomayor's theorem (Pirayesh et al., 2016) for local bifurcation, the saddle node bifurcation does not occur near to the equilibrium point $E^2(S^*, I^*, 0)$. For Bogdanov– Takens bifurcation, there must be two equilibria : saddle and non-saddle. Therefore, BT bifurcation cannot appear here also.
We noted that the first condition $W^T F_\xi(E^2, \hat{\xi}) = 0$ of Sotomayor's theorem for the existence of transcritical bifurcation is satisfied. Now,

$$DF_\xi(E^2, \hat{\xi}) = \begin{pmatrix} 0 & 0 & 0 \\ 0 & 0 & 0 \\ 0 & 0 & -1 \end{pmatrix} \Longrightarrow DF_\xi(E^2, \hat{\xi})V = \begin{pmatrix} 0 & 0 & 0 \\ 0 & 0 & 0 \\ 0 & 0 & -1 \end{pmatrix} \begin{pmatrix} \Psi_1\mathbf{e} \\ \mathbf{e} \\ \Psi_2\mathbf{e} \end{pmatrix} = \begin{pmatrix} 0 \\ 0 \\ -\Psi_2\mathbf{e} \end{pmatrix}$$

So, we have $W^T[DF_\xi(E^2, \hat{\xi})V] = -\Psi_2\mathbf{ef} \neq 0$. Moreover,

$$D^2F(E^2, \hat{\xi})(V, V) = \begin{pmatrix} -2V_1^2 + \dfrac{2\gamma\eta S^*}{(1+\eta I^*)^3}V_2^2 - 2\left(\left(\kappa + \dfrac{\gamma}{(1+\eta I^*)^2}\right)V_1V_2 + \theta_1\psi_S'(S^*)V_3V_2\right) \\ \dfrac{-2\gamma\eta S^*}{(1+\eta I^*)^3}V_2^2 + 2\left(\dfrac{\gamma}{(1+\eta I^*)^2}V_1V_2 - \theta_2\psi_I'(I^*)V_2V_3\right) \\ 2V_3(\psi_S'(S^*)V_1 + \psi_I'(I^*)V_2) \end{pmatrix}$$

Thus, we have $W^T[D^2F(E^2, \hat{\xi})(V, V)] = 2V_3\mathbf{f}(\psi_S'(S^*)V_1 + \psi_I'(I^*)V_2) \neq 0$. Therefore, by Sotomayor's theorem, transcritical bifurcation occurs near to the predator-free stationary point $E^2(S^*, I^*, 0)$.

Appendix B

The Jacobian matrix of the system (3) at the infection free equilibrium point $E^3(S^*, 0, P^*)$ denote by $J(E^3) = (\overline{D_{ij}})_{3\times3}$ as

$$J(E^3) = \begin{pmatrix} 1 - 2S^* - \theta_1\psi_S'(S^*)P^* & -\kappa S^* - \gamma S^* & -\theta_1\psi_S(S^*) \\ 0 & \gamma S^* - \zeta - \theta_2\psi_I'(0)P^* & 0 \\ \psi_S'(S^*)P^* & \psi_I'(0)P^* & \psi_S(S^*) - \xi \end{pmatrix}.$$

Thus, $J(E^3)$ has zero eigenvalue, while, $\lambda_1 = \nabla_2 = \gamma_2 S^* - \zeta - \theta_2\psi_I'(0)P^* = 0$. and the model bifurcate when

$$\zeta^{[0]} = \frac{\theta_1\xi\gamma S^* - \theta_2\psi_I'(0)S^*(1 - S^*)}{\theta_1\xi}.$$

To perform the Jacobian matrix $J^{[0]}(E^3) = (D_{ij})_{3\times3}$ at $\zeta = \zeta^{[0]}$ which is same as above $J(E^3)$ except $D_{22} = 0$. The eigenvectors of $J^{[0]}(E^3, \zeta^{[0]})$ and $(J^{[0]}(E^3, \zeta^{[0]}))^T$, corresponding to the zero eigenvalue are, respectively

$$V = \begin{pmatrix} \Upsilon \\ \dfrac{D_{13}D_{31} - D_{11}D_{33}}{D_{12}D_{33} - D_{32}D_{13}}\Upsilon \\ \dfrac{D_{11}D_{32} - D_{12}D_{13}}{D_{12}D_{33} - D_{32}D_{13})}\Upsilon \end{pmatrix} = \begin{pmatrix} V_1 \\ V_2 \\ V_3 \end{pmatrix} \text{ and } W = \begin{pmatrix} 0 \\ \Gamma \\ 0 \end{pmatrix}$$

where,Υ and Γ are nonzero real numbers. From our model system (3), use derivative we get:

$$F_\zeta(X, \zeta) = \begin{pmatrix} 0 \\ -I \\ 0 \end{pmatrix} \Longrightarrow F_\zeta(E^3, \zeta^{[0]}) = \begin{pmatrix} 0 \\ 0 \\ 0 \end{pmatrix}$$

Thus, applying Sotomayor's theorem first condition $W^T F_\zeta(E^3, \zeta^{[0]}) = 0$. Hence, the dynamical system (3) saddle node bifurcation does not demonstrate at the disease free equilibrium point $E^3(S^*, 0, P^*)$.
Now we try to perform the other conditions of Sotomayor's theorem for the existence of transcritical bifurcation. Thus,

$$DF_\zeta(X, \zeta) = \begin{pmatrix} 0 & 0 & 0 \\ 0 & -1 & 0 \\ 0 & 0 & 0 \end{pmatrix}$$

$$\Longrightarrow DF_\zeta(E^3, \zeta^{[0]})V = \begin{pmatrix} 0 & 0 & 0 \\ 0 & -1 & 0 \\ 0 & 0 & 0 \end{pmatrix} \begin{pmatrix} \Upsilon \\ \dfrac{D_{13}D_{31} - D_{11}D_{33}}{D_{12}D_{33} - D_{32}D_{13}}\Upsilon \\ \dfrac{D_{11}D_{32} - D_{12}D_{13}}{D_{12}D_{33} - D_{32}D_{13})}\Upsilon \end{pmatrix} = \begin{pmatrix} 0 \\ \dfrac{D_{11}D_{33} - D_{13}D_{31}}{D_{12}D_{33} - D_{32}D_{13}}\Upsilon \\ 0 \end{pmatrix}$$

Hence, we arrived that $W^T[DF_\zeta(E^3, \zeta^{[0]})V] = \dfrac{D_{11}D_{33} - D_{13}D_{31}}{D_{12}D_{33} - D_{32}D_{13}}\Upsilon\Gamma \neq 0$. In addition,

$$D^2F(E^3, \zeta^{[0]})(V, V) = \begin{pmatrix} (-2 - \theta_1\psi_S''(S^*)P^*)V_1^2 + 2\gamma\eta S^* V_2^2 - 2\left((\kappa + \gamma 1)V_1V_2 + \theta_1\psi_S'(S^*)V_3V_2\right) \\ (-2\gamma\eta S^* - \theta_2\psi_I''(0)P^*)V_2^2 + 2(\gamma V_1V_2 - \theta_2\psi_I'(0)V_2V_3) \\ \psi_S''(S^*)P^*V_1^2 + \psi_I''(0)P^*V_2^2 + 2V_3(\psi_S'(S^*)V_1 + \psi_I'(0)V_2) \end{pmatrix}$$

Thus, we have

$$W^T[D^2F(E^3, \zeta^{[0]})(V, V)] = -(2\gamma\eta S^* + \theta_2\psi_I''(0)P^*)V_2^2\Upsilon + 2(\gamma V_1V_2\Upsilon - \theta_2\psi_I'(0)V_2V_3)\Upsilon \neq 0.$$

Therefore, according to Sotomayor's theorem (Pirayesh et al., 2016), our dynamical system (3) experience transcritical bifurcation at the disease-free fixed point $E^3(S^*, 0, P^*)$.

East African Journal of Biophysical and Computational Sciences
ISSN (Online): 2789-3618 and ISSN (Print): 2789-360X

ARTICLE

Computational Study of MHD Blood Flow through Bifurcated Artery Using Caputo-Fabrizio Fractional Derivative, Thermal Radiation, and Magnetic Field for Tumor Therapies

ARTICLE INFO
Volume 7(1), 2026
https://dx.doi.org/10.4314/eajbcs.v7i1.2S

ARTICLE HISTORY
Received: March 10, 2026
Accepted: 23 May, 2026
Published Online: 10 June, 2026

CITATION
Abdullahi et.al (2026). Computational Study of MHD Blood Flow through Bifurcated Artery Using Caputo-Fabrizio Fractional Derivative, Thermal Radiation, and Magnetic Field for Tumor Therapies. *East African Journal of Biophysical and Computational Sciences* Volume 7(1), 2026. .https://dx.doi.org/10.4314/eajbcs.v7i1.2S.18-26

OPEN ACCESS

Isah Abdullahi[1], Dauda Gulibur Yakubu[1,*], Muhammad Shamsuddeen Dauda[2], Mahmood Abdulhameed[3],Saidu Abubakar Kadas[4],Mohammed Abdulhameed[5], and Garba Tahiru Adamu[6]

[1]Department of Mathematical Sciences, Abubakar Tafawa Balewa University, Bauchi, Nigeria
[2]Department of Biological Sciences, Abubakar Tafawa Balewa University, Bauchi, Nigeria
[3]Department of Electrical Electronic Engineering, Abubakar Tafawa Balewa University, Bauchi, Nigeria
[4]Department of Obstetrics Gynaecology, ATBU, Teaching Hospital, Bauchi, Nigeria
[5]School of Science and Technology, The Federal Polytechnic Bauchi, Nigeria
[6]Department of Mathematical Sciences, Bauchi State University, Gadau, Bauchi, Nigeria

*Corresponding author: dgyakubu@atbu.edu.ng

Abstract

This study investigates the impact of heat sources, thermal radiation, and chemical reactions on the magnetohydrodynamic blood flow through a bifurcated artery in the presence of a slanted magnetic field. Using Laplace transform and the method of undetermined coefficients, the constitutive equations for the mathematical model of Caputo-Fabrizio fractional derivative order were solved. Blood flow velocity, temperature distribution, and concentration were found to have analytical expressions. The effects of certain physical parameters on blood velocity, temperature and concentration are graphically represented, and these representations accurately depict the flow disturbances. We discovered that the bifurcation apex of the artery with a symmetrical divider has steady blood flow. This may lead to significant shear stresses on either side of the bifurcation. Near the apex, when the flow is substantially different, obstruction may result from the formation of boundary layers on the inner walls of the bifurcation. Sluggish flow also occurred along the outer walls of the bifurcation. It has also been discovered that the temperature distribution, concentration, and arterial blood flow velocity are significantly influenced by the fractional order parameter, the slanted magnetic fields, the heat source, and the chemical reaction parameter. This study offers significant benefits for medical applications in biomechanical engineering, biomedical engineering, and medicine.

Keywords: Chemical reaction; Heat source; MHD Blood flow; Slanted magnetic field; Thermal radiation

1 Introduction

Bio-magnetic fluid dynamics (BFD), which is the study of bio-fluid flow in the presence of magnetic field, is a rapidly developing subject of study in fluid mechanics (Tzirtzilakis, 2005). This field of study is of tremendous importance to the field of medical science and has the possibility to be utilized in a diversity of domains, including the delivery of medications via the utilization of magnetized particles, the management of severe bleeding, and the assistance in dealing with malignant cancers (Shit & Majee, 2015). Understanding many facets (aspects) of the medical sciences, such as homeostasis, treating cancerous tumors, and administering medication using magnetic particles, depends on the study of biomagnetic fluid dynamics (Shaw & Murthy, 2010). Blood's hemoglobin molecules are regarded as biomagnetic fluids with magnetic properties. Blood can also be considered as a Newtonian fluid if it flows through the bigger arteries at a high shear rate. These arteries are thought to be homogenous whose flow behavior can be described by a Newtonian model (see, Caro et al., 2011; MacDonald, 1979). Numerous researchers have looked into various possibilities for studying physiological fluids

using porous media (see, Bhatti & Lu, 2019; Dash et al., 1996; Ramesh & Devakar, 2015; Shit & Roy, 2015) developed blood flow model via porous medium. Based on Darcy's law, Bhargava et al. (2007) and Ghasemi et al. (2015) investigated the pulsatile flow and mass transfer of an electrically conducting Newtonian bio-fluid via a channel comprising porous media using blood as the porous medium fluid. Bhatti et al. (2018) developed a mathematical model to investigate heat transfer, mass transfer, and blood flow in a porous medium channel while accounting for the integrated Darcy-Brinkman-Forchheimer model. Blood behaves non-Newtonian even in larger arteries at low shear rates, as demonstrated by Liepsch (1986). When blood flows through arteries at a low shear rate, it can be treated as Cassons fluid (Srivastava & Srivastava, 1984). Many researches have supported the Casson fluid model for blood flow via tiny arteries at low shear rates (see,Hayat et al., 2016; Nagarani et al., 2006; Venkatesan et al., 2013). Many authors (see, Abdulhameed et al., 2017; Misra & Shit, 2009; Mondal & Shit, 2017; Yakubu et al., 2020; Zeeshan et al., 2017) have regarded blood as a non-Newtonian fluid, because of its electrical conductivity, displays magneto hydrodynamic behavior.

Many authors considered the examination of the heat and mass transfer occurrences generated from these processes to be a highly relevant element with respect to modeling physiological processes (Prasad et al., 2025) and industrial processes (Sademaki et al., 2026). Electromagnetohydrodynamics is the study of fluids whose motion is constantly affected by externally applied magnetic field and electric field. In order to comprehend the impact of magnetohydrodynamic (MHD) and electrohydrodynamic (EHD) forces on the flow of normal fluids, including blood, several studies have mostly concentrated on the theoretical, computational, and experimental aspects of these forces. Cell-based therapies, medication delivery, and biological processes are just a few of the fields where the application of (EHD) has shown notable advancement. Additional force components, primarily the Lorentz and Coulomb forces, are incorporated into momentum equations and have a direct effect on fluid velocity. Magnetohydrodynamics or MHD has been used in a wide variety of biomedical applications (Vardanyan, 1973).

The heat transmission and magnetohydrodynamic (MHD) blood flow in a restricted artery were studied by Majee and Shit (2017). Akbar and Butt (2017) considered ferromagnetic blood flow in a restricted, smaller artery with a porous wall. The radiant heat transfer that takes place in the blood vessels must also be considered while treating hyperthermia. Oncology professionals are familiar with the medical practice of using heat therapy to cancer patients. Chinyoka and Makinde (2014) investigated the effects of magnetic fields and heat radiation on arterial blood flow. Sinha and Shit (2015) investigated the magnetic hydrodynamic blood flow in the presence of thermal radiation. Tabi et al. (2017) studied the combined effects of magnetic fields and external radiation on blood flow in the major blood arteries. Yakubu et al. (2022) examined blood flow of Oldroyd-B fluids in order to investigate the erratic flow, with magnetic field applied perpendicular to the flow direction. Heat transfer processes were studied in the peristaltic flow of blood with variable viscosity particle-liquid suspensions by Bhatti et al. (2016). Blood flow is greatly affected when the human body is exposed to a vibratory environment, as occurs when operating machines or traveling in spacecraft. When the human body undergoes body acceleration, a number of health problems might arise, such as an elevated heart rate and vision loss. In the study of the impact of body acceleration, a number of researches have produced mathematical simulations of oscillatory blood flow (see, Chaturani & Palanisamy, 1990; Ghasemi et al., 2016; Sud & Sekhon, 1984). Bhatti and Lu (2019) investigated the propagation of a hydro elastic single wave in a channel with uniform flow. Blood flow characteristics have been discovered to promote blood velocity in a vibratory environment using fractional order derivative differential equation problems. Fractional differential equations are the most used method for modeling natural phenomena. This is due to the fact that equations offer the possibility for a system to either retain memory or to be hereditary with the properties of its history, similar to how dynamic systems work (Syed et al., 2026).

Fractional order derivatives have been applied in many fields of study, including the complicated dynamics and rheological properties of different kinds of fluids. The behavior of fluid flow is well depicted by substituting fractional-order derivatives for the ordinary time derivative in the constitutive equations (see, Atangana and Baleanu, 2016; Caputo and Fabrizio, 2015; Samko et al., 1993). The concept of fractional calculus was initially proposed by L'Hôpital in 1695, more than four centuries ago. Therefore, it wasn't until the last few decades that a significant number of scholars started to highlight the fact that differential equations and fractional derivatives have numerous applications in a variety of domains (see, Abdulhameed et al., 2023; Imoro et al., 2024). These days, fractional derivative order differential equation problems are the most effective and successful ways to model the nonlinear processes that emerge in many domains of applied study, including biology, chemistry, ecology, engineering, and many other application areas. Several mathematical models have shown that they offer a more realistic depiction of the phenomenon under research. Examples of these models include those employed in biomedical engineering, viscoelastic mechanics, boundary layers, electromagnetic, and porous media. Bansi et al. (2018) investigated a fractional blood flow model in the oscillatory artery with magnetic field and heat radiation effects. With the aid of fractional time derivative, (Yakubu et al., 2021) examined the effects of pressure gradient, body acceleration, and magnetic field on blood flow through artery. The effects of blood flow parameters, Caputo's time fractional derivatives, and the external magnetic field on the cylindrical domain were studied by (Shah et al., 2016). Ali et al. (2017) solved a fractional order model for Cassons fluid flow using the Hankel transform and Laplace transform techniques to determine the exact solutions. He and collaborators (2019) used the fractional order Caputo derivative to investigate the complexity of blood in arteries under various forces. In the field of medicine, magneto hydrodynamic flow plays a crucial role. It is considered for the reduction of bleeding from wounds and for the treatment of malignant tumors. Kumar et al. (2021) employed a chemical reaction, heat source, and inclined magnetic field to cure malignancies.

The fractional order time derivative of MHD blood flow via a bifurcated artery in the presence of a slanted magnetic field, as well as the coupling impact of heat transfer and blood flow concentration, are described here using Newtonian fluid. The goal is to investigate how magneto-hydrodynamic blood flow through a bifurcated artery is affected by thermal radiation and a slanted magnetic field during tumor treatments. The Laplace transform and the indeterminate coefficients approach were used to find the exact solutions, which were then simulated to produce graphical outputs and the implications of several important parameters on the outcomes were explored. The study was motivated by the fact that there is currently very little information available on the flow in arterial bifurcation since the phenomena is currently not stringent to mathematical analysis or precise experimental measurement. The present investigation shows that the vast number of variables involved are the main challenge in both situations.

2 Methods

2.1 Physical Structure and Mathematical formulation

Blood considered in this study, is Newtonian, incompressible, homogeneous, sticky fluid that flows from the trunk to the branches. A mass stream's rate at any cross-section that is perpendicular to its direction is equal to $m = 2bv$, where b is the stream's radius and v is its mean speed. The mass stream's speed at any cross section of the extended channel is equal to $m/2$, and the bifurcating divider (internal apical curve) has no effect on this (see Figure 1). The magnetic field is applied to the flow at an angle (ϕ) since the evaluated magnetic Reynolds number is low. Therefore, it is believed that the magnetic and electric fields produced by blood flow are insignificant, the angle of bifurcation is set to zero ($\Theta = 0$), that is, the blood flow region is bifurcated into two streams that flow parallel to the principal artery (the trunk). Figure 2 demonstrates the smooth muscle fibers of the three concentric layers that make up the walls of a typical elastic artery. These fibers are controlled by the sympathetic nervous system to contract or relax.

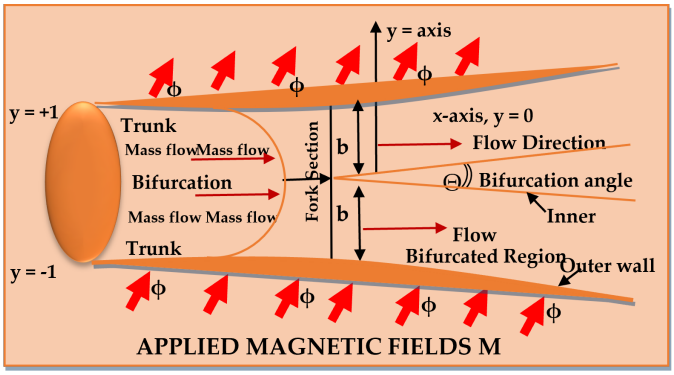

Figure 1: Physical flow diagram of the bifurcated artery with zero angle of bifurcation

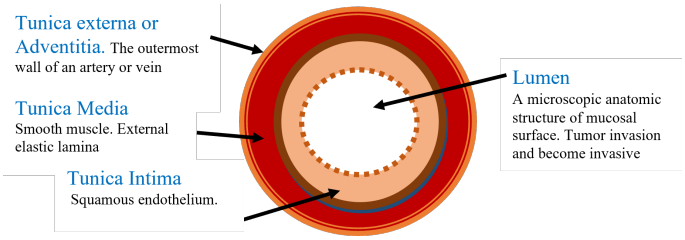

Figure 2: The structure of an artery walls (Transverse section through an artery)

2.2 Fundamental flow equations and their solutions

Blood flows through a porous media as two-limit layers when it is subjected to magnetic fields and heat, with the assumptions made in the numerical definition guiding its movement. In the stream field headings of x and y at time t , let u and v be the speed parts, η and ρ denote blood density and thickness, respectively. Blood pressure is represented by p , warm conductivity (K_T), C_p is the specific heat capacity at steady strain, hotness is represented by Q , temperature is represented by T , the volumetric development boundary is represented by β , the angle of the slanted (inclined) magnetic field is represented by ϕ, and porosity parameter is represented by K . With these, we have the equations provided by (see, Ali et al., 2017; He et al., 2019; Kumar et al., 2021), with some additional terms as follows:

$$\frac{\partial \overline{u}}{\partial \overline{t}} + \frac{1}{\rho}\frac{\partial \overline{p}}{\partial \overline{x}} = \frac{\eta}{\rho}\frac{\partial^2 \overline{u}}{\partial \overline{y}^2} + g\beta(T - T_\infty) + g\beta'(C - C_\infty) - \frac{c\mathcal{B}_\alpha^2 \sin^2\phi}{\rho}\overline{v} - \frac{\overline{v}}{\overline{k}} \tag{1}$$

$$\frac{\partial \overline{T}}{\partial \overline{t}} = \frac{\bar{k}_T}{\rho C_o}\frac{\partial^2 \overline{T}}{\partial \overline{y}^2} + \frac{Q}{\rho C_o}(T - T_o) - \frac{\partial \overline{q}}{\partial \overline{y}} \tag{2}$$

$$\frac{\partial \overline{u}}{\partial \overline{x}} + \frac{\partial \overline{v}}{\partial \overline{y}} = 0 \tag{3}$$

where, $\frac{\partial}{\partial \bar{t}}$ is the material time derivative. On the other hand, the dimensionless concentration equation for medication (concentration) delivery in magneto hydrodynamic blood flow through permeable bifurcated artery is provided by,

$$\frac{\partial \overline{C}}{\partial \overline{f}} = D\frac{\partial^2 \overline{C}}{\partial \overline{y}^2} + G \tag{4}$$

where D is the diffusion coefficient and $G = -k_1(C - C_\infty)$ represents chemical reaction rate in the fluid flow. It is important to mention that the effect of an electric field in the concentration equation was also ignored.

$$\begin{aligned} \theta = \ell^{-\bar{z}_1}, \quad u = \ell^{-\bar{z}_1}, \quad v = \ell^{-\bar{z}_1}, \quad C = \ell^{-\bar{z}_1} \quad \text{at } y = -1, \\ \text{and } \theta \to 0, \quad u \to 0, \quad v \to 0, \quad C \to 0 \quad \text{at } y = 1. \end{aligned} \tag{5}$$

However, by using the proper normalizing factors, the governing equations (1)–(4) can be converted to dimensionless form. We present the non-dimensional parameters as follows:

$$x = \frac{\bar{x}}{b}, y = \frac{\bar{y}}{b}, u = \frac{\bar{u}}{mu_{HS}/2b\rho}, \quad v = \frac{\bar{v}}{mu_{HS}/2b\rho}, h(x,t) = \frac{d\bar{p}/d\bar{x}}{u_{HS}\eta m/2b^3\rho}$$

$$\text{k}=\frac{\bar{k}}{(b^2\rho/\eta)}, C = \frac{\bar{C}\left(2b^3\rho^2\right)}{m\eta u_{HS}}, \theta = \frac{\bar{\theta}\left(2b^3\rho^2\right)}{m\eta u_{HS}}, \tau = \frac{\eta}{\rho}, \quad t = \frac{\bar{t}}{(b^2\rho/\eta)},$$

and

$$\bar{q} = \frac{-16\delta T_0^3}{3k'}\frac{\partial \bar{T}}{\partial \bar{y}} \tag{6}$$

Applying (5) and (6) to eqns. (1)- (4) and removing the bars we obtain:

$$\frac{\partial u}{\partial t} + h = \frac{\partial^2 u}{\partial y^2} + g\beta\theta + g\beta' C - M^2\sin^2\phi - \frac{u}{k} \tag{7}$$

$$\frac{\partial \theta}{\partial t} = \left(\frac{1}{\tau p_r} + R\right)\frac{\partial^2 \theta}{\partial y^2} + \left(\frac{S}{\tau p_r}\right)\theta \tag{8}$$

$$\frac{\partial u}{\partial x} + \frac{\partial v}{\partial y} = 0 \tag{9}$$

$$\frac{\partial C}{\partial t} = \frac{1}{S_C}\frac{\partial^2 C}{\partial y^2} - \omega C \tag{10}$$

where

$$M^2 = \frac{\sigma B_0^2}{\rho}, \; p_r = \frac{\rho C_\rho}{k_T}, \; R = \frac{16\delta T_0^3}{3k'\tau}, \; S = \frac{Qb^2}{k_T}, \; S_C = \frac{\tau}{bD}, \; \omega = \frac{k_1 b^2}{\tau}$$

are the magnetic field parameter, Prandtl number, thermal radiation parameter, heat source parameter, Schmidt number, chemical reaction parameter and θ is the temperature conveyance. Now, using the Caputo-Fabrizio fractional derivative as stated in (Caputo and Fabrizio 2015), we consider the time fractional momentum equations as:

$$^{CF}D_t^\alpha u(y,t) = \frac{1}{1-\alpha}\int_0^t \frac{\partial u(y,\tau)}{\partial \tau}\exp\left(-\frac{\alpha(t-\tau)}{1-\alpha}\right)d\tau, \quad 0 < \alpha < 1$$

$$L\left\{^{CF}D_t^\alpha u(y,t)\right\} = \frac{su(y,s) - u(y,0)}{(1-\alpha)s + \alpha} \tag{11}$$

$$u(y,0) = \tag{12}$$

The Caputo-Fabrizio derivative corresponding to equations (7), (8) and (10) are as follows:

$$ {}^{CF}D_t^{\alpha}u(y,t) + h = \frac{\partial^2 u}{\partial y^2} + g\beta\theta + g\beta' C - M^2 \sin^2\phi - \frac{u}{k} \tag{13} $$

$$ {}^{CF}D_t^{\alpha}\theta(y,t) = \left(\frac{1}{\tau p_r} + R\right)\frac{\partial^2\theta}{\partial y^2} + (\frac{S}{\tau p_r})\theta \tag{14} $$

$$ {}^{CF}D_t^{\alpha}C\,(y,t) = \frac{\partial C}{\partial t} = \frac{1}{S_C}\frac{\partial^2 C}{\partial y^2} - \omega C. \tag{15} $$

Applying Laplace transform to equations (13)-to-(15), and using the boundary condition in equation (12) we have;

$$ \frac{su(y,s)}{(1-\alpha)s+\alpha} + h = \frac{\partial^2\bar{u}}{\partial\bar{y}^2} + g\beta\bar{\theta} + g\beta'\bar{C} - M^2\sin^2\phi - \frac{\bar{u}}{k} \tag{16} $$

$$ \frac{su(y,s)}{(1-\alpha)s+\alpha} = \left(\frac{1}{\tau p_r} + R\right)\frac{\partial^2\bar{\theta}}{\partial\bar{y}^2} + (\frac{S}{\tau p_r})\bar{\theta} \tag{17} $$

$$ \frac{su(y,s)}{(1-\alpha)s+\alpha} = \frac{1}{S_C}\frac{\partial^2\bar{C}}{\partial\bar{y}^2} - \omega\bar{C}. \tag{18} $$

2.3 Exact solutions

Here we assume the following as the arbitrary solutions of equations (9), (16), (17) and (18),

$$ \bar{u} = \bar{F}(y)\frac{1}{s+\lambda^2}, \tag{19} $$

$$ \bar{\theta} = \bar{H}(y)\frac{1}{s+\lambda^2}, \tag{20} $$

$$ \bar{v} = \bar{G}(y)\frac{1}{s+\lambda^2}, \tag{21} $$

$$ \bar{C} = \bar{I}(y)\frac{1}{s+\lambda^2}, \tag{22} $$

then the boundary conditions in eqns. (5) reduce to;

$$ \begin{aligned} H = 1, \quad I = 1, \quad F = 1, \quad \text{at } y = -1, \\ H \to 0, \quad I \to 0, \quad F \to 0, \quad \text{at } y = 1. \end{aligned} \tag{23} $$

As a result, the following are the simplified governing equations of motions with arbitrary solutions:

$$ \frac{d^2\bar{F}}{dy^2} - A_2\bar{F} = A_3 - g\beta\bar{H} - g\beta'\bar{I}, \tag{24} $$

$$ \frac{d^2\bar{H}}{dy^2} + A_6^2\bar{H} = 0, \tag{25} $$

$$ G = A_1\,(\text{constant}), \tag{26} $$

$$ \frac{d^2\bar{I}}{dy^2} - A_9^2\bar{I} = 0. \tag{27} $$

Equation (23)'s boundary conditions are used to solve equations (24) through (27) and the following solutions are obtained:

$$ \bar{H} = \left(\frac{\cos A_6\bar{y}}{2\cos A_6}\right) - \frac{\sin A_6\bar{y}}{2\sin A_6} \tag{28} $$

$$ \bar{I} = \frac{\cosh A_9\bar{y}}{2\cosh A_9} - \frac{\sinh A_9\bar{y}}{2\sinh A_9} \tag{29} $$

$$ F = \left\{ \begin{matrix} A_7 + A\cosh A_2 y + B\sinh A_2 y + A_8\cos A_6 y + A_9\sin A_6 y + \\ + A_{10}\cosh\Lambda y + A_{11}\sinh\Lambda y \end{matrix} \right\}. \tag{30} $$

We now have blood velocity in the axial direction, using equation (30) and equation (19) as

$$ \bar{u}(y,s) = \begin{pmatrix} A_7 + A\cosh A_2\bar{y} + B\sinh A_2\bar{y} + A_8\cos A_6\bar{y} + \\ A_9\sin A_6\bar{y} + A_{10}\cosh\Lambda\bar{y} + A_{11}\sinh\Lambda\bar{y} \end{pmatrix}\frac{1}{s+\lambda^2} \tag{31} $$

Equation (26) and equation (21) together provide the usual direction of blood velocity in the bifurcated artery, which is given by

$$ \bar{v}(y,s) = A_1\frac{1}{s+\lambda^2} \tag{32} $$

According to equations (28) and (20), the temperature distribution in the bifurcated artery is given as follows:

$$ \bar{\theta}(y,s) = \left(\left(\frac{\cos A_6\bar{y}}{2\cos A_6}\right) - \frac{\sin A_6\bar{y}}{2\sin A_6}\right)\frac{1}{s+\lambda^2} \tag{33} $$

Equations (22) and (29) provide the drug's concentration in the flowing blood in the carotid artery as follows:

$$ \bar{C}(y,s) = \left(\frac{\cosh A_9\bar{y}}{2\cosh A_9} - \frac{\sinh A_9\bar{y}}{2\sinh A_9}\right)\frac{1}{s+\lambda^2}. \tag{34} $$

Equations (31) through (34) yield the inverse Laplace transform. Using Mathcad software, we simulated the given solutions using Gaver-Stehfest's algorithm, and the results are shown graphically in the next section.

3 Results and Discussion

To get the flow information, we simulated the solutions of equations (31), (33), and (34) using Mathcad software. The influence of the fractional-parameter (α) on velocity, temperature and blood concentration are displayed graphically and discussed. Axial fluid velocity, temperature distribution, and concentration are explored as functions of several dimensionless factors, including: slanted (inclined) magnetic field parameter (M), radiation parameter (R), fractional parameter (α), heat source parameter (S), and Schmidt number (S_C). In all the dimensionless parameter calculations, we vary the value of the fractional parameter (α), but we maintain other values constant, such as, $t = 1$, $S_C = 0.5$, $\omega = 0.5$, $S = 1$, $P_r = 2$, $K = 2$, $R = 0.5$, $h = 0.5$, $\beta = 0.5$, $\phi = 30^{\circ}$.

3.1 Velocity Profile

Consequently, the magnetic field always has a greater influence on the blood velocity profile. The application of the magnetic field to the system, as shown in Figure 3, increases the Lorentz force, a resistive force that primarily restricts the flow of fluid Bunonyo and Ebiwareme (2023) and Vardanyan (1973). For fractional order ($\alpha = 0.4$), as the magnetic field parameter's strength increases, as seen in Figure 3(a), the blood velocity reduces sharply, whereas it declines gradually for ($\alpha = 1$) as shown in Figure 3b.

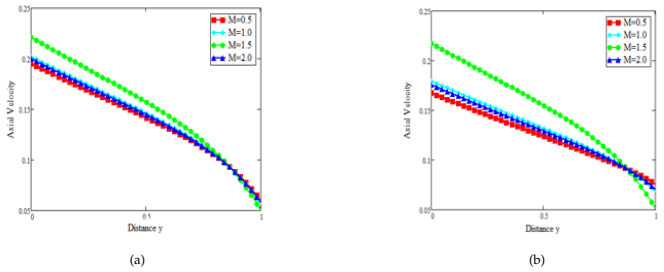

Figure 3: Axial velocity profile for different values of magnetic parameter: (a) $\alpha = 0.4$ (b) $\alpha = 1$, $\omega = 0.5$, $S = 1$, $P_r = 2$, $K = 2$, $R = 0.5$, $t = 1$, $h = 0.5$, $\beta = 0.5$, $\phi = 30°$, $Sc = 0.5$.

For therapeutic purposes and treatment procedures related to atherosclerosis, bone fractures, controlled tissue damage, and malignant tumors, to mention a few, a regulated magnetic field can therefore be a useful tool (Imoro et al., 2024). For both the fractional parameter ($\alpha = 0.4$) and the integer order model blood flow ($\alpha = 1$), Figure 4 shows the variation in blood flow at different heat source parameter (S) values. It is clear that an increase in the heat source has an impact on blood velocity and the fractional fluid parameter ($\alpha = 0.4$) (see Figure 4a). As seen in Figure 4b, the axial velocity does, however, drop symmetrically as the heat source parameter increases.

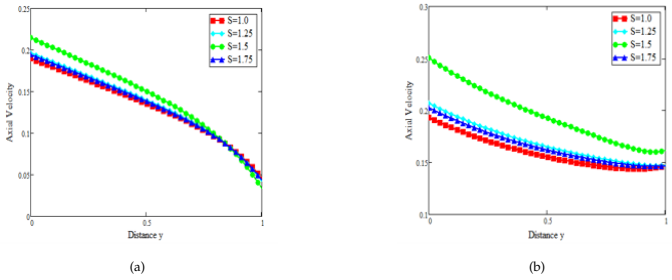

Figure 4: Profile of axial velocity for various heat source parameter: (a) $\alpha = 0.4$ (b) $\alpha = 1$, $\omega = 0.5$, $M = 0.5$, $P_r = 2$, $K = 2$, $R = 0.5$, $t = 1$, $h = 0.5$, $\beta = 0.5$, $\phi = 30°$, $Sc = 0.5$.

Figure 5 displays the velocity distribution based on different thermal radiation parameters (R). The blood velocity increases as the radiation parameter (R) increases, as indicated by both the fractional parameter ($\alpha = 0.4$) and the classical order parameter ($\alpha = 1$). Remarkably, comparable results for a related fluid model were discussed in Tabi et al. (2017). According to Yakubu et al. (2022), heat radiation possesses the capability to modify the effective viscosity of fluids, hence potentially causing an indirect influence on the velocity profile.

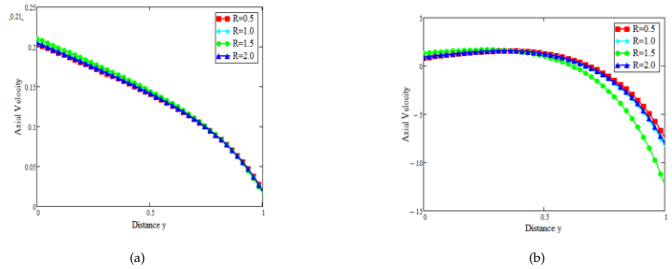

Figure 5: Profile of axial velocity for various heat source parameter: (a) $\alpha = 0.4$ (b) $\alpha = 1$, $\omega = 0.5$, $M = 0.5$, $P_r = 2$, $K = 2$, $R = 0.5$, $t = 1$, $h = 0.5$, $\beta = 0.5$, $\phi = 30°$, $Sc = 0.5$.

The applied magnetic field parameter for various tilted values is displayed in Figure 6. Blood flow is reduced over the affected area when the applied magnetic field's angle of inclination is increased for both the fractional order parameter and the classical order parameter ($\alpha = 1$). However, for the fractional order parameter in Figure 6a and 6b, the flow velocity vanishes between angles of (80° to 85°).

Because several of the related parameters' values have changed, the graphs in Figure 6c and 6d behave very differently from one another. Using Figure 6c as an example, $y = 0.004$, $p = 4$, and the fractional parameter ($\alpha = 0.2$), whereas Figure 6d also includes the fractional parameter ($\alpha = 0.4$) and $y = 0.004$, $p = 3$.

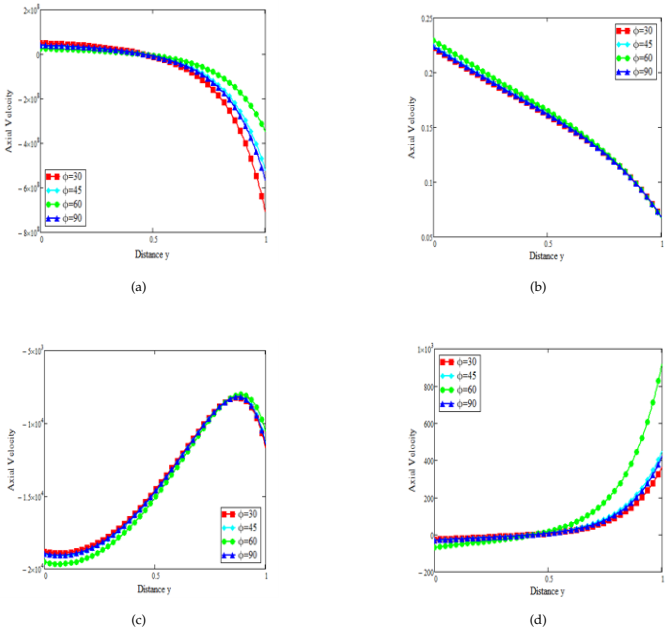

Figure 6: Axial velocity profile for various angles of inclination of the magnetic field: (a) $\alpha = 0.4$ (b) $\alpha = 1$ (c) $y = 0.004$, $p = 4$ and $\alpha = 0.2$ (d) $y = 0.004$, $p = 3$, $\alpha = 0.4$, $\omega = 0.5$, $S = 1$, $P_r = 2$, $K = 2$, $M = 0.5$, $t = 1$, $h = 0.5$, $\beta = 0.5$, $\phi = 30°$, $Sc = 0.5$.

The blood flow velocity profile at two independent times, $t = 0.01$ and 0.5, is shown in Figure 7 with five different values of the fractional parameter ($\alpha = 0.2$, 0.4, 0.6, 0.8, and 1). It has been observed that the fractional parameter (α) plays a critical role in regulating blood velocity. The fractional derivative fluid velocity initially moves faster than the integer order fluid model when the time is relatively small ($t = 0.01$). However, for a longer period of time ($t = 0.5$), the reverse behavior is seen, that is, fluids with integer order have a faster velocity than those with fractional order parameters. Naturally, this results from the system's stability, which can improve over longer timescales. For both fractional order derivative fluid models and integer order derivative fluid models, it is often observed that blood velocity increases with increasing time t. Figure 7a shows the evolution of the primary velocity profile, showing how the flow develops into fully formed Poiseuille flow, which is distinguished by the typical parabolic profile. Figure 7b clearly depicts the velocity profile at the fork section for various values of the fractional parameter. It is significant to note that when ($\alpha = 1$), a zone of sluggish flow appears along the outside wall and gets worse as time goes on, as was previously observed by Gade et al. (2026).

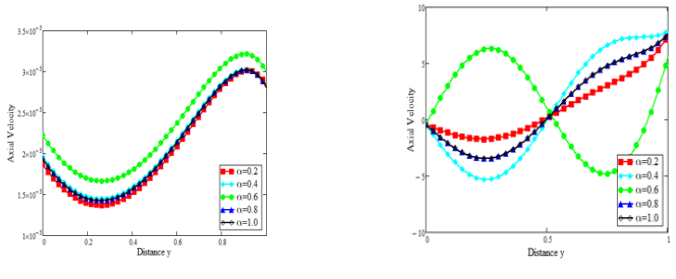

Figure 7: Axial velocity profile for different values of α at: (a) $t = 0.01$ (b) $t = 0.5$ $\omega = 0.5$, $S = 1$, $P_r = 2$, $K = 2$, $M = 0.5$, $t = 1$, $h = 0.5$, $\beta = 0.5$, $\phi = 30°$, $Sc = 0.5$

3.2 Temperature profile

Temperature profiles for different radiation parameters (R), fractional parameters , and heat source parameters (S) are shown in Figures 8–??. The temperature change for different values of the radiation parameter R, as shown in Figure 8. It is evident that when the thermal radiation increases, temperature increases for both fractional and integer order derivatives. The temperature varies near the center line for both the integer order and the fractional order derivative, as shown in Figure 8a and 8b. Consequently, it is more visible in the graphs of Figure 8b.

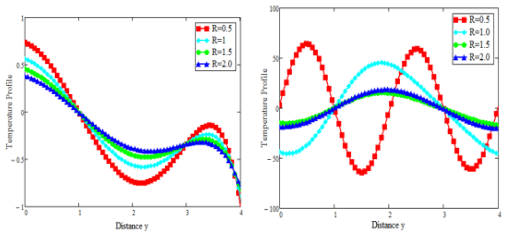

Figure 8: Temperature profile for different values of radiation parameter: (a) $\alpha = 0.4$ (b) $\alpha = 1$, $\omega = 0.5$, $S = 1$, $P_r = 2$, $K = 2$, $M = 0.5$, $t = 1$, $h = 0.5$, $\beta = 0.5$, $\phi = 30°$, $Sc = 0.5$

During hyperthermia, the temperature distribution is very important. It is commonly recognized that hyperthermia results from a breakdown in thermoregulation, which takes place when the body absorbs heat from outside sources like radiation or a body temperature that is being generated or absorbed. When a person has hyperthermia, the blood's internal temperature increases without damaging the tissues around the blood vessel. We have not taken into account the temperature exchange at the artery wall to account for this, meaning that the wall's temperature is zero. In light of this, the blood temperature in the current model is low at the artery wall and high at the midline for classical fluid. Numerous theoretical and experimental studies for Newtonian and non-Newtonian fluids of integer order reported similar phenomena, for example in (Ramesh & Devakar, 2015). Similar to radiation, the heat source (S) another crucial factor, has a large impact on the bloodstream's temperature distribution. More mitochondria per cell increase the thermal activity involved with the heat production process, as seen in Figure 9, which raises the system's temperature. The heat source improves the temperature distribution and supplies more heat to the blood flow system even though the wall temperature must remain zero in order to meet the boundary conditions. The temperature distribution at the channel walls, which decreases and becomes more flattened toward the channel's center line when the heat source is increased as shown in Figure 9a, which is amplified to maintain a constant flow rate, as seen in Figure 9a

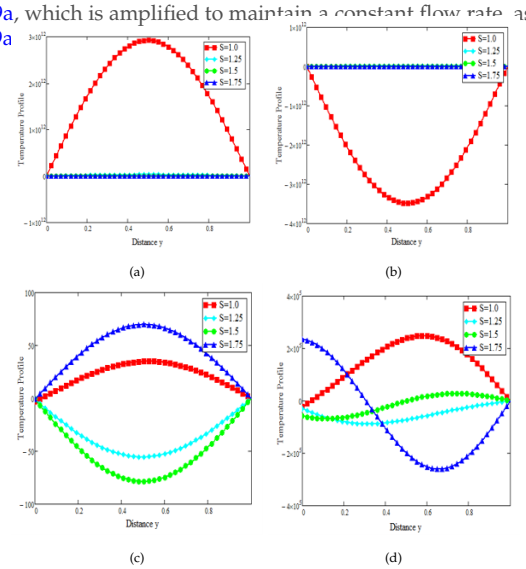

Figure 9: Temperature profile for different values of heat source parameter: (a) $\alpha = 0.4$ (b) $\alpha = 1$, $\omega = 0.5$, $R = 0.5$, $P_r = 2$, $K = 2$, $M = 0.5$, $t = 1$, $h = 0.5$, $\beta = 0.5$, $\phi = 30°$, $Sc = 0.5$

It's noteworthy to see in Figure 9b that the temperature at the middle line of the channel decreases as the heat source's values rise. The temperature exhibits oscillating behavior for different amounts of the heat source in Figures 9c and 9d. As the values of the heat source rise, the temperature is maximum at the center, decreases, and finally approaches zero at the artery walls. The different values of the fractional parameter really cause a shift in the temperature distribution, as shown in Figure 10. It illustrates how temperature increases with increasing fractional parameter . This implies that the fractional order fluid model's temperature distribution is more faster and higher over a longer period of time, which is what causes the variation shown in Figures 10a and 10b, as mentioned earlier. The temperature gradually decreases toward the artery's axis in Figures 10c and 10d, eventually tending to align with the axis.

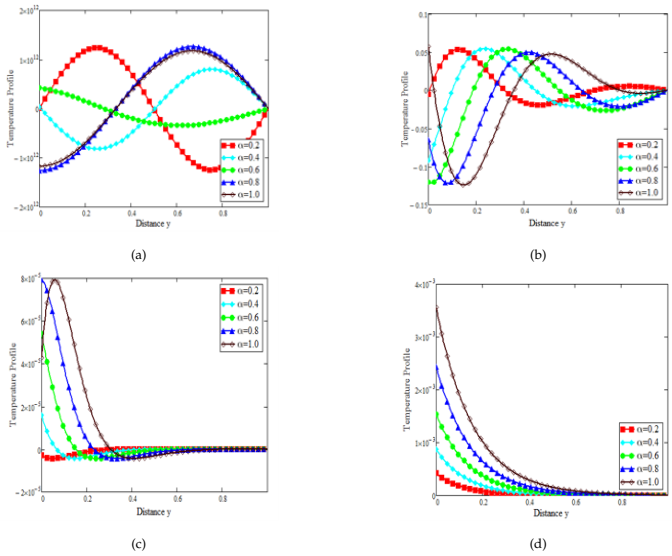

Figure 10: Temperature profile for different values of α at: (a) $t = 0.05$, $y = 0.004$, $p = 1$ and $\alpha = 1$, $t = 0.1$ (b) $t = 0.25$, $\omega = 0.5$, $S = 1$, $P_r = 2$, $K = 2$, $M = 0.5$, $t = 1$, $h = 0.5$, $\beta = 0.5$, $\phi = 30°$, $Sc = 0.5$, $y = 0.004$, $p = 3$, $\alpha = 0.4$. (c) $y = 0.004$, $p = 2$ and $\alpha = 1$, $t = 0.1$ (d) $y = 0.004$, $p = 10$, $\alpha = 0.01$, $t = 0.1$.

3.3 Concentration profile

The concentration profile for different values of fractional order parameter (α) , Schmidt number (Cs) , and chemical process (ω) is shown in Figures 11 to 13. There is a relationship between the blood concentration and the quantity of blood cells floating in the plasma. Red blood cells (RBCs) are important blood cells because of their size and density in the bloodstream. RBCs assembled at the center of the vessel, where there is a greater concentration of solutes, due to their revolving nature. However, because the off-axis zone is an area predominantly represented by cells that carry plasma, the solute concentration there decreases to a minimum. This observation is displayed in all of the concentration graphs in this section. The fractional model fluid in Figure 11 reaches a greater concentration more quickly than the integer order fluid (Imoro et al., 2024).

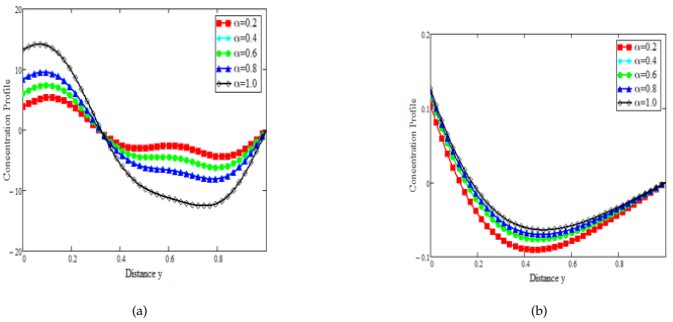

Figure 11: Concentration profile for different values of α at: (a) $t = 0.1$ (b) $t = 0.5$ $Sc = 0.5$, $S = 1$, $R = 0.5$, $P_r = 2$, $K = 2$, $M = 0.5$, $t = 1$, $h = 0.5$, $\beta = 0.5$, $\phi = 30°$

This is because a fractional order derivative that restricts fluid flow is included in the model. The Schmidt number exhibits the opposite pattern. The blood cells show an additional force of the temperature gradient in the presence of the Schmidt number, as seen in Figure 12, which further increases the concentration. Therefore, lower Schmidt number values, for example in industrial applications, physically represent hydrogen gas as the species diffusing (Sademaki et al., 2026).

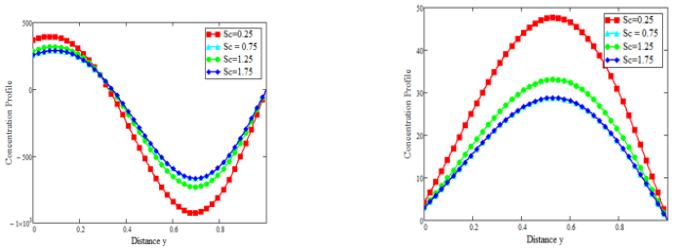

Figure 12: Concentration profile for different values of Schmidt number: (a) $\alpha = 0.4$ (b) $\alpha = 1$, $\omega = 0.5$, $S = 1$, $R = 0.5$, $P_r = 2$, $K = 2$, $M = 0.5$, $t = 1$, $h = 0.5$, $\beta = 0.5$, $\phi = 30^\circ$

Figure 12 illustrates how the species' chemical molecular diffusivity decreases dramatically with increasing Schmidt number (Sc) , making it easier for the species to enter the flow field and raising the mass transfer function. Higher Schmidt number compounds can enhance mass transfer and dispersion properties in the bloodstream, especially for pharmaceutical diffusion in pulse blood flow. The amplitude of the blood flow concentration is larger for the integer order derivative. As demonstrated in Figure 13a and 13b, this phenomena is clearly seen along the flow axis $(0 \leq y \leq 0.5)$ and slowly declines in the region $(0 \leq y \leq 1)$ for both fractional and integer order derivatives, respectively. As can be observed from all of the graphs in Figure 13, the blood flow decreases along the distensible tube's length where the graphs begin to fluctuate because of the size of the chemical reaction parameter's peak value (pressure gradient) (see, Abdul-Wahab & Al-Saif, 2024). Furthermore, it has been demonstrated that the variation is more pronounced in the larger section of the artery wall, permitting the flow to pass without producing a perceptible pressure gradient. Nevertheless, the substantial pressure gradient is usually required to maintain a consistent flow rate as it passes through the constrictions in the artery.

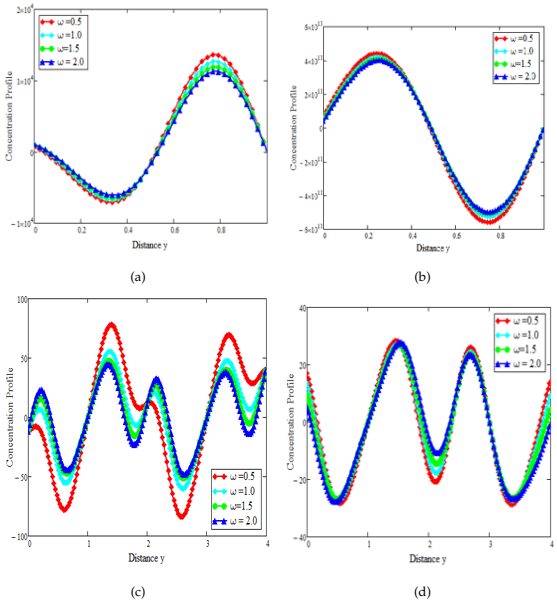

Figure 13: Concentration profile for different values of the chemical reaction parameter: $Sc = 0.5$, $S = 1$, $P_r = 2$, $K = 2$, $M = 0.5$, $t = 1$, $h = 0.5$, $\beta = 0.5$, $\phi = 30^\circ$, $R = 0.5$ (a) $\alpha = 0.4$ (b) $\alpha = 1$.

4 Conclusion

Currently, a fractional-order model of the magneto hydrodynamic blood flow via a bifurcated artery under the influence of thermal radiation, a slanted magnetic field, and a heat source during tumor treatment is being developed. The Laplace transform and the combined methods of indeterminate coefficients were used to solve the mathematical models. The fractional order parameter has a major effect on the blood velocity profiles, concentration, and temperature distribution. It has been noted that fluids with fractional order can occasionally move faster than those with integer order. Fractional model fluid flow is slower than integer-order fluid flow over longer dimensionless durations. The impact of fluid velocity is demonstrated by the fact that the rate of increase in fluid velocity is slower at larger levels of the magnetic field parameter. As the chemical reaction parameter rises, the blood flow concentration falls. The blood concentration rises as the Schmidt number rises. As the fractional parameter and the heat source increase, the blood flow's dimensionless temperature rises, which also affects the radiation parameter. We noted that the outcomes will be intriguing to comprehend and evaluate throughout cancer therapy using hyperthermia. Additionally, it will be useful in understanding the drug particle concentration phenomena for applications and administrations involving drug delivery. Our research's findings should serve as a foundation for the study of increasingly sophisticated blood flow models and also serve as a basis for in vitro and in vivo testing, particularly in the application areas like medicine, biomedical engineering, biology, pathology, and other related domains.

Acknowledgments

This work was supported by Tertiary Education Trust Fund (TETFund) Ref. No. TETF/ DR&D/CE /UNI /BAUCHI /IBR /2025/ VOL.1. Therefore, the authors gratefully acknowledged the financial support of the TETFUND. The authors would like to express their sincere gratitude to the handily editor and the reviewers for their helpful and informative comments, which have enhanced the manuscript.

Declaration of Generative AI

The authors declare that they do not used generative AI in the scientific writing.

References

Abdulhameed, M., Babagana, B., Markus, S., Yakubu, D. G., & Adamu, G. T. (2023). The effects of fractional relaxation time and magnetic field on blood flow through arteries along with nanoparticles. *Defect and Diffusion Forum*, *424*, 59–76.

Abdulhameed, M., Vieru, D., & Roslan, R. (2017). Modeling electro-magnetohydrodynamic thermo-fluidic transport of biofluids with new trend of fractional derivative without singular kernel. *Physica A*, *484*, 233–252.

Abdul-Wahab, M. S., & Al-Saif, A. S. J. A. (2024). A new method for studying blood flow through stenotic artery in the presence of a magnetic field. *Intern. J. Appl. Comput. Math.*, *10*(49). https://doi.org/10.1007/s40819-024-01684-x

Akbar, N. S., & Butt, A. W. (2017). Entropy generation analysis in convective ferromagnetic nano blood flow through a composite stenosed arteries with permeable wall. *Commun. Theor. Phys.*, *67*, 554–560.

Ali, F., Sheikh, N. A., Khan, I., & Saqib, M. (2017). Magnetic field effect on blood flow of casson fluid in axisymmetric cylindrical tube: A fractional model. *J. Magn. Magn. Mater.*, *423*, 327–336.

Atangana, A., & Baleanu, D. (2016). New fractional derivative with non-local and non-singular kernel: Theory and application to heat transfer model. *Thermal Science*, *21*(2), 761–766. https://doi.org/10.2298/TSCI160517180A

Bansi, C. D. K., Tabi, C. B., Motsumi, T. G., & Mohamadoud, A. (2018). Fractional blood flow in oscillatory arteries with thermal radiation and magnetic field effects. *J. Magn. Magn. Mater.*, *456*, 38–45.

Bhargava, R., Rawat, S., Takhar, H. S., & Bég, O. A. (2007). Pulsatile magnetobiofluid flow and mass transfer in a non-darcian porous medium channels. *Meccanica*, *42*, 247–262.

Bhatti, M. M., & Lu, D. Q. (2019). Analytical study of the head-on collision process between hydroelastic solitary waves in the presence of a uniform current. *Symmetry*, *11*, 333.

Bhatti, M. M., Zeeshan, A., & Ellahi, R. (2016). Heat transfer analysis on peristaltically induced motion of particle-fluid suspension with variable viscosity: Clot blood model. *Comput. Math. Prog. Biomed.*, *137*, 115–124.

Bhatti, M. M., Zeeshan, A., Ellahi, R., & Shit, G. C. (2018). Mathematical modeling of heat and mass transfer effects on MHD peristaltic propulsion of two-phase flow through a Darcy-Brinkman-Forchheimer porous medium. *Adv. Powder Tech.*, *29*, 1189–1197.

Bunonyo, K. W., & Ebiwareme, L. (2023). Mathematical analysis of a magnetic and conducting fluid flow through blood vessel along with an inclination and chemical radiation. *European J. Theoretical and Applied Sciences*, *1*(6), 3–15.

Caputo, M., & Fabrizio, M. (2015). A new definition of fractional derivative without singular kernel. *Progress in Fractional Differentiation and Applications*, *1*(2), 73–85.

Caro, C. G., Pedley, T. J., Schroter, R. C., & Seed, W. A. (2011). *The mechanics of the circulation*. Cambridge University Press.

Chaturani, P., & Palanisamy, V. (1990). Casson fluid model for pulsatile flow of blood under periodic body acceleration. *Biorheology*, *27*(5), 619–630.

Chinyoka, T., & Makinde, O. D. (2014). Computational dynamics of arterial blood flow in the presence of magnetic field and thermal radiation therapy. *Adv. Math. Phys.*, *2014*, 915640.

Dash, R. K., Mehta, K. N., & Jayaraman, G. (1996). Casson fluid flow in a pipe filled with homogeneous porous medium. *Int. J. Engg. Sci.*, *34*, 1146–1156.

Gade, M. R., Kalakuntla, S. R., Adigoppula, R., & Itikela, S. (2026). Prediction of micropolar fluid flow characteristics in a stenosed bifurcated artery using feed-forward neural networks trained by the Levenberg Marquardt Algorithm. *Partial Diff. Equat. Appl. Math.*, *18*, 101366.

Ghasemi, S. E., Hatami, M., Hatami, J., Sahebi, S. A. R., & Ganji, D. D. (2016). An efficient approach to study the pulsatile blood flow in femoral and coronary arteries by differential quadrature method. *Physica A*, *443*, 406–414.

Ghasemi, S. E., Hatami, M., Sarokolaie, A. K., & Ganji, D. D. (2015). Study on blood flow containing nanoparticles through porous arteries in presence of magnetic field using analytical methods. *Physica E*, *70*, 146–156.

Hayat, T., Asad, S., & Alsaedi, A. (2016). Flow of casson fluid with nanoparticles. *Appl. Math. Mech.*, *37*(4), 479–470.

He, S., Fataf, N. A. A., Banerjee, S., & Sun, K. (2019). Complexity in the muscular blood vessel model with variable fractional derivative and external disturbances. *Physica A*, *526*, 120904.

Imoro, I., Etwire, C. J., & Musah, R. (2024). MHD flow of blood-based hybrid nanofluid through a stenosed artery with thermal radiation effect. *Case Studies in Thermal Engin.*, *59*, 104418.

Kumar, D., Satyanarayana, B., Rajesh, K., Narendra, D., & Sanjeev, K. (2021). Application of heat source and chemical reaction in magnetohydrodynamic blood flow through permeable bifurcated arteries with inclined magnetic field in tumor treatments [1-13]. *Results in Applied Mathematics*, *10*, 100151.

Liepsch, D. (1986). Flow in tubes and arteries - A comparison. *Biorheology*, *23*, 395–433.

MacDonald, D. A. (1979). On steady flow through modeled vascular stenosis. *J. Biomech.*, *12*(1), 13–20.

Majee, S., & Shit, G. C. (2017). Numerical investigation of MHD flow of blood and heat transfer in a stenosed arterial segment. *J. Magn. Magn. Mater.*, *424*, 137–147.

Misra, J. C., & Shit, G. C. (2009). Flow of a biomagnatic visco-elastic fluid in a channel with stretching walls. *J. Appl. Mech.*, *76*(6), 061006.

Mondal, A., & Shit, G. C. (2017). Transport of magneto-nanoparticles drugging electro-osmotic flow in a micro-tube in the presence of magnetic field for drug delivery application. *J. Magn. Magn. Mater.*, *442*, 319–328.

Nagarani, P., Sarojamma, G., & Jayaraman, G. (2006). Exact analysis of unsteady convective diffusion in casson fluid flow in an annulus-Application to catheterized artery. *Acta Mechanica*, *187*, 189–202.

Prasad, K. V., Vaidya, H., Choudhari, R., Tripathi, D., Karanth, S., & Hanumantha. (2025). Advancing blood flow in stenotic arteries through magnetohydrodynamic peristaltic motion of hybrid nanoparticles. *Chinese Journal of Physics*, *96*, 1144–1163.

Ramesh, K., & Devakar, M. (2015). Magneto hydrodynamic peristaltic transport of couple stress fluid through porous medium in an inclined asymmetric channel with heat transfer. *J. Magn. Magn. Mater.*, *394*, 335–348.

Sademaki, L. J., Reddy, B. P., & Matao, P. M. (2026). Dissipative and radiative consequences on diffusional reactive MHD nanofluid flow over an inclined vertical cone in a porous medium with reactive species: FEM study. *Partial Diff. Equat. Appl. Math.*, *18*, 101365.

Samko, S. G., Kilbas, A. A., & Marichev, O. I. (1993). *Fractional integrals and derivatives: Theory and applications*. Gordon; Breach Science Publishers.

Shah, N. A., Vieru, D., & Fetecau, C. (2016). Effects of the fractional order and magnetic field on the blood flow in cylindrical domains. *J. Magn. Magn. Mater.*, *409*, 10–19.

Shaw, S., & Murthy, P. V. S. N. (2010). Magnetic drug targeting in the permeable blood vessel - The effect of blood rheology. *J. Nanotechnol. Eng. Med.*, *1*(2), 021001–11.

Shit, G. C., & Majee, S. (2015). Pulsatile flow of blood and heat transfer with variable viscosity under magnetic and vibration environment. *J. Magn. Magn. Mater.*, *388*, 106–115.

Shit, G. C., & Roy, M. (2015). Effect of slip velocity on peristaltic transport of a magneto-micropolar fluid through a porous non-uniform channel. *Int. J. App. Compt. Math.*, *1*, 121–141.

Sinha, A., & Shit, G. C. (2015). Electromagnetohydrodynamic flow of blood and heat transfer in a capillary with thermal radiation. *J. Magn. Magn. Mater.*, *378*, 143–151.

Srivastava, L., & Srivastava, V. (1984). Peristaltic transport of blood: Casson model-11. *J. Biomech.*, *17*(11), 821–829.

Sud, V. K., & Sekhon, G. S. (1984). Blood flow subject to a single cycle of body acceleration. *Bull. Math. Biol*, *46*, 937–949.

Syed, M. H., Mustansar, S. H. S., Hijaz, A., Nazar, T., Wasim, J., Mohamed, R. E., et al. (2026). Thermal characteristics of magnetic blood-based hexa-hybrid nanofluids in stenotic arteries with heat source/sink by applying Caputo-Fabrizio fractional derivatives [In Press]. *Results in Surfaces and Interfaces*.

Tabi, C. B., Motsumi, T. G., Kamdem, C. D. B., & Mohamadou, A. (2017). Nonlinear excitations of blood flow in large vessels under thermal radiations and uniform magnetic field. *Commun. Nonl. Sci. Numer. Simul.*, *49*, 1–8.

Tzirtzilakis, E. E. (2005). A mathematical model for blood flow in magnetic field. *Phys. Fluids*, *17*(7), 077103.

Vardanyan, V. A. (1973). Effect of magnetic field on blood flow. *Biofizika*, *18*, 491–496.

Venkatesan, J., Sankar, D., Hemalatha, K., & Yatim, Y. (2013). Mathematical analysis of casson fluid model for blood rheology in stenosed narrow arteries. *J. Appl. Math.*, *2013*, 1–11.

Yakubu, D. G., Abdulhameed, M., Adamu, G. T., & Kwami, A. M. (2020). A study of fractional relaxation time on blood flow in arteries with magnetic radiation effects. *Diff. Found.*, *26*, 126–144.

Yakubu, D. G., Abdulhameed, M., Adamu, G. T., Roslan, R., Issakhov, A., Rahimi-Gorji, M., & Bakouri, M. (2021). Towards the exact solution of Burger's fluid flow through arteries with fractional time derivative magnetic field and thermal radiation effects. *J. Proce. Mech. Eng.*, *235*, 1618–1627.

Yakubu, D. G., Mohammed, A., Garba, T. A., Usman, H., & Muhammad, L. K. (2022). Construction of the exact solution of blood flow of Oldroyd-B fluids through arteries with effects of fractional derivative magnetic field and heat transfer. *J. Mech. Med. Biol.*, *22*(10), 2250068.

Zeeshan, A., Bhatti, M. M., Akbar, N. S., & Sajjad, Y. (2017). Hydromagnetic blood flow of Sisko-fluid in a non-uniform channel induced by peristaltic wave. *Commun. Theor. Phys.*, *68*, 103–110.

Appendix

$$A_1 = 1, \quad A_2 = M^2 \sin^2\phi - \frac{1}{k} - \frac{s}{(1-\alpha)s+\alpha}, \quad A_3 = h(s+\lambda^2), \quad A_4 = \frac{\tau p_r}{R\tau p_r + 1},$$

$$A_3 = h(s+\lambda^2), \quad A_4 = \frac{\tau p_r}{R\tau p_r + 1}, \quad A_5 = \left(\frac{S}{\tau p_r} - \frac{S}{(1-\alpha)s+\alpha}\right)(s+\lambda^2), \quad A_6 = \sqrt{A_4 A_5}, \quad A_7 = \frac{A_3}{A},$$

$$A_9 = \sqrt{Sc(\omega + s((1-\alpha)s+\alpha))}, \quad A_{10} = \frac{-g\beta}{2(A_9^2 - A_2)\cosh A_9}, \quad A_{11} = \frac{g\beta}{2(A_9^2 - A_2)\sinh A_9}$$

East African Journal of Biophysical and Computational Sciences
ISSN (Online): 2789-3618 and ISSN (Print): 2789-360X

ARTICLE

Prevalence and Determinant Factors of Malaria Infection among Patients Attending Gimbichu Primary Hospital, Soro District, Central Ethiopia, Ethiopia

Melese Birmeka [1,*], Gebremedhin Gebrezgabiher[2], Tekleweyni Asayehegn[3], and Mohammed Kasso[4]

[1]Department of Biology, Hawassa University, Hawassa, P. O. Box 05,
[2]Department of Veterinary Medicine, College of Veterinary Medicine and Animal Sciences, Samara University, P. O. Box 132, Samara, Afar, Ethiopia
[3]Department of Aquatic Sciences, Fisheries and Aquaculture, Hawassa University, Hawassa, P. O. Box 05,
[4]Department of Biology, Hawassa University, Hawassa, P. O. Box 05.

*Corresponding author: melesebirmeka@yahoo.com

ARTICLE INFO
Volume 7(1), 2026
https://dx.doi.org/10.4314/eajbcs.v7i1.3S

ARTICLE HISTORY
Received: 12 June, 2025
Accepted: 21 January, 2026
Published Online: 10 June, 2026

CITATION
Birmeka M. et.al (2026). Prevalence and Determinant Factors of Malaria Infection among Patients Attending Gimbichu Primary Hospital, Soro District, Central Ethiopia, Ethiopia. *East African Journal of Biophysical and Computational Sciences* Volume 7(1), 2026. .https://dx.doi.org/10.4314/eajbcs.v7i1.3S.27-33

OPEN ACCESS

Abstract

In the world, particularly in Ethiopia, malaria has a great influence on human health and economy. This study intended to determine the prevalence, trends and associated risk factors of malaria patients visiting Gimbichu Primary Hospital, Ethiopia. To assess the trend and parasitological examination, a hospital-based cross-sectional study was carried out. To determine factors that significantly associated with infection, a bivariate and multivariable logistic regression analyses were performed with statistical significance set at $p < 0.05$. The findings of the study revealed the overall malaria prevalence of 72.4% among suspected patients. The study also revealed that males (AOR = 3.5, 95% CI; 1.5 - 3.8, p<0.001), individuals under five years (AOR = 2.8, 95% CI: 1.13 - 2.2), 5-20 years (AOR = 1.75, 95% CI: 1.1 - 1.91) and 21-45 years (AOR = 1.65, 95% CI: 1.01 - 1.49) were at higher risk. Additionally, study participants living close to mosquito breeding sites (AOR = 2.54, 95% CI: 2.53 - 4.14), rural (AOR = 2.13, 95% CI: 1.01 - 2.6), houses with thatch roof (AOR = 1.43, 95% CI: 1.01-2.30), not using bed nets (AOR = 1.51, 95% CI: 2.01 - 4.1), homes with wall openings (AOR = 1.6, 95% CI: 1.13 - 2.57), monthly income of less than 1,000 Ethiopian Birr (AOR = 2.93, 95% CI: 1.3 - 4.6), and pregnant women (AOR = 1.6, 95% CI: 1.13 - 2.57) had maximum risk for malaria infection. The analysis from the retrospective data showed the overall decreasing trend in malaria infection rates, despite the fluctuations recorded between 2015 - 2021. The study indicates that malaria is persistent and a significant public health challenge which is driven by a complex interrelationship of demographic, social and environmental factors. Plasmodium vivax infection is the most prevalent species known to cause malaria in the study area. These findings necessitate targeted interventions focusing on housing improvements, economic support, and vector control measures.

Keywords: Determinants; Malaria; Prevalence; Soro District, Trend

1 Introduction

Malaria is a contagious disease that is caused by parasitic proatozoa (Ferede et al., 2013). It has great impact on world population health and economy (Baird, 2013). It is dominantly caused by *Plasmodium falciparum* and *Plasmodium vivax*. Out of the two species *P. falciparum* is the stronger pathogenic species that causes most deaths by malaria diseases at world scale, accounting for more than 90% of the world malaria mortality (Baird, 2013; Ferede et al., 2013). The malaria disease is a severe disease particularly in children and pregnant women. Pregnant women are more susceptible due to decreased immunity during pregnancy, endangering both mother and the child. Similarly, children under five are at higher risk because their immune systems are not fully developed, with a child dying of malaria every 45 seconds worldwide.

As an infectious vector-borne disease, malaria continues to be a key public health challenge in the country, with transmission patterns varying across regions depending on climatic conditions, rainfall, and altitude. In Ethiopia, malaria is known to be dominantly caused by *P. falciparum* (60%) and P. vivax (40%) (FMOH (Federal Ministry of Health), 2018). In the country, about 75% of areas located below 2,000 meters above sea level are susceptible to malaria epidemics and the persistent risk of transmission (Girum et al., 2019). Annually, approximately 4,782,000 reported cases

and related deaths, with morbidity and mortality increasing markedly during epidemic periods were recorded in the country (Alemayehu et al., 2014). Of this, the large-scale epidemics tend to occur every five to eight years although smaller, localized outbreaks are reported annually (Tsige et al., 2011). An estimated 68% of Ethiopians, a country with a population of over 100 million people, are at risk of contracting malaria (WHO (World Health Organization), 2016).

In Ethiopia, malaria transmission shows a considerable variation across seasons, years, and geographic settings. The high impact of malaria is particularly pronounced in rural areas (Donnelly et al., 2005), largely due to proximity to mosquito breeding sites, limited coverage of control interventions, widespread poverty, low literacy levels, land-use practices and poor housing conditions (Stratton et al., 2008). Exceptionally, a yearly based transmission observation is evident in the southwestern lowland regions bordering neighboring countries (Zhou et al., 2016). The communities with lower socioeconomic status are known to be disproportionately affected (WHO (World Health Organization), 2012), because it limits access to medical care and preventative measures like indoor spraying, bed nets treatment and efficient antimalarial therapy (Yamamoto et al., 2010). The drug-resistant strains of *P. falciparum* and P. vivax have also emerged and spread, posing a significant challenge to the control of malaria which contributed to the recent increase in malaria cases in the nation (Yarcho, 2010).

The Government of Ethiopian has made significant progresses since 2005 in malaria control interventions such as diagnostic testing, rapid case treatment, and prevention strategies for pregnant women through intermittent preventive therapy. High efforts also implemented on the distribution of IRS and ITNs. However, the widespread emergence of drug resistance in parasites and insecticide resistance in vectors have obstructed efforts of malaria eradication (Abeku et al., 2015; Tafese et al., 2018), particularly in the Hadiya Zone of central Ethiopia. This situation underscores the need for continuous evaluation and monitoring of malaria control interventions to address existing gaps.

2 Materials and Methods

2.1 Study Area

The study was conducted at Gimbichu Primary Hospital which provides care for the Soro District in Hadiya Zone, central Ethiopia region. The district is about 264 kilometers south of the nation's capital, Addis Ababa. Soro District is home to a substantial population of 233,015 people, nearly evenly split between genders (115,825 men and 117,190 women), giving the hospital a wide and diverse community to serve.

2.2 Study Design and Period

An institution-based cross-sectional study was carried out between October 2022 and January 2023.

2.3 Study Population

All individuals who presented to Gimbichu Primary Hospital with suspected malaria during the data collection period and satisfied the eligibility requirements were involved in the study population

2.4 Eligiblity Criteria

Inclusion criteria: Malaria suspected patients who were consented to participate in the study.

Exclusion criteria: Malaria suspected patients who were not to give consent for participation in this study.

Sampling and Sample Size Determination All patients suspected of having malaria were consecutively selected during their visits to the outpatient department of Gimbichu Primary Hospital till the compulsory sample size was achieved. The sample size was estimated using Daniel's formula (Daniel, 2004).

$$N = \frac{z^2(1-p)}{d^2} \quad (1)$$

Where - p = 50%, because of the absence of previous malaria prevalence studies in the area, - d = margin of error at 5% and - z = 1.96 at 95% CI Consequently, the sample size was determined to be 384.

2.5 Data Collection

The structured pretested questionnaires were used to collect information on socio-demographic and economic status of study participants. Blood sample collection was done by finger prick by healthcare professional, and on the same slide both thick and thin blood smears were prepared. Throughout the data collection process, continuous monitoring and supervision were maintained. The activities performed by laboratory technicians, interviewers and nurses were closely overseen. Additionally, retrospective data spanning for seven years (2015 -2021) was retrieved from hospital registration records.

2.6 Data Analysis

Following a completeness check, the data was analyzed by using SPSS version 24. Logistic regression studies were performed to identify the relationship between a few possible risk variables and malaria infection. To determine the existence and strength of a connection, AOR at 95% CI were calculated; if p < 0.05, statistical significance was proclaimed.

2.7 Ethical Consideration

The Institutional Research Ethics Review Committee of CNCS of Hawassa University examined and approved the study proposal and ethical clearance was received (Ref.no. IRB/279/13). Additional, permission was also granted by the Hadiya Zone Health Department and the Soro District Primary Hospital. Confidentiality and privacy were strictly upheld, and participation in the study was entirely voluntary. After awareness made on the objectives of the study, participants gave their consent participation. Confidentiality was also maintained.

3 Results

3.1 Characteristics of Study Participants in Retrospective Study of Malaria in Soro District, 2015 - 2021

A total of 65,211 clients were registered in the laboratory logbooks of Gimbichu Primary Hospital. Of these, 36,132(55.4%) were males and 29,089(44.6%) were females. Between 2015 and 2021, 65,211 blood films were microscopically examined. The majority of the cases were males accounting 17,813(49.3%). Although malaria prevalence fluctuated from 2016 to 2021, there was an overall decreasing trend. Over the seven year period, a considerable malaria cases were recorded in the age 15 - 24 years old (18,718 cases, 28.7%), followed by 5 - 14 years old (15,131 cases, 23.2%). The lowest number of cases was over 54 years (8,740 cases, 13.4%) (Table 1).

Table 1: The social and demographic characteristics of microscopically examined suspected patients in Soro District, 2015 - 2021.

Socio-demographic variables	Category	Total examined (%)	Smear Microscopy Results	
			Positive (%)	Negative (%)
Sex	Male	36132(55.4)	17813(49.3)	18319(50.7)
	Female	29089(44.6)	11868(40.8)	17221(59.2)
	Total	**65221(100)**	**29,681(45.5)**	**35540(54.5)**
Age	<5	11283(17.3)	5114(45.3)	6169(54.6)
	5 - 14	15131(23.2)	5447(36.0)	9684(64.0)
	15 - 24	18718(28.7)	7674(41.0)	11044(59.0)
	25 - 54	11349(17.4)	8040(70.0)	3309(29.0)
	>54	8740(13.4)	3421(39.1)	5319(60.8)
	Total	**65221(100)**	**29681(45.5)**	**35540(54.5)**
Resident	Urban	29415(45.1)	10310(35.05)	19105(64.95)
	Rural	35806(54.9)	19371(54.1)	16435(45.9)
	Total	**65221(100)**	**29681(45.5)**	**35540(54.5)**

3.2 The Prevalence of Malaria cases by Mex and Age among the Study Population in Soro District, 2015–2021

Among the 65,211 blood films examined, 36,132 (55.4%) were males and 29,089 (44.6%) were females. Of the 29,681 individuals who tested positive for malaria, 17,813 (60%) were males 11,868 (40%) were females (Table 2).

The age specific prevalence rates of malaria was as follows: 5,114 cases (45.3%) in children under five years old, 5,447(36%) in 5 - 14 years old, 7,674 cases (41%) in the 15-24 years old, 8,040 cases (70%) in the 25 - 54 years age group, and 3,421 cases (39.1%) in individuals over 54 years old. The infections malaria was recorded along all age groups considered in the study with an overall rate of 70%. The maximum prevalence was observed in the age group of 25 - 54 years. The next highest prevalence was in children below five years old, at 45.3%, though the lowest prevalence was in the 5 - 14 years age group, at 36% (Table 2).

Table 2: The *Plasmodium* species distribution across sex and age among study participants in Soro District, 2015 - 2021

Variable	Category	Total examined (%)	Positive (%)	Negative (%)	*P. falciparum* (%)	*P. vivax* (%)	Mixed infection (%)
Sex	Male	36132(55.4)	17813(49.3)	18319(50.7)	9860(55.4)	7173(40.3)	765(4.3)
	Female	29089(44.6)	11868(40.8)	17221(59.2)	6550(55.2)	4866(41)	452(3.8)
	Total	**65221(100%)**	**29,681(45.5)**	**35540(54.5)**	**16414(55.3)**	**12051(40.6)**	**1217(4.1)**
Age	<5	11283(17.3)	5114(45.3)	6169(54.6)	2915(57)	1994(39.0)	204(4.0)
	5 - 14	15131(23.2%)	5447(36.0)	9684(64)	2724(50.3)	2521(46.0)	202(3.7)
	15 - 24	18718(28.7)	7674(41.0)	11044(59)	4014(52.3)	3400(44.3)	260(3.4)
	25 - 54	11349(17.4)	8040(70.0)	3309(29)	5017(62.3)	2734(34.0)	289(3.6)
	>54	8740(13.4)	3421(39.1)	5319(60.8)	1757(51.0)	1402(41.0)	262(7.6)
	Total	**65221(100)**	**29681(45.5)**	**35540(54.5)**	**16414(55.3)**	**12051(40.6)**	**1217(4.1)**

*The numbers inside the brackets indicate percentages (%)

3.3 Trends of Malaria Incidence in Soro District, 2015 - 2021

Figure 1 illustrates trends of malaria prevalence among patients from 2015 - 2021, based on data obtained from the malaria records of Gimbichu Primary Hospital. Over seven years period, 65,221 blood films were examined for malaria, with 29,663 (45.5%) testing positive. The annual prevalence rates were 74.5% in 2015, 54.5% in 2016, 44.6% in 2017, 58.7% in 2018, 10.4%; in 2019, 15.7% in 2020 and 13.4 % in 2021. The highest annual prevalence was recorded in 2015 at 74.5 %, significantly higher than in subsequent years. Overall, the data indicates fluctuating trends in malaria cases, with a general decrease over the seven-year period (Figure 1).

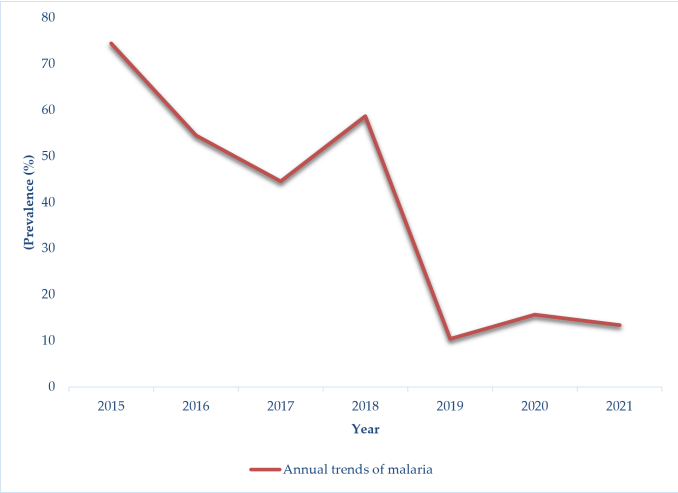

Figure 1: Malaria Incidence Trends among patients at Gimbichu Primary Hospital (2015 -2021)

3.4 Annual Malaria Prevalence Trends by Plasmodium Species in Soro District, 2015–2021

From 2015 to 2021, malaria cases at Gimbichu Primary Hospital were attributed *P. falciparum* (16,392 cases, 55.3%), P. vivax (12055 cases, 40.6%), and mixed infections (1201 cases, 4.1%). The trends in malaria cases by species showed fluctuations and an overall decrease over the years. The annual occurrence rates for *P. falciparum* were 58% in 2015, 54% in 2016, 42% in 2017, 70.1% in 2018, 42.5% in 2019, 32% in 2020, and 20% in 2021. For P. vivax, the rates were 39% in 2015, 44% in 2016, 57% in 2017, 16.9% in 2018, 56.7% in 2019, 67.6% in 2020, and 79.9% in 2021. Mixed infections were recorded as follows: 3.4% in 2015, 1.5% in 2016, 1% in 2017, 12.9% in 2018, 0.8% in 2019, 1.4% in 2020, and 1.7% in 2021. The highest case of *P. falciparum* was recorded in 2018 (70.1%), while P.vivax showed a fluctuating trend with the maximum rate in 2021 (79.9%). Mixed infection peaked in was recorded 2018 at 12.9% (Figure 2).

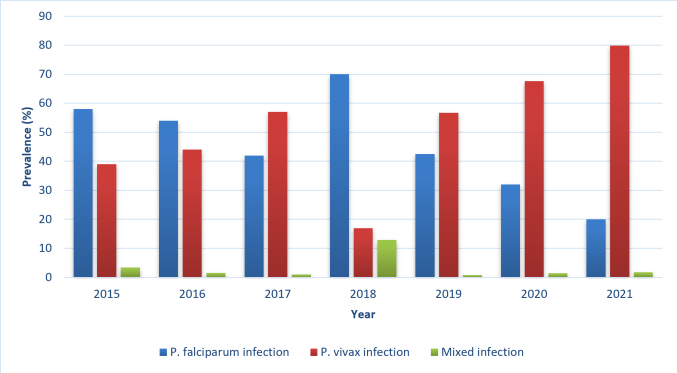

Figure 2: Malaria infection distribution trends by Plasmodium species among patients at Gimbichu Primary Hospital (2015 - 2021)

3.5 Socio-demographic Profile of the Study Population in Soro District, South-Central Ethiopia (Oct 2022 – Jan 2023)

During the study period, 384 suspected malaria patients were sampled in Soro District, comprising of 214 (55.7%) males and 170 (44.3%) females. Of these, majority of the participants (52.6%) were 5 - 20 years old, and 80 (20.8%), 58 (15.1%), and 44 (11.5%) of participants were below five years, 21 - 45 years, above 45 years, respectively. Most participants (219, 57%) resided in rural areas. The monthly income per month distribution of the study participants were: 118 (30.7%) had 3,000 - 5,000 ETB, 110 (28.6%) had less than 1000 ETB. Additionally, 199 (52%) respondents were homes near mosquito breeding sites, 237 (61.7%) respondents had homes with wall opening, 167 (43.5%) of respondents were sleeping under mosquito net,101(26.3%) respondents had IRS in the past five months, and 266 (69.3%) respondents had homes with corrugated roofs (Table 3).

3.6 Prevalence and Determinant Factors of Malaria Infection

The findings indicated that 278 (72%) of the participants were infected with malaria parasites. Analyses of determinant risk factors for suspected patients found significant associations with sex, age, residence, pregnancy status, income level, bed nets usage, IRS in the past five months, availability of mosquito breeding places, porous wall for mosquito's entrance, and types of roofing material.

Males were found to have a 3.5 times more likelihood of malaria infection compared with females (AOR = 3.5, 95% CI: 1.5 – 3.8, p < 0.001). Higher infection rates were observed for children under five years of age (AOR = 2.8, 95% CI: 1.13 – 2.2), individuals aged 5–20 years (AOR = 1.75, 95% CI: 1.1 – 1.91), and those aged 21 – 45 years (AOR = 1.65, 95% CI: 1.01 – 1.49) when compared with participants older than 45 years.

Table 3: The participants socio-demographic characteristics in Soro District, South-Central Ethiopia (Oct 2022 – Jan 2023)

Characteristics	Categories	Number	Percent (%)
Gender	Male	214	55.7
	Female	170	44.3
Age	<5	80	20.8
	5 - 20	202	52.6
	21 - 45	58	15.1
	>45	44	11.5
Residence	Urban	165	43
	Rural	219	57
Pregnancy-Self reported	Present	107	28
	Absent	277	72
Income level	< 1,000	110	28.6
	100-3,000	91	23.7
	3,000-5,000	118	30.7
	>5,000	65	16.9
Home closer to breeding site	Yes	199	52
	No	185	48
Opening hole in the wall	Yes	107	28
	No	277	72
Sleep under mosquito net	Yes	167	43.5
	No	217	56.5
IRS in the past five month	Yes	101	26.3
	No	283	73.7
House roof type	Corrugated	266	69.3
	Thatch	118	30.7

Participants living in households around mosquito breeding sites in the surrounding environment were nearly three times more likely to be infected than those without such sites (AOR = 2.54, 95% CI: 2.53–4.14, p < 0.001). Rural residents had approximately twice the odds of malaria infection compared with urban dwellers (AOR = 2.13, 95% CI: 1.01–2.6, p = 0.01).

Housing characteristics were also showed significant association with malaria infection. Individuals residing in houses with thatched roofs were 1.43 times more likely to be infected compared to those living in houses with corrugated iron roofs (AOR = 1.43, 95% CI: 1.01 – 2.30, p < 0.001). Participants who did not use bed nets had a higher risk of malaria infection than their counterparts who used bed nets (AOR = 1.51, 95% CI: 2.01 – 4.1). Similarly, the existence of wall openings in dwellings increased the likelihood of malaria infection by 1.6 times (AOR = 1.6, 95% CI: 1.13 – 2.57, p = 0.01).

Furthermore, participants with a monthly income of less than 1,000 Ethiopian Birr were infected with malaria nearly triple times when compared with those earning more than 1,000 Birr per month (AOR = 2.93, 95% CI: 1.3 – 4.6, p = 0.004) (Table 4).

Table 4: Logistic Regression Analysis for Predictors of Malaria in Suspected Patients in Soro District, Central Ethiopia, (Oct 2021 – Jan 2022)

Characteristics	Category	Malaria+ve(%)	COR(95%CI)	P-value	AOR(95%CI)	P-value
Sex	Female	106(62.4)	1		1	
	Male	172(80.4)	1.67(1.3 - 2.65)	< 0.001	3.5(1.5 - 3.8)	< 0.001
Age	<5	27(34)	1.6(2.13 - 3.1)	0.01	2.8(1.13 - 2.2)	0.024
	5 - 20	161(79)	1.86(1.14 - 2.16)	< 0.001	1.75(1.1 - 1.91)	< 0.001
	21 - 45	50(86)	1.75(1.01 - 2.79)	0.03	1.65(1.01 - 1.49)	0.03
	>45	40(90)	1		1	
Residence	Urban	110(66.7)	1		1	
	Rural	168(76.7)	1.43(1.14 - 2.31)	< 0.001	2.13(1.01 - 2.6)	0.01
Income level of Household	< 1000	90(81.8)	1.55(1.06 - 4.62)	< 0.001	2.93(1.3 - 4.6)	0.004
	100-3000	65(71.4)	0.56(0.22 - 5.6)	0.324	0.86(0.21 - 5.2)	0.31
	3000-5000	83(70.3)	1.63(0.11 - 2.6)	0.234	2.75(0.14 - 4.3)	0.22
	>5000	40(61.5)	1		1	
Use of bed nets	Yes	112(67.1)	1		1	
	No	166(76.5)	1.54(2.03 - 5.12)	< 0.001	1.51(2.01 - 4.1)	< 0.001
IRS in the past twelve month's	yes	70(69.3)	1		1	
	No	208(73.5)	1.9(1.23 - 2.96)	< 0.001	1.89(1.3 - 2.76)	< 0.001
Mosquito Breeding Site near to home	Yes	145(72.8)	1.54(2.03 - 5.16)	< 0.001	2.54(2.53 - 4.14)	< 0.001
	No	133(71.9)				
Home wall opening	Yes	67(62.6)	1.89(1.23 - 2.96)	< 0.001	1.6(1.13 - 2.57)	0.01
	No	211(76.2)	1		1	
House Roof Type	Corrugated iron sheet	191(71.8)	1		1	
	Thatch	87(73.7)	1.63(1 - 2.2)	0.02	1.43(1 - 2.30)	0.001

*For each respective characteristic, the percentage calculated is from total examined

3.7 Discussion

This study was conducted to examine trends in malaria infection over time, estimate its prevalence and identify factors associated with malaria infection among patients attending Gimbichu Primary Hospital in Soro District, South-central Ethiopia.

A study by Deressa et al., 2006 reported that malaria has been one of the major causes of mortality, hospital admissions and outpatient visits in Ethiopian health facilities for a long time. In line with these findings, the present analysis showed that malaria cases peaked in 2015, accounting for 74.5% of all reported cases, while the lowest prevalence was observed in 2019 (10.4%). From the year 2015- 2021, overall trend analysis demonstrated the fluctuations in malaria incidence, with an overall declining pattern across the seven-year period.

Results from the current study revealed an overall malaria prevalence of 72.4% among suspected patients. This prevalence differs from reports of similar studies conducted in other parts of Ethiopia either higher or lower. For instance, the prevalence rate observed in this study was higher than those reported from Dilla District by Ehsetu and Besha, 2015 , Kola Diba District by Abebe et al., 2012, Wolkite Health Center by Degefie, 2017, Arba Minch Hospital by Belayneh, 2014, Sibu Sira District by Girum, 2014 and the East Shewa Zone of Oromia Region by Firew and Andrew, 2018. In contrast, it was lower than the prevalence reported from Hallaba District by Girum (2014). These differences might be due to variations in study period, season, altitude, local communities' awareness and differences in malaria prevention and control strategies.

In the study area, P. vivax was the predominant Plasmodium species (86.1%), followed by *P. falciparum* (8.3%) and mixed infections of *P. falciparum* and P. vivax (5.6%). Hence, the result of present study contradicts with the national estimates which indicate as *P. falciparum* accounts for approximately 60% of malaria incidences while P. vivax accounts for the remaining 40% in Ethiopia (Eliyas, 2014). Similar predominance of *P. falciparum* has been documented in studies conducted in Ayire District (Eliyas, 2014) and Arba Minch Hospital (Belayneh, 2014). Such inconsistencies may be explained by topographical differences, as *P. falciparum* transmission is more common in lowland areas. Conversely, the predominance of P. vivax observed in this study is agree with reports from Wolkite Health Center (Degefie, 2017) , Dilla District (Ehsetu & Besha, 2015), Hallaba District (Girum, 2014) , and East Shewa Zone (Firew & Andrew, 2018) **(Firew and Andrew, 2017)**. This similarity may be related to comparable altitudinal conditions or the relapsing nature of P. vivax, particularly during cooler seasons.

The present study showed as the infection malaria was significantly more common among males than females which seem males being 3.5 times more likely to be infected. This result differs from case reported by Graves et al., 2009 , although it is consistent with other Ethiopian studies (Abebe et al., 2012; Girum, 2014). More than half proportion of the malaria infection was observed among individuals aged 5–20 years, followed by those aged 21–40 years. This may be attributed to increased outdoor activities such as farming and other productive work, which elevate exposure to mosquito bites. Additionally, malaria prevalence was assumed to be higher among individuals residing in rural areas when compared with those living in urban settings. This observation aligns with findings from Dilla District (Ehsetu & Besha, 2015). Such higher burden in rural areas may be due to lower levels of awareness, substandard housing conditions, limited resources and reduced access to effective malaria control measures.

The record of the higher prevalence of malaria cases among pregnant women when compared with non-pregnant women probably due to immunity reduction associated with pregnancy. Low household income may also significantly associate with increased malaria infection. For instance, individuals with lower income levels may face greater malaria risk due to limited access to preventive tools and healthcare services, inadequate housing that permits mosquito entry, and compromised health and nutrition status (Dejene, 2014). These findings are also consistent with studies from Muleba District in the Kagera region of Tanzania, which reported a similar association between family employment status and malaria prevalence among children under five (Mushashu, 2012). WHO (World Health Organization), 2012 also pointed out as economically disadvantaged households may have limited access to healthcare facilities and insufficient resources to afford vector control

interventions including insecticide-treated nets (ITNs), indoor residual spraying (IRS) and antimalarial medications.

The result of present study regarding the use of indoor residual spraying within the past 12 months was significantly associated with malaria infection. In similar way, Sintasath et al., 2005 also indicated as IRS remains a cornerstone of the national malaria control strategy, particularly for epidemic prevention and mitigation. Their study also has shown substantially reduces in malaria morbidity and mortality. These findings are also consistent with reports from the Jiga area in northwest Ethiopia (Seble, 2014) , although they contrast with findings from Muleba District in Tanzania (Mushashu, 2012).

For the malaria infection, the environmental and housing-related factors such as proximity to mosquito breeding sites, wall openings, wall type and roofing material were identified as important contributors. These results agree with previous studies conducted by Ghebreyesus et al., 2000 and Loha, 2013 which have highlighted the role of housing quality and environmental conditions in malaria transmission.

4 Conclusions

The findings of this study indicated that malaria remains a major public health concern in Soro District; P. vivax was identified as the predominant infecting species. Although retrospective analysis over the seven-year period revealed fluctuations in malaria incidence, the overall trend showed a gradual decline. Several factors were significantly associated with malaria infection, including low household income, proximity to mosquito breeding sites, the presence of wall openings, lack of indoor residual spraying, and inadequate use of insecticide-treated bed nets.

Addressing existing burden of malaria in the study area requires coordinated and multi-sectorial interventions. The control efforts should be prioritize to strengthen the health service accessibility and quality, prompt treatment of infected individuals, enhancement of community socio-economic conditions, implementation of effective and well-coordinated vector control measures. The active community engagement action is also needed to mitigate the identified risk factors in Soro District, Ethiopia.

Declarations

Availability of data

The data used during this study will be available up on request.

Conflict of interests

The authors declare no conflict of interest.

Consent for publication

Not applicable.

Funding

None

Authors' contributions

MB was responsible for conceptualization, investigation, data collection, analysis and writing the original draft. TA, MK and GG contributed to supervision, methodology, data analysis and reviewing and editing the manuscript. All authors read and approved the final manuscript.

Acknowledgments

The authors are grateful for laboratory technical staff of Gimbichu Primary Hospital and Hawassa University for technical support.

References

Abebe, A., Teshome, G., & Meshesha, B. (2012). Abundance and dynamics of anopheline larvae in a highland malarious area of south-central ethiopia. *Parasites and Vectors*, *5*, 117.

Abeku, T., Helinski, M., Kirby, M., Kefyalew, T., Awano, T., Batisso, E., Tesfaye, G., Ssekitooleko, J., Nicholas, S., Erdmanis, L., Nalwoga, A., Bass, C., Cose, S., Assefa, A., Kebede, Z., Habte, T., Katamba, V., Nuwa, A., Bakeera-Ssali, S., … Meek, S. (2015). Monitoring changes in malaria epidemiology and effectiveness of interventions in ethiopia and uganda: Beyond garki project baseline survey. *Malar J.*, *14*, 337.

Alemayehu, N., Gadissa, H., Dawit, G., Solomon, G., Sarah, A., Savitah, S., Tadesse, A., Kifle, G., & Atinafu, D. (2014). Can training health extension workers in the integrated pharmaceutical logistics system (ipls) be effective, affordable and opportunistic. *Ethiopian. Medical J.*, *52*(3), 11–12.

Baird, J. (2013). Evidence and implications of mortality associated with acute plasmodium vivax malaria. *Clin Microbiol Rev.*, *26*(1), 36–57.

Belayneh, R. (2014). Magnitude of malaria infection in ethiopia. *Global Journal of Medical Research: C Microbiology and Pathology*, *14*, 7.

Daniel, W. (2004). *Biostatistics, a foundation for the analysis in the health sciences* (7th). John Wiley; Sons (Asia) Pvt. Ltd.

Degefie, B. (2017). *Prevalence of malaria among patients attending wolkite health center, south-central ethiopia* [Unpublished work].

Dejene, H. (2014). *Malaria prevention and control in ethiopia* [Ph.D. Thesis]. University of South Africa.

Deressa, W., Ali, A., & Berhane, Y. (2006). Review of the interplay between population dynamics and malaria transmission in ethiopia. *Ethiop. J. Health Dev.*, *20*(3), 137–144.

Donnelly, M., McCall, P., Lengeler, C., Bates, I., D'Alessandro, U., Barnish, G., Konradsen, F., Klinkenberg, E., Townson, H., Trape, J., Hastings, I., & Mutero, C. (2005). Malaria and urbanization in sub-saharan africa. *Malar J.*, *4*, 12.

Ehsetu, M., & Besha, A. (2015). Prevalence of malaria and associated factors in dilla town and the surrounding rural areas. *Ethiop J Health Sci.*, *25*(3), 229–236.

Eliyas, N. (2014). *Prevalence of malaria and its biomedical knowledge among households in ayira district, western ethiopia* [MSc Thesis]. Haramaya University.

Ferede, G., Worku, A., Getaneh, A., Ahmed, A., Haile, T., Abdu, Y., & Tessema, B. (2013). Prevalence of malaria from blood smears examination: A seven-year retrospective study from metema hospital, northwest ethiopia. *Malar Res Treat.*, *2013*, 705730.

Firew, T., & Andrew, W. (2018). Prevalence and associated risk factors of malaria among adults in east shewa zone of oromia regional state, ethiopia: A cross-sectional study. *Trop Med Health.*, *46*, 4.

FMOH (Federal Ministry of Health). (2018). *Malaria: Diagnosis and treatment guidelines for health workers in ethiopia* (4th). Addis Ababa.

Ghebreyesus, T., Haile, M., Witten, K., Getachew, A., Yohannes, M., & Lindsay, S. (2000). Household risk factors for malaria among children in the ethiopian highlands. *Trans. R. Soc. Trop. Med. Hyg.*, *94*(1), 17–21.

Girum, T. (2014). Prevalence of malaria and associated factors among patients attending at hallaba health center, southern ethiopia. *Immunol. Infect. Dis.*, *2*(3), 25–29.

Girum, T., Shumbej, T., & Misgun, S. (2019). Burden of malaria in ethiopia, 2000–2016: Findings from global health estimates 2016. *Trop. Dis. Travel Med. Vaccines*, *5*(1), 11.

Graves, P., Richards, F., & Ngondi, J. (2009). Individual, household and environmental risk factors for malaria infection in amhara, oromia and snnp regions of ethiopia. *Trans. R. Soc. Trop. Med. Hyg.*, *103*(12), 1211–1220.

Loha, E. (2013). *Variation in malaria transmission in southern ethiopia: The impact of prevention strategies and a need for targeted intervention* [Doctoral dissertation, University of Bergen].

Mushashu, U. (2012). *Prevalence of malaria infection among under-fives and the associated factors in muleba district-kagera region tanzania* [MSc Thesis]. Muhimbili University of Health and Allied Sciences.

Seble, A. (2014). *The prevalence of malaria and the associated risk factors in jiga area, northwest ethiopia* [MSc Thesis]. Addis Ababa University.

Sintasath, D., Ghebremeskel, T., Lynch, M., Kleinau, E., Bretas, G., Shililu, J., Brantly, E., Graves, P., & Beier, J. (2005). Malaria prevalence & associated risk factors in eritrea. *Am J Trop Med Hyg.*, *72*(6), 682–687.

Stratton, L., O'Neill, M., Kruk, M., & Bell, M. (2008). The persistent problem of malaria: Addressing the fundamental causes of a global killer. *Soc. Sci. Med.*, *67*(5), 854–862.

Tafese, H., Hemming-Schroeder, E., Koepfi, C., Tesfaye, G., Lee, M., Kazura, J., Yan, G., & Zhou, G. (2018). Malaria epidemiology and interventions in ethiopia from 2001 to 2016.

Tsige, K., Kefelegn, G., & Ketema, B. (2011). Therapeutic efficacy of chloroquine for treatment of plasmodium vivax malaria cases in halaba district, south ethiopia. *Parasites and Vectors*, *4*(1), 46.

WHO (World Health Organization). (2012). *World malaria report 2012*. Geneva, WHO.

WHO (World Health Organization). (2016). *World malaria report*. Geneva, WHO.

Yamamoto, S., Louis, V., Sie, A., & Sauerborn, R. (2010). Household risk factors for clinical malaria in a semi-urban area of burkina faso: A case–control study. *Trans. R. Soc. Trop. Med. Hyg.*, *104*(1), 61–65.

Yarcho, Y. (2010). *The effect of social and environmental variability on malaria epidemiology and transmission in some selected village around arbaminch towns' southern ethiopia* [MSc Thesis]. Haramaya University.

Zhou, G., Yewhalaw, D., Lo, E., Zhong, D., Wang, X., Degefa, T., Zemene, E., Lee, M., Kebede, E., Tushune, K., & Yan, G. (2016). Analysis of asymptomatic and clinical malaria in urban and suburban settings of southwestern ethiopia in the context of sustaining malaria control and approaching elimination. *Malaria J.*, *15*, 250.

East Afr. J. Biophys. Comput. Sci. (2026), Vol. 7, Issue. 1, 34-42

East African Journal of Biophysical and Computational Sciences

ISSN (Online): 2789-3618 and ISSN (Print): 2789-360X

ARTICLE

Feeding Habits and Trace Metal Concentrations in Organs of the Nile Catfish, *Synodontis schall* (Bloch & Schneider) (Pisces: Mochokidae), in Lake Abaya, Ethiopia

Elias Dadebo [1], Daniel WM-Bekele[2], Abnet Woldesenbet [1], Tamirat Handago[3], Tekleweyni Asayehegn[1], Tiruken Aziz[1], and Teshome Belay [4,*]

[1]Department of Aquatic Sciences, Fisheries and Aquaculture, Hawassa University, P. O. Box 5, Hawassa, Ethiopia
[2]Biology Department, Environmental Toxicology Program, Hawassa University, P. O. Box 5, Hawassa, Ethiopia
[3]Department of Biology, Wachemo University, PO Box 667, Hosaena, Ethiopia
[4]Department of Animal Sciences, Dilla University, PO Box 419, Dilla, Ethiopia.

[*]Corresponding author: teshimeansc@gmail.com

ARTICLE INFO
Volume 7(1), 2026
https://dx.doi.org/10.4314/eajbcs.v7i1.4S

ARTICLE HISTORY
Received: 14 April, 2026
Accepted: 26 May, 2026
Published Online: 10 June, 2026

CITATION
Dadebo et.al (2026). Feeding Habits and Trace Metal Concentrations in Organs of the Nile Catfish, *Synodontis schall* (Bloch & Schneider) (Pisces: Mochokidae), in Lake Abaya, Ethiopia . *East African Journal of Biophysical and Computational Sciences* Volume 7(1), 2026. .https://dx.doi.org/10.4314/eajbcs.v7i1.4S.34-42

Abstract

This study investigated the feeding habits and trace metal concentrations in different organs of the Nile catfish, *Synodontis schall*, in Lake Abaya, Ethiopia. Stomach content analysis was conducted using frequency of occurrence and volumetric analysis. The results of the study indicated that *S. schall* is an omnivore with polyphagous feeding habits; dominant food categories included phytoplankton, detritus, insects, zooplankton, and macrophytes. Seasonal shifts were observed: phytoplankton was the primary food source during the dry season, whereas zooplankton predominated during the wet season. Ontogenetic dietary shifts were also noted with juveniles consuming mainly phytoplankton and zooplankton, while adults mainly fed insects, detritus and phytoplankton. Trace metal analysis identified copper (Cu), cadmium (Cd), nickel (Ni), zinc (Zn), and manganese (Mn) in liver, kidney and muscle tissues, while lead (Pb) and cobalt (Co) were not detected. Metal concentrations in the liver were ranked as Cu > Zn > Mn > Ni > Cd, while in muscle and kidney tissues, the order was Zn > Cu > Mn > Ni > Cd. Significant difference ($p < 0.05$) in mean concentrations of Cu, Cd, and Zn were noted among tissues. All detected heavy metals were within the FAO and EU safety limits, suggesting that *S. schall* from Lake Abaya is safe for human consumption.

Keywords: Feeding habits; Lake Abaya; Omnivory; *S. schall*; Trace metals

East African Journal of Biophysical and Computational Sciences (EAJBCS) is already indexed on known databases like AJOL, DOAJ, CABI ABSTRACTS and FAO AGRIS.

1 Introduction

The genus Synodontis is widely distributed across African freshwaters ranging from the Nile basin, Chad, Niger, and much of the West African region (Paugy et al., 2003) (Cuvier, 1816,). In Ethiopia, the Nile catfish *Synodontis schall* (Bloch and Schneider, 1801) is found in Lakes Abaya and Chamo in the south, the Baro River and its tributaries in the west, and in the Wabishebele River in the southeast (Golubtsov & Habteselassie, 2010; Golubtsov et al., 1995). Generally, *S. schall* is classified as an omnivore and benthic fish species, and its diet covers a wide spectrum of food ranging from plankton to invertebrates and plants (Lalèyè et al., 2006). This dietary flexibility, combined with a high tolerance for adverse environmental conditions, allows the species to remain abundant

in most African fresh waters (Lowe-Mcconnell, 1987).

In Lake Abaya, *S. schall* is abundant in both littoral and pelagic environments, likely due to low predation and minimal fishing pressure (Dadebo et al., 2012) . While the species is among the most favored edible fishes in some African countries (Lalèyè et al., 2006), it currently holds low commercial importance in Lake Abaya. Although, it remains ecologically indispensable as a primary prey species for the commercially significant catfish, *Bagrus docmac* (Forsskål, 1775) (Anja & Mengistou, 2001). Previous studies across Africa have highlighted the species' opportunistic feeding nature (Adeyemi, 2010; Akombo et al., 2014; Arame et al., 2021; Dadebo et al., 2012). Yongo et al. (2019) reviewed the feeding habits of some *Synodontis* species in African freshwaters, and reported that the genus feeds on a variety of food items, including vegetable materials, insects, mollusks, detritus, macrophytes, fish scales, and plankton. In Quémé River, the most frequent food items in the stomachs of *S. schall* were macrophytes, algae, crustaceans, rotifers, and mollusks (Lalèyè et al., 2006). Ofori-Danson (1992) reported that the frequent food items of *S. schall* in the Kpong head pond were benthic macroinvertebrates. Adeosun et al. (2017) indicated the importance of insects, rotifers, crustaceans, fish parts and phytoplankton in the diet of *S. schall*.

Beyond ecological dynamics, the health of fish populations is increasingly threatened by the accumulation of trace metals from natural and anthropogenic sources (Ali & Khan, 2018). Because fish occupy various trophic levels, they can accumulate toxic substances in vital organs and muscle tissues, posing risks not only to aquatic biota but also to human consumers through trophic transfer (Garai et al., 2021). Given the benthic feeding habits of *S. schall*, it is particularly susceptible to metals associated with lake sediments.

Despite its ecological importance, there is lack of information regarding the biology and ecology of *S. schall* in Ethiopia. To the knowledge of the researchers, there is no published data regarding the feeding habits and heavy metal load in the organs of *S. schall* specifically within Lake Abaya. Therefore, the aim of this study was to investigate the dietary patterns and concentrations of trace metals in different organs of this species. Such information is vital for future management of the fish stock for assessing the environmental health of the Lake Abaya ecosystem.

2 Materials and Methods

2.1 Study Area

Lake Abaya is the second largest lake in Ethiopia and geographically located between 5°55′9″ and 6°35′30″ N latitude, and 37°36′90″ and 38°03′45″ E longitude in the southern part of the Ethiopian Rift Valley, East of the Guge Mountains (Figure 1) (Shishitu, 2024) . The lake is fed on its northern shore by the Bilate River, which rises on the southern slope of mount Gurage (Golubtsov & Habteselassie, 2010). Other rivers that drain in to the lake include, Gelana, Milate, Gidabo, Harre, Baso, and Amesa. The only outflow of the lake is through the lower reaches of Kulfo River directly below an alluvial pan at an elevation of 1,190 m. Arba Minch town lies on its southwestern shore and the southern shores are part of the Nechisar National Park (Teffera et al., 2019).

Lake Abaya has a length of 79 km, a width of 29 km, and a surface area of 1,160 km2 (Baxter, 2002). It has a maximum depth of 13 m and is located at an elevation of 1,268 m (Baxter, 2002; Grove et al., 1975). Lake Abaya is a home to 21 different fish species that have economic and ecological roles (Golubtsov & Habteselassie, 2010).

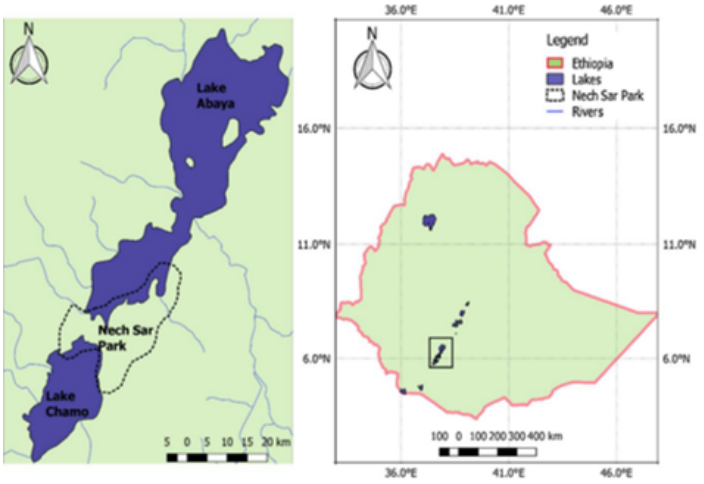

Figure 1: Geographic location of Lake Abaya (Source: adopted from Shishitu, 2024)

2.2 Sampling and Measurements

A total of 849 *S. schall* specimens were collected during the dry season (January to February, 2020) and the wet season (June to July, 2020) (wet season). Sampling was conducted at both littoral and pelagic sites of the lake using a beach seine (25 m long and three meters wide with a mesh size of 0.6 cm) in the shallow littoral area and Nordic survey multi-mesh monofilament nylon gillnets (Appelberg et al., 1995) at the pelagic area of the lake.

The multi-mesh gillnets consisted of twelve randomly distributed panels of the mesh sizes 5, 6.25, 8, 10, 12.5, 15.5, 19.5, 25, 29, 35, 43, and 53 mm (bar mesh). Each panel was 2.5 m long, and hence the total length of each net was 30 m. The gillnets were set between three to five meters depths in the open water, about 1.5 km inward from the littoral sampling station. The gillnets were set early in the morning around 7.00 a.m. local time and pulled around 3.00 p.m. in the afternoon.

For each specimen, fork lengths (FL) and standard length (SL) were measured to the nearest mm using a measuring board. Total weight (TW) was measured to the nearest 0.1g using a SCALTEC digital balance (model 23565, USA). The stomach of each fish was split open, and the contents were collected and preserved in 5% formalin solution and transported to Hawassa University Fishery Laboratory for further analysis.

2.3 Stomach Content Analysis

The stomach contents of each specimen were examined visually to identify macroscopic food items, whereas a dissecting microscope (Leica, MS5, magnification- 40x) and a compound microscope (Leica DME, magnification- 1000x) were used to identify microscopic food items. Quantitative analysis of the diet

was conducted using frequency of occurrence and volumetric methods of analyses.

Frequency of occurrence (%FO): the number of stomach samples containing one or more individuals of each food category was expressed as a percentage of all stomachs containing food (Hyslop, 1980). In volumetric analysis (%V), the food items found in each stomach were sorted into different food categories, and the water displaced by the group of volume of items in each category was measured (Bowen, 1996). The relative importance of each category was then expressed as a percentage of the total volume of food categories.

2.4 Ontogenetic Dietary Shift and Dietary Overlap

To assess ontogenetic dietary shifts, specimens were categorized into five size classes (Class I: 5- 9.9 cm; Class II: 10-14.9 cm; Class III: 15-19.9 cm; Class IV: 20-24.9 cm; Class V: 25- 29.9 cm). The total volume of food items in each size class was determined and volumetric contribution of each category of food items was then expressed as a percentage of total volume of food consumed in each size class. The dietary overlap between different size-classes was calculated as percentage overlap using the Schoener Diet Overlap Index (SDOI) (Schoener, 1970; Wallace Jr, 1981) based on Eq.(1) :

$$\alpha = 100[l - 0.5]\left(\sum_{i=1}^{n} |P_{xi} - P_{yi}|\right) \quad (1)$$

where α is percentage overlap SDOI, between size group x and y, Pxi and Pyi are proportions of food category (type) i used by size group x and y, and n is the total number of food categories. Diet overlap in the index is generally considered to be strong dietary similarity and overlap when α value exceeds 0.60 (Mathur, 1977; Zaret & Rand, 1971).

2.5 Fish Samples Collection and Preservation for Determination of Heavy Metals

A total of 20 *S. schall* specimens were collected from Lake Abaya for heavy metal analysis using gill nets and a beach seine. For each specimen, fork length (FL) and total weight (TW) of each fish were recorded to the nearest 0.1 cm and 0.1 g, respectively. Fish dissection for muscle, kidney, and liver samples followed the EMERGE protocol, ensuring proper handling (Gupta & Mullins, 2010). The separated organs and muscles were quickly wrapped in aluminum foil and then placed in plastic bags. These bags were subsequently stored in an icebox and transported to the deep freezer at Hawassa University Laboratory. Finally, the samples were preserved at a temperature of -20 °C in the deep freeze.

2.6 Sample Preparation for Atomic Absorption Spectroscopy (AAS) Analysis

Muscle, liver, and kidney tissues were mechanically crushed with a stainless steel knife and partially air-dried overnight. They were then fully dried in a laboratory oven at 175°C for three hours and processed separately except for Pb and Cd. For Pb and Cd 60°C were considered. A solution of aqua regia (3:1 hydrochloric to nitric acid) was prepared as per Nwani et al. (2010). One gram of dried muscle and 0.5 grams of liver and kidney were added to a 100 ml flask with 10 ml of aqua regia and refluxed overnight to dissolve organic materials and release trace metals, following Muinde et al. (2013) method. After refluxing, samples were digested at 60°C for three hours to enhance reaction kinetics. Each sample was digested in triplicates and diluted to a final volume in a 50 ml volumetric flask and filtered with the attached monochromater filter.

2.7 Determination of Heavy Metals

The digested fish organ and muscle were analyzed for Cd, Co, Cu, Mn, Ni, Pb, and Zn using flame atomic absorption spectrometry (FAAS) with a dual background correction system (BUCK SCIENTIFIC, Model 210VGP, USA). An air-acetylene flame was employed, utilizing aqueous calibration standards from stock solutions of the metals. Three standard solutions and a blank solution, made from the acid used in digestion, were prepared to minimize errors and avoid overestimating heavy metal concentrations due to contamination. The trace metal concentrations in the organs were calculated by subtracting the levels in the stock solution from those measured in the acid. Each sample was aspirated into the FAAS for direct readings, and the blank was created by combining all reagents in a 50 ml volumetric flask and diluting with deionized water. Finally, the FAAS was adjusted with the following detection limit capacity of the element as Cd (0.03 mg/kg), Co (0.02 mg/kg), Cu (0.005 mg/kg), Mn (0.03 mg/kg), Ni (0.02 mg/kg), Pb (0.03 mg/kg), and Zn (0.005 mg/kg), respectively.

2.8 Statistical Analysis

The chi-square test was employed to compare the variations of the frequency of occurrence of the different food categories during the dry and wet seasons (Worms and Touati, 2017). For volumetric data, the Mann-Whitney U test was used to assess seasonal differences (Worms & Touati, 2017). This non-parametric test was used because the data violated the assumption of homogeneity of variance required for parametric test. For the comparisons of ontogenetic dietary overlap between different size classes, their schooner dietary overlap index was considered depending on the benchmark (0.6). The concentration of considered trace metals from the muscle, kidney, and liver of *S. schall* was compared using one-way analysis of variance with the aid of SPSS v20 software at a 95% confidence interval.

3 Results

3.1 Diet Composition

From a total of 849 *S. schall* specimens examined, 751 (88.5%) contained food, while 98 (11.5%) had empty stomachs. The sampled fish ranged in size from 5.4 to 33.0 cm in fork length and weighed between 2.6 and 566 g in total weight. The diet of *S. schall* in Lake Abaya was diverse, consisting of phytoplankton,

zooplankton, insects, macrophytes, detritus, ostracods, nematodes, hydracarina and fish scales at different proportion (Table 1). Of these, the frequency of occurrences of detritus, insects, macrophytes, zooplankton and phytoplankton were identified as major food categories, while ostracods, nematodes, fish scales and Hydracarina were found to be of minor importance (Table 1). Volumetrically, the contributions of Phytoplankton (31.20%), detritus (20.10%), insects (16.80%), zooplankton (13.40%) and macrophyte (12.80%) were dominant as a diet of *S. schall*. While, the volumetric contributions of other identified food categories were negligible (Table 1).

Table 1: Diet Compositions of *S. schall* (n = 751) in Lake Abaya, Ethiopia

	Frequency of occurrences		**Volumetric contribution**	
Food type	**FO**	**%FO**	**VC(ML)**	**%VC**
Phytoplankton	**352**	**46.90**	**154.70**	**31.20**
Blue green algae	236	31.40	87.23	17.60
Green algae	57	7.60	8.72	1.80
Diatoms	133	170	58.51	11.80
Euglinoids	3	0.40	0.20	0.04
Zooplankton	**411**	**54.70**	**66.42**	**13.40**
Cladocera	343	45.70	58.35	11.80
Calanoid copepods	87	11.60	6.11	1.20
Cyclopoid copepods	35	4.70	1.76	0.40
Rotifera	5	0.70	0.19	0.04
Insects	**484**	**64.40**	**83.24**	**16.80**
Diptera	354	47.10	50.90	10.30
Ephemeroptera	101	13.40	8.70	1.80
Plecoptera	80	10.70	12.01	2.40
Coleoptera	59	7.90	4.35	0.90
Hymenoptera	23	3.10	1.32	0.30
Tricoptera	8	1.10	1.52	0.30
Anisoptera	7	0.90	4.12	0.80
Hemiptera	8	1.10	0.12	0.02
Macrophytes	**431**	**57.40**	**63.54**	**12.80**
Detritus	**490**	**65.20**	**99.77**	**20.10**
Ostracods	**203**	**27.00**	**22.26**	**4.50**
Hydracarina	**10**	**1.30**	**0.23**	**0.05**
Nematodes	**93**	**12.40**	**3.38**	**0.68**
Fish scales	**14**	**1.90**	**3.02**	**0.60**

3.2 Seasonal Variation in the Diet Composition

Significant seasonal variations were observed in the diet of *S. schall* in Lake Abaya (Table 2). The frequency of occurrence of phytoplankton and zooplankton significantly varied during the dry (64.80%) and wet (29.30%) seasons (x^2 test, $p < 0.05$; Table 2). The occurrences of insects (68.8%), phytoplanktons (64.8%), detritus (62.20%), and macrophytes (53.3%) were the major food items of *S. schall* during dry season. While, during wet season, the occurrences of zooplanktons (70.50%), detritus (68.20%), and macrophytes (58.80%) were the three most ingested food items of *S. schall*. The remaining food categories in both dry and wet seasons were negligible (Table 2). Volumetrically, during dry season the contribution of phytoplankton (41.20%), detritus (19.60%), insects (17.40%), and macrophytes (13.10%) were the major food categories of *S. schall*. On the other hand, during wet season, zooplankton (26.40%), detritus (21.00%), phytoplanktons (18.33%) were the dominant food categories of *S. schall*. The contributions of other food categories were relatively low (Table 2).

Table 2: Diet Compositions of *S. schall* during the Dry (n = 304) and Wet (n = 447) Seasons in Lake Abaya.

	Frequency of occurrence (%)		Volumetric contribution (%)	
Food items	**Dry**	**Wet**	**Dry**	**Wet**
Phytoplankton	**64.80**	**29.30**	**41.20**	**18.33**
Blue green algae	48.40	12.80	28.60	3.60
Green algae	13.20	3.10	2.80	0.40
Diatoms	17.80	18.30	9.80	14.30
Euglinoids	-	-	-	-
Zooplankton	**28.60**	**70.50**	**3.00**	**26.40**
Cladocera	10.50	69.60	0.80	25.40
Copepoda	22.40	7.60	2.20	0.90
Rotifera	-	0.90	-	0.20
Insects	**68.80**	**59.50**	**17.41**	**15.94**
Diptera	61.50	37.40	13.00	6.80
Ephemeroptera	10.90	15.40	1.70	2.80
Plecoptera	2.30	15.90	0.50	3.80
Coleoptera	3.00	11.20	0.30	1.70
Hymenoptera	5.90	1.10	0.40	0.10
Tricoptera	-	1.10	-	0.70
Anisoptera	2.30	-	1.50	-
Hemiptera	0.70	0.90	0.010	0.040
Macrophytes	**53.60**	**58.80**	**13.10**	**12.5**
Detritus	**62.20**	**68.20**	**19.60**	**21.00**
Ostracods	**203**	**25.50**	**4.60**	**4.30**
Hydracarina	**-**	**2.20**	**-**	**0.05**
Nematodes	**4.30**	**17.90**	**0.10**	**0.580**
Fish scales	**3.00**	**1.10**	**1.00**	**0.90**

3.3 Ontogenetic Diet Shift and Dietary Overlap

The diet of *S. schall* exhibited distinct changes across the five size classes (Figure 1). *S. schall* in size class 5-9.9 cm FL widely relied on phytoplankton (60.3%) and zooplankton (17.4%) compared to the contributions of other identified food categories (Figure 1). When *S. schall* attained 10-14.9 cm FL size class, the importance of detritus, insects, macrophytes and ostracods increased while the contributions of phytoplankton and zooplankton decreased (Figure 2). As the fish grew to the 15-19.9 cm FL size range, it relied mainly on phytoplankton (30.6%), detritus (19.8%), insects (17.4%), macrophytes (12.4%) and ostracods (4.1%). When the fish further grew to 20-24.9 cm FL size range, it mainly consumed phytoplankton (25.6%), detritus (21.5%), insects (18.2%), macrophytes (11.6%) and ostracods (4.1%) (Figure 2). The major food categories of the largest size class (25-29.9 cm FL) were phytoplankton (45.5%), macrophytes (17.4%), detritus (16.5%) and insects (16.1%) by volume (Figure 2). Other food categories, namely fish scales and zooplankton had negligible role and unimportant in the diet of the largest size class.

The Schoener Diet Overlap Index (SDOI) indicated significant diet similarity (> 60%) between several size classes, with the highest overlap observed between classes III and IV (α = 93.3%) and II and III α = 81.8%). Other significant overlaps were recorded for combinations III and V (α = 79.9%), IV and V (α = 77.8%), II and V (α = 69.0%), I and IV (α α = 66.9%), and I and V (α = 65.1%) (Table 3). In contrast, diet overlap was not biologically significant for size classes I and II (α = 52.0%), I and III (α = 58.8%), and II and IV (α = 55.0%), suggesting a higher degree of dietary partitioning among these groups.

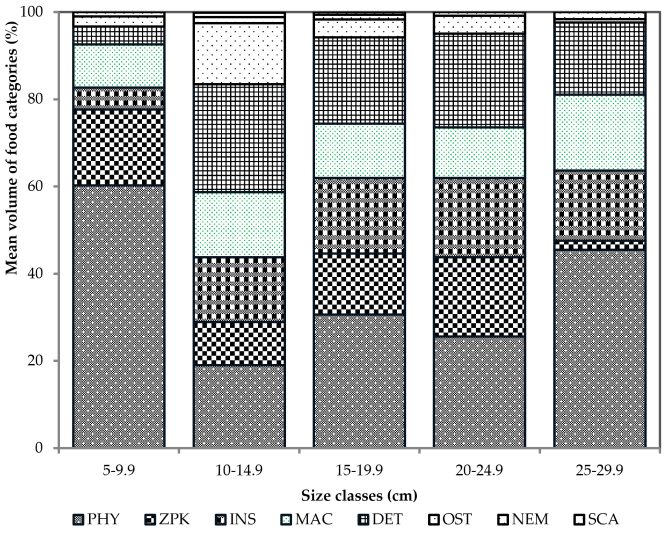

Figure 2: Mean volume of food items consumed by different size class of *S. schall* sampled from Lake Abaya.

Table 3: Schoener Diet Overlap Index (SDOI) in five size classes of *S. schall* from Lake Abaya, Ethiopia

Size class	SDOI (%)
I and II	52.0
I and III	58.8
I and IV	65.1*
I and V	66.9*
II and III	81.8*
II and IV	55.0
II and V	69.0*
III and IV	93.3*
III and V	79.6*
IV and V	77.8*

*indicated SDOI value showed strong dietary overlap between considered size classes

3.4 Concentration of Some Heavy Metals in Muscle, Liver and Kidney

The concentrations of seven heavy metals in liver, muscle, and kidney tissues of *S. schall* from Lake Abaya are summarized in Table 3. The findings indicated that five heavy metals - Cu, Cd, Ni, Zn, and Mn - were detected in all tissue types at levels exceeding the analytical detection limits (see the detection limit from material and method at sub section of determination of heavy metals). Conversely, Pb and Co were found at levels below the detection threshold of the equipment, as detailed in Table 4. The distribution of metals in the liver was ranked as Cu > Zn > Mn >Ni > Cd, while in the muscle and kidney tissues, the order was Zn > Cu > Mn > Ni > Cd.

Mean concentrations exhibited significant tissue specific variations (Table 3). The mean concentration of Cu was notably higher in the liver (3.847±0.341 mg/kg DW) compared to the kidney (1.211±0.168 mg/kg DW) and muscle (0.944±0.028 mg/kg DW). Similarly, Zn levels were elevated in the liver (1.85±0.153 mg/kg DW) relative to the kidney (1.38±0.179 mg/kg DW) and muscle (1.26±0.169 mg/kg DW). Conversely, more Cd concentration was detected in the kidney (0.03±0.006 mg/kg DW), followed by the liver (0.017±0.002 mg/kg DW) and muscle (0.011±0.00). The mean concentrations of Cu in muscle (0.94), kidney (1.21), and liver (3.85) exhibited significant differences ($p < 0.05$). Likewise, Cd levels in muscle (0.01), kidney (0.03), and liver (0.02) also showed significant variation ($p < 0.05$). The mean Zn concentrations in muscle (1.26), kidney (1.38), and liver (1.85) indicated significant differences ($p < 0.05$). In contrast, the concentrations of Ni and Mn did not show significant differences ($p > 0.05$) across the three tissues.

Table 4: Mean concentrations of trace metals in muscle, kidney and liver (mean concentration in mg/kg dry weight ± standard error) of *S. schall* in Lake Abaya.

Element	Muscle	Kidney	Liver
Cu	0.94 ± 0.028^{a}	1.21 ± 0.168^{a}	3.85 ± 0.341^{b}
Cd	0.01 ± 0.000^{a}	0.03 ± 0.006^{b}	0.02 ± 0.002^{a}
Ni	0.05 ± 0.006^{a}	0.05 ± 0.007^{a}	0.04 ± 0.006^{a}
Zn	1.26 ± 0.169^{a}	1.38 ± 0.179^{a}	1.85 ± 0.153^{b}
Mn	0.07 ± 0.008^{a}	0.09 ± 0.011^{a}	0.09 ± 0.009^{a}
Pb	ND	ND	ND
Co	ND	ND	ND

Note: Superscript represented by different letters indicate significant difference ($p < 0.05$), ND–Not detected.

3.5 Discussion

The results of the present study indicated that *S. schall* feeds on various food items including phytoplankton, zooplankton, insects, detritus, macrophytes, ostracods, nematodes, fish scales and Hydracarina in Lake Abaya (Table 1). From the various food items, phytoplankton, detritus, insects, zooplankton and macrophytes were the major food items while ostracods, nematodes, fish scales and Hydracarina were of minor importance. Various authors studied the feeding habits of *S. schall* and reported its polyphagous nature. Hickley and Bailey (1987) studying *S. schall* in the Sudd Swamps of River Nile (Sudan) have pointed out the importance of detritus, benthic algae, macrophytes, benthic crustaceans, insects and fish scales in its diet. Ofori-Danson (1992) working on the ecology of some *Synodontis* species in Kpong Head-pond (Ghana) have reported the dominant food items of *S. schall* as detritus, insects, oligochaets, nematodes and Hirudinae. Dadebo et al. (2012) reported a similarly diverse diet for *S. schall* in Lake Chamo, including zooplankton, plant materials, insects, fish fry, fish eggs, gastropods, and fish scales. Moreover, various other workers studying the food and feeding habits of *S. schall* in different African water bodies have indicated the polyphagus nature of the species (Adeyemi, 2010; Akombo et al., 2014; Arame et al., 2021) .

The high frequency and substantial volumetric contributions of both plant materials and macro- invertebrates in the stomachs of *S. schall* were a good evidence for its omnivorous feeding habits in Lake Abaya. Various authors have also reported the omnivorous feeding habits of *S. schall* in different African inland water bodies. Baras and Laleye (2003) reported the omnivorous feeding habit of *S. schall* with a strong tendency to predation. Willoughby (1974) described *S. schall* as an omnivorous species feeding on insect larvae and nymph, fish eggs and detritus. Dadebo et al. (2012) also reported the omnivorous feeding habits of *S. schall* in Lake Chamo.

Seasonal variations in the diet of *S. schall* were observed during the present study (Table 2). During the dry season, the diet was dominated by phytoplankton, detritus, insects and macrophytes

(Table 2). The reason for the abundance of phytoplankton during the dry season might be attributed to higher light penetration and reduced water turbulence, which favor autotrophic production (Drakare et al., 2002). Detritus was the second important food of *S. schall* in the dry season (Table 2). The contribution of insects was considerable during the dry season (17.4%). Among insects, Diptera (Chironomidae larvae) was the most important contributing more than 70% by volume of all insect groups. This high contribution of Diptera was probably due to the ease of capture and also their ability to flourish in wide range of environmental conditions (Drakare et al., 2002). Ofori-Danson (1992) also reported the importance of Diptera and other insects in the diet of S, schall in the Kpong Head-pond in Ghana.

Macrophytes were ingested in considerable quantities during the dry season. It is probable that the fish might ingest part of macrophytes incidentally as they pursue their prey in the littoral region where the prey normally seek refuge from predators (Thomaz et al., 2025). More focused study is needed to determine the importance of macrophytes to the nourishment of the species by comparing the nutritive values of the plant fragments in the fore and hind guts of the fish (Thomaz et al., 2025). During the wet season, the contributions of zooplanktons were dominated and widely represented by Daphnia (Table 2). The reason for this was probably due to seasonal reproductive cycle of the cladocerans population, which often peak during rainy season in tropical lakes (Choedchim et al., 2017). Detritus was also an important food item during the wet season. The source of this food category could be the floods that introduce different plant materials into the lake and plant leaves falling into the lake and undergoing partial decomposition. Araoye (1999) reported that the contribution of plant materials and detritus in the diet of *S. schall* during the wet season was high, and such food items were dispersed along the surface water column at this period due to floods and overturn.

From the results of the present study, it was evident that *S. schall* showed a clear ontogenetic dietary shift during its life cycle (Figure 1). Smaller individuals relied widely on phytoplankton and zooplankton, whereas larger fish incorporated more insects, detritus, and macrophytes. Bishai and GideirI (1965) reported that some members of the genus *Synodontis* switch from benthic feeding to surface feeding or vice versa by using ventrally positioned mouth depending on food availability and their size. According to Lalèyè et al. (2006), large size *S. schall* browse on benthic deposit as can be seen from the presence of detritus and mud in the stomachs of large fish. The same authors also noted the importance of fish scales in the diet of *S. schall* as its size increases. Similarly, Dadebo et al. (2012) reported that fish scales become important food items in large size *S. schall* in the neighboring Lake Chamo. Bishai and GideirI (1965) found a significant difference between the diets of large and small *S. schall* in Khartoum. Several other investigators also demonstrated that *S. schall* showed an ontogenetic diet shift as a result of the change in habitat use in different water bodies (Araoye, 1999; Dadebo et al., 2012; Ofori-Danson, 1992). The other probable factor for such dietary variations across size classes might be aligned with the habitat that they survive. Juvenile *S. schall* hide themselves from the risk of predators (Baras & Laleye, 2003). Similar to the present finding, Araoye (1999) and Dadebo et al. (2012) reported that, fry and fingerlings of *S. schall* were usually restricted to the flooded littoral zone of the lake where they feed mainly on zooplankton, insect larvae and other macro-invertebrates.

The concentrations of the five heavy metals detected were generally higher in the kidney and liver compared to muscle tissue (Table 5). For example, Cu levels were elevated in the liver relative to both the kidney and muscle tissues, consistent with findings of Gerenfes et al. (2019) for Enteromious species in Lake Chamo, Ethiopia and Shahid et al. (2016) for *Cyprinus carpio*. This distribution can be explained by the liver's function in detoxification and synthesis of copper-binding metallothioneins, highlighting its role as a crucial bio-indicator for evaluating Cu levels in aquatic ecosystems (Javed & Usmani, 2013). In terms of Cd levels, *S. schall* from Lake Abaya exhibited a muscle tissue concentration of 0.01 mg/kg, which is higher than that of bream (0.009 mg/kg) and mandarin fish (0.0009 mg/kg) from Poyang Lake (Wei et al., 2014). Additionally, Cd concentrations ranging from 0.001 to 0.009 mg/kg were identified in eleven fish species from Rio de Janeiro State, Brazil (Medeiros et al., 2012), but the finding in this study is lower than the 0.03 to 1.57 mg/kg detected in fish from the Pearl River Delta (Cheung et al., 2008). All observed concentrations of the detected heavy metals fall below the limits set by the EU (2001), TFC (2002) and FAO (1983) guideline for human consumption.

Table 5: Comparisons of Concentration of Trace Metals in Fish Muscle Relative to the Standards (mg/kg dry weight).

Parameter (guidelines)	Cu	Zn	Mn	Cd	Ni	References
Present study in fish muscle	0.94	1.26	0.07	0.01	0.05	
FAO	30	50	30	–	–	FAO (1983)
EU	4	–	–	–	–	EU (2002)
Turkish Food Codex	20	50	20	–	–	TFC (2002)

4 Conclusion

This study has clearly shown that *S. schall* in Lake Abaya ingests a wide range of plant based and animal origin of food categories. However, the diet composition of *S. schall* was different based on their size classes and season of sampling. With the exception of some size classes, strong dietary overlap was seen across different size classes. Trace metals analysis revealed that Cu, Cd, Ni, Zn, and Mn were found in all three tissues, while Pb and Co were absent. In the liver, the concentration ranking was Cu > Zn > Mn > Ni > Cd, whereas in muscle and kidney tissues, it was Zn > Cu > Mn > Ni > Cd. From the present study, *S. schall* is an omnivorous in its feeding strategy. Overall, heavy metal concentrations were generally higher in the kidney and liver than in muscle. The level in muscle showed below FAO and EU maximum acceptable limits for human consumption. The present result

suggested conducting further metal analysis is required based on simultaneous study including water quality analysis, sediment analysis, and the interaction between feeding ecology with trace metal concentration for further comparisons.

Conflict of Interest

None declared.

Funding

This research was supported by NORAD project

Acknowledgements

The authors are grateful to the Department of Aquatic Sciences, Fisheries and Aquaculture for providing laboratory facilities and the logistics for the field trips. Dr. Andargachew Gedebo, NORAD project coordinator and Hawassa University are acknowledged for providing a vehicle for the field trips. We thank fisherman Asaminew Matte for his assistance during sample collection.

References

Adeosun, O., Adebayo, A., Ajayi, S., & Olabode, G. (2017). Gas chromatography-mass spectrometric (gc-ms) analysis of ethanolic extract of the peel of dioscorea bulbifera linn (air potatoe). *Journal of Natural Sciences Research*, *7*, 1281–1286. https://core.ac.uk/download/pdf/234657521.pdf

Adeyemi, S. O. (2010). Food and feeding habits of synodontis resupinatus (boulenger, 1904) at idah area of river niger, kogi state, nigeria. *Animal Research International*, *7*, 1281–1286. https://www.ajol.info/index.php/ari/article/view/79781

Akombo, P., Akange, E., Adikwu, I., & Araoye, P. (2014). Length-weight relationship, condition factor and feeding habits of synodontis schall (bloch and schneider, 1801) in river benue at makurdi, nigeria. *International Journal of Fisheries and Aquatic Studies*, *1*, 42–48. https://doi.org/10.1016/j.ejar.2018.11.004

Ali, H., & Khan, E. (2018). Bioaccumulation of non-essential hazardous heavy metals and metalloids in freshwater fish. risk to human health. *Environmental chemistry letters*, *16*, 903–917. https://doi.org/10.1007/s10311-018-0734-7

Anja, H., & Mengistou, S. (2001). Food and feeding habits of the catfish, bagrus docmak (forsskal, 1775) (pisces: Bagridae) in lake chamo, ethiopia. *SINET: Ethiopian Journal of Science*, *24*, 239–254. https://doi.org/10.4314/sinet.v240.18189

Appelberg, M., Berger, H.-M., Hesthagen, T., Kleiven, E., Kurkilahti, M., Raitaniemi, J., & Rask, M. (1995). Development and intercalibration of methods in nordic freshwater fish monitoring. *Water, Air, and Soil Pollution*, *85*, 401–406. https://doi.org/10.1007/BF00476862

Arame, H., Adite, A., Adjibade, K. N., Imorou, R. S., Sossoukpe, E., & Stanislas, S. P. (2021). Food habits, ecomorphological patterns and niche breadth of the squeaker, synodontis schall (pisces: Siluriformes: Mochokidae) from niger river in northern benin. *International Journal of Aquatic Biology*, *9*, 41–54. https://doi.org/10.22034/ijab.v9i1.973

Araoye, P. (1999). Spatio-temporal distribution of the fish synodontis schall (teleostei: Mochokidae) in asa lake, ilorin, nigeria. *Revista de biología tropical*, *47*, 1061–1066. https://doi.org/10.15517/rbt.v47i4.19311

Baras, E., & Laleye, P. (2003). Ecology and behavior of catfish. In G. Arratia, B. G. Kapoor, M. Chardon, & R. Diogo (Eds.), *Catfish*. Science Publishers.

Baxter, R. (2002). In: Ethiopian rift valley lakes. In C. Tudorancea & W. D. Taylor (Eds.). Backhuys Publishers.

Bishai, H., & GideirI, Y. (1965). Studies on the biology of the genus synodontis at khartoum: Ii. food and feeding habits. *Hydrobiologia*, *26*, 98–113. https://doi.org/10.1007/BF00731551

Bowen, S. H. (1996). Quantitative description of the diet. In *Fisheries techniques* (2nd, pp. 513–532). American Fisheries Society.

Cheung, K., Leung, H., & Wong, M. H. (2008). Metal concentrations of common freshwater and marine fish from the pearl river delta, south china. *Archives of environmental contamination and toxicology*, *54*, 705–715. https://doi.org/10.1007/s00244-007-9064-7

Choedchim, W., Van-Damme, K., & Maiphae, S. (2017). Spatial and temporal variation of cladocera in a tropical shallow lake. *International Journal of Limnology*, *53*, 233–252. https://doi.org/10.1051/limn/2017006

Dadebo, E., Gebre-Mariam, Z., & Ahlgren, G. (2012). Feeding habits of the catfish synodontis schall (bloch & schneider)(pisces: Mochokidae) with emphasis on its scale-eating habits in lake chamo, ethiopia. *Ethiopian Journal of Biological Sciences*, *11*, 117–132.

Drakare, S., Blomqvist, P., Bergström, A. K., & Jansson, M. (2002). Primary production and phytoplankton composition in relation to doc input and bacterioplankton production in humic lake örträsket. *Freshwater Biology*, *47*, 41–52. https://doi.org/10.1046/j.1365-2427.2002

EU. (2002). Commission's regulation as regards heavy metal directive 2001 ec no. 466/2001.

FAO. (1983). *Compilation of legal limits for hazardous substances in fish and fishery products* (tech. rep. No. FAO Fishery Circular No. 464).

Garai, P., Banerjee, P., Mondal, P., & Saha, N. (2021). Effect of heavy metals on fishes: Toxicity and bioaccumulation. *Journal of Clinical Toxicology*, *18*, 001. https://www.longdom.org/open-access/effect-of-heavy-metals-on-fishes-toxicity-and-bioaccumulation-82260.html

Gerenfes, D., Teju, E., & Kebede, T. (2019). Selected metal (fe, cu and zn) levels in fish and water at abaya and chamo rift valley lakes. *Biochemistry and Molecular Biology*, *4*, 17–27. https://doi.org/10.11648/j.bmb.20190402.11

Golubtsov, A. S., Darkov, A. A., Dgebua, Y. Y., & Mina, M. V. (1995). An artificial key to fish species of gambella region, addis ababa, joint ethio-russian biological expedition. https://www.librarycat.org/lib/newcrossbooks/item/92429599

Golubtsov, A. S., & Habteselassie, R. (2010). Fish faunas of the chamo-abaya and chew bahir basins in southern portion of the ethiopian rift valley: Origin and prospects for survival. *Aquatic Ecosystem Health & Management*, *13*, 47–55. https://doi.org/10.1080/14634980903578506

Grove, A. T., Street, F. A., & Goudie, A. (1975). Former lake levels and climatic change in the rift valley of southern ethiopia. *Geographical Journal*, *141*, 177–194. https://doi.org/10.2307/1797205

Gupta, T., & Mullins, M. C. (2010). Dissection of organs from the adult zebrafish. *Journal of Visualized Experiments*, *37*, 1717. https://doi.org/10.3791/1717

Hickley, P., & Bailey, R. (1987). Food and feeding relationships of fish in the sudd swamps (river nile, southern sudan). *Journal of Fish Biology*, *30*, 147–159. https://doi.org/10.1111/j.1095-8649.1987.tb05741.x

Hyslop, E. (1980). Stomach contents analysis—a review of methods and their application. *Journal of fish biology*, *17*, 411–429. https://doi.org/10.1111/j.1095-8649.1980.tb02775.x

Javed, M., & Usmani, N. (2013). Assessment of heavy metal (cu, ni, fe, co, mn, cr, zn) pollution in effluent dominated rivulet water and their effect on glycogen metabolism and histology of mastacembelus armatus. *SpringerPlus*, *2*, 390. https://doi.org/10.1186/2193-1801-2-390

Lalèyè, P., Chikou, A., Gnohossou, P., Vandewalle, P., Philippart, J.-C., & Teugels, G. (2006). Studies on the biology of two species of catfish synodontis schall and synodontis nigrita (ostariophysi: Mochokidae) from the ouémé river, bénin. *Belgian Journal of Zoology*, *136*, 193–201. https://agris.fao.org/search/en/providers/122397/records/64747068425ec3c088f1b96f

Lowe-Mcconnell, R. H. (1987). *Ecological studies in the in tropical fish communities*. Cambridge University Press.

Mathur, B. C. (1977). Book reviews. *Indian Journal of Public Administration*, *23*, 423–425. https://doi.org/10.1177/0019556119770225

Medeiros, R. J., Dos santos, L. M. G., Freire, A. S., Santelli, R. E., Braga, A. M. C., Krauss, T. M., & Jacob, S. D. C. (2012). Determination of inorganic trace elements in edible marine fish from rio de janeiro state, brazil. *Food control*, *23*, 535–541. https://doi.org/10.1016/j.foodcont.2011.08.027

Muinde, V., Nguu, E., Ogoyi, D., & Shiundu, P. M. (2013). Effects of heavy metal pollution on ω3 polyunsaturated fatty acids levels in tilapia fish from winam gulf of lake victoria. *The Open Environmental Engineering Journal*, *6*, 22–31. https://doi.org/10.2174187482950130601002 2

Nwani, C. D., Nwachi, D., Okogwu, O., Ude, E., & Odoh, G. (2010). Heavy metals in fish species from lotic freshwater ecosystem at afikpo, nigeria. *Journal of Environmental Biology*, *31*, 595–601. https://europepmc.org/article/MED/21387908

Ofori-Danson, P. K. (1992). Ecology of some species of catfish synodontis (pisces: Mochocidae) in the kpong headpond in ghana. *Environmental biology of fishes*, *35*, 49–61. https://doi.org/10.1007/BF00001157

Paugy, D., Lévêque, C., & Teugels, G. G. (2003). *Faune des poissons d'eaux douces et saumâtres de l'afrique de l'ouest* (Vol. 2). IRD (Paris), MHN (Paris), MRAC (Tervuren). https://pascal-francis.inist.fr/vibad/index.php?action=getRecordDetail&idt=16360680

Schoener, T. W. (1970). Nonsynchronous spatial overlap of lizards in patchy habitats. *Ecology*, *51*, 408–418. https://doi.org/10.2307/1935376

Shahid, M., Shazia, K., Farhat, J., Sultana, S., Sultana, T., Al-ghanim, K., Bilal, H., Al-Misned, F., & Ahmed, Z. (2016). Effect of heavy metals on liver, kidney, gills and muscles of cyprinus carpio and wallago attu inhabited in the indus. *Brazilian Journal of Biology*, *59*, 16150275. https://doi.org/10.1590/1678-4324-2016150275

Shishitu, B. (2024). Length-based estimates of growth parameters and mortality rates of nile tilapia (oreochromis niloticus, l. 1758) in lake abaya, southern ethiopia. *East African Journal of Biophysical and Computational Sciences*, *5*, 51–67.

Teffera, F. E., Lemmens, P., Deriemaecker, A., Deckers, J., Bauer, H., Gamo, F. W., Brendonck, L., & De Meester, L. (2019). Why are lake abaya and lake chamo so different? a limnological comparison of two neighboring major ethiopian rift valley lakes. *Hydrobiologia*, *829*, 113–124. https://doi.org/10.1007/s10750-018-3707-8

TFC. (2002). Turkish food codes [Official Gazette, 23 September 2002, No. 24885].

Thomaz, S., Cardozo, A., Quirino, B., Yofukuji, K., Aleixo, M., & Fugi, R. (2025). A review of the ecological role of aquatic macrophytes on freshwater fish. *Hydrobiologia*, *852*(13), 3257–3290. https://doi.org/10.1007/s10750-025-05819-z

Wallace Jr, R. K. (1981). An assessment of diet-overlap indexes. *Transactions of the American Fisheries Society*, *110*, 72–76. https://doi.org/10.1557/1548.8659

Wei, Y., Zhang, J., Zhang, D., Tu, T., & Luo, L. (2014). Metal concentrations in various fish organs of different fish species from poyang lake, china. *Ecotoxicology and environmental safety*, *104*, 182–188. https://doi.org/10.1016/j.ecoenv.2014.03.001

Willoughby, N. G. (1974). *The ecology of the genus synodontis (pisces: Silaroidei) in lake kainji, nigeria* [Doctoral dissertation, University of Southampton]. https://eprints.soton.ac.uk/458942/

Worms, J., & Touati, S. (2017). *Parametric and non-parametric statistics for program performance analysis and comparison* (tech. rep. No. RR-8875). INRIA Sophia Antipolis - I3S. https://inria.hal.science/hal-01286112

Yongo, E., Iteba, J., & Agembe, S. (2019). Review of food and feeding habits of some synodontis fishes in african freshwaters. *Oceanography and Fisheries*, *10*, 27–31. https://doi.org/10.19080/FOAJ.2019.10.555781

Zaret, T. M., & Rand, A. S. (1971). Competition in tropical stream fishes: Support for the competitive exclusion principle. *Ecology*, *52*, 336–342. https://doi.org/10.2307/1934593

East African Journal of Biophysical and Computational Sciences
ISSN (Online): 2789-3618 and ISSN (Print): 2789-360X

ARTICLE

ARTICLE INFO
Volume 7(1), 2026
https://dx.doi.org/10.4314/eajbcs.v7i1.5S

ARTICLE HISTORY
Received: 03 March, 2026
Accepted: 04 June June, 2026
Published Online: 10 June, 2025

CITATION
Teferi H.T (2026). Intuitionistic Fuzzy Multi-objective Optimization Method for Determination of Optimal Cropping Pattern. *East African Journal of Biophysical and Computational Sciences* Volume 7(1), 2026. .https://dx.doi.org/10.4314/eajbcs.v7i1.5S.43-63

OPEN ACCESS

Intuitionistic Fuzzy Multi-objective Optimization Method for Determination of Optimal Cropping Pattern

Habtamu Tsegaye Teferi [1,*]

[1] Department of Mathematics, College of Natural and Computational Sciences, Wolkite University, Ethiopia

*Corresponding author: hbtmtsgy@gmail.com

Abstract

Agriculture has become a difficult occupation due to inadequate farming resources and cultivation risks. Thus, proficient utilization of resources alongside risk-alleviation strategies is essential aspect to realize sustainable farm benefits. Most of the earlier studies have reported the capability of Operations research in solving agricultural problems and enhancing farm productivity. However, they have not addressed effectively the distinctive nature of decision-makers, uncertainties, and associated risks of agriculture. This study mainly aims to fill these lacunae by applying an intuitionistic fuzzy optimization method to determine optimal cropping pattern that maximizes overall net benefits, minimizing cultivation costs and workforce concurrently with regard to procurable agricultural resources. For this purpose, an effective multi-objective optimization method is formulated, and its effectiveness is verified through proof and numerical example. The comparison between existing and proposed cropping patterns showed that the proposed patterns offer several advantages in enhancing overall agricultural benefits sustainably for farmers in the study area.

Keywords: Multi-objective optimization; Intuitionistic fuzzy optimization; Agricultural production planning; Cropping pattern.

1 Introduction

Today, the burgeoning world's population increases the demand for agricultural products and this in turn increasing pressure on the resources required for production (Wang, 2022). However, to meet the ever-escalating demand for nourishment, crop production must be boosted either by increasing land area for cultivation or by enhancing production per unit area of land (FAO, 2017; Mirkarimi et al., 2013). Since agricultural resources for farming are very limited all over the world (Guo et al., 2021), increasing land area for crop production regardless of limiting factors causes deterioration of available resources. Moreover, climate change, drought, political disputes, and disease are holding back agricultural advancement and remain key determinants of food security and poverty alleviation (Luo et al., 2023; Zerssa et al., 2021). Therefore, it is crucial to design means of efficient utilization of resources and risk alleviation strategies to improve the overall agricultural returns sustainably.

In this regard, the decision of agricultural stakeholders has its own impact on the achievement of the desired objectives. Even if decision-making for the optimum utilization of resources is a challenging task for farmers and agricultural managers, it can be scientifically addressed using optimization models to support farm activities and contribute to feeding the steadily growing population (Carravilla & Oliveira, 2013; Weintraub & Romero, 2006).

Agriculture is the primary sector of the Ethiopian economy, employing approximately 85% of the country's population as workers (Zerssa et al., 2021). It contributes 50% of Ethiopia's gross domestic product and earns over 90% of the foreign exchange (Haile & Kasa, 2015; Zerssa et al., 2021). The country's goal for achieving overall economic growth mainly depends on the accomplishment of agriculture sector (Haile & Kasa, 2015).

Despite the country's vast irrigable land and water resources, farming is weather dependent and the production of which depends heavily on the availability of rainfall (Awulachew & Ayana, 2011). Consequently, most farmers are exposed to inconsistent rainfall patterns and weather conditions (Zerssa et al., 2021). Even though Ethiopia is vulnerable to the vagaries of natural weather conditions, it has substantial agricultural potential because of its vast areas of fertile land, enormous labor, abundant water resources, and diverse climate conditions (Awulachew & Ayana, 2011; Kelbore, 2014).

Due to seasonal variation, Ethiopia has three distinct seasons: Kiremt

(June – September), Bega (October – January), and Belg (February – May) (Gebremichael et al., 2014). Kiremt is the main rainy season, accounting for about 90% of agricultural production, while Bega is dry and Belg is a short rainy season contributing the remaining 10% of production (Kelbore, 2014).

A cropping pattern is the proportion of land area under various crops that changes over space and time (G. Singh, 2012). It is the annual succession of different crops and fallow in a particular region and can be reported at the farm level to address the collective issues of a farming system (Andrews & Kassam, 1976).

The principal objective of optimal cropping pattern (OCP) is to identify the combination of several crops to be cultivated which maximizes the net return of farming by managing agricultural risks with respect to available resources (Ouda et al., 2017).

As the population grows, agricultural resources have been decreasing and the situation worsens with the spread of drought (Carravilla & Oliveira, 2013). These circumstances continue to generate many agricultural inquiries in search for more productive alternatives on a given land area for the optimal utilization of other agricultural resources (Paudel, 2016). Therefore, OCP is one of the important and feasible mechanisms to increase productivity with other integrated scientific agricultural practices (Luo et al., 2023; Ouda et al., 2017).

Determining the OCP remains a complex task for farmers and managers (Pawar et al., 2026), as decisions on machinery selection, input use, operation timing, and cultivation practices must be made in each cropping season (Duan et al., 2021).

In Ethiopia, where most farmers practice traditional agriculture, these decisions are largely based on experience, fluctuating market prices, and other operational factors (Kelbore, 2014). Conversely, policies and guidelines delivered through extension services often fail to account for multiple agricultural objectives and constraints, such as weather variability and production risk. Therefore, more effective strategies are required through the use of optimization models.

The problem of optimizing multiple goals simultaneously under given constraints is called multi-objective optimization (MOO). It involves concurrent optimization of incommensurate and conflicting goals subject to different constraints (V. Singh & Yadav, 2018).

Many real-life problems are inherently characterized by multiple and conflicting goals with uncertainties (Gupta et al., 2000). So, it is difficult to deal with such problems using classical optimization techniques. Hence, intuitionistic fuzzy sets (IFSs) can be used to represent insufficient information, imprecise concept, uncertainties and the diverse perspectives of decision-makers (DMs) in a more generalized way compared to fuzzy sets (Roszkowska et al., 2024). Thus, intuitionistic fuzzy modelling is more relevant than other classical optimization methods (Pawar et al., 2026).

Several researchers have attempted to address agricultural production planning (APP) problems employing various MOO methods to recommend an alternative cropping system for improved outcomes (Luo et al., 2023; Weintraub & Romero, 2006). However, the ambiguity of the parameters in the problem, inconsistent natural conditions, the distinctive perspective of DMs, and associated operational risks in agriculture have not been well addressed in their studies.

To overcome the above difficulties, it is imperative to formulate an effective optimization model and design OCP at the farm level by considering the available resources to assist sustainable crop production.
This study aims to investigate the application of an intuitionistic fuzzy multi-objective optimization (IFMOO) model and to propose OCP for the study area that improves farmers' welfare concerning scarce resources and reduces various challenges of farming.

The rest of this paper is organized as follows. In Section 2, the related literature is reviewed. The optimization method for addressing the practical problem is outlined in Section 3. A comparative analysis of the proposed method is presented in Section 4. Section 5 provides the model application in three subsections: study area description, data collection and analysis, and problem formulation. A detailed analysis of the results is given in Section 6. Section 7 summarizes the findings, discusses limitations, and provides recommendations for future research.

2 Literature Review

Agriculture is one of the fields where Operations research (OR) models were first employed and they have been extensively applied (Rădulescu et al., 2014). The capability of addressing MOO problems for decision-making helps out OR to play a fundamental role in agriculture (Rădulescu et al., 2014; Weintraub & Romero, 2006).

Carravilla and Oliveira (2013) reviewed studies demonstrating the applications of OR in agriculture at farm and sector levels. Depending on problem complexity, some used linear programming (LP), while others employed multi-objective and fuzzy optimization models to address APP problems.

Weintraub and Romero (2006) demonstrated the potential of OR in the management of agricultural resources and forestry, and their advantages in simplifying DM in farming activities. In their article, the applications of OR in APP problems at the farm and regional levels were comprehensively reviewed. They address uncertainties, risks, environmental conservation, and discuss future research directions in these areas.

Environmental, social, and economic factors make agricultural data inherently uncertain (Bairwa et al., 2013), leading to decision-making under ill-defined objectives and constraints (Li et al., 2017). Accordingly, risks in agriculture are better represented with fuzzy numbers than crisp values, prompting the development and application of fuzzy multi-objective optimization (FMOO) methods to handle APP problems.

Although many researchers employed FMOO approaches to deal with APP problems (Amini, 2015; Biswas & Pal, 2005; Gupta et al., 2000; Mirajkar & Patel, 2012; Mirkarimi et al., 2013; Rasikh et al., 2024; Wang, 2022; X. Zeng et al., 2010) their studies were limited in scope and did not represent the real nature of the problems very well (Mahapatra & Roy, 2009). This is due to insufficient information, incomplete attributes, ill-definedness, uncertainties, and vagueness in every aspect of MOO problems (Sen et al., 2018). Consequently, different advanced generalizations are ascertained. From that, IFS, which is originated by Atanassov (1986), is an effective generalization of fuzzy sets. It has been used in a wide range of operations because of its ability to address uncertainties and vagueness in practical problems. Thus, intuitionistic fuzzy optimization (IFO) (Angelov, 1995) was introduced to handle different pragmatic problems.

IFO technique is a relatively recent research field in contrast to fuzzy optimization approaches (Angelov, 1995). It enhances understanding of the addressed problems and provides valuable insights into their nature (Roszkowska et al., 2024). Moreover, the output of an investigation employing IFO is a more valuable analytical means for researchers, practitioners, and experts.

In APP problem, interactions among various natural entities and correlated factors complicate the management process. These factors enforce DMs to use advanced optimization models for proficient usage of resources and to gain better overall benefits.

Nishad and Singh (2015) employed an intuitionistic fuzzy goal programming to resolve the land use planning problem. They considered the agricultural system undertaken by Biswas and Pal, 2005 in which several seasonal crops were cultivated in a year and different productive resources are taken into account in the model. Their study revealed that IFO method gives better results in all aspects compared to the results obtained by the fuzzy optimization method.

Li et al. (2017) formulated an IFMOO model that incorporates MOO, nonlinear programming (NLP) and intuitionistic fuzzy number (IFN) to deal with the uncertainties of conflicting targets in irrigated agriculture to support sustainable farming. They employed an IFMOO model to allocate limited accessible water to rice during growth stages to maximize crop yield, minimize utilized water and cost of water supply in Heping irrigation area of northeast China.

Li et al. (2019) used a multi-objective NLP model in an intuitionistic fuzzy environment (IFE) for the management of the water-energy-food nexus in irrigational agriculture, considering the cropping system of the Heihe River basin in northwest China. In their study, both optimistic and pessimistic views of DMs were considered under different scenarios to maximize system profit and minimize carbon dioxide emissions, subject to water, energy, land, and other input resources for cultivating wheat, corn, and vegetables in the three regions of the basin.

Pawar et al., 2022 applied an IFMOO method to determine the OCP of the Ukai irrigation area in India. Their approach combined minimizing the aggregated hesitation level of objectives with maximizing the minimum membership degree and minimizing the maximum non-membership degree. This produced an OCP that maximized net returns and employment, while minimizing farming expenditures under constraints of arable land and irrigation water.

Li et al., 2020 developed an optimization model for sustainable irrigated agriculture combining IFMOO, nonlinear mixed-integer, and fuzzy credibility-constrained programming. Their study aimed to allocate water and farmland to crops across subareas and seasons to optimize net returns while considering socioeconomic and ecological objectives. The algorithm was successfully applied to crop planning in the Heping irrigation area of China.

Kousar et al., 2022 formulated an IFO method considering all parameters and variables as IFN to optimize the production of five types of fruits in Baluchistan region, Pakistan.Their results showed that the fully IFO technique has an imperative advantage to consider the fluctuating nature of prices and input resources more efficiently.

L. Zeng et al. (2020) studied sustainable resource management for the Zhanghe Reservoir irrigation in central China using an interval stochastic multi-objective mixed-integer model in an IFE. Their objectives were to maximize crop production, hydroelectricity, and water allocation while optimizing cropland under constraints of water availability, crop demand, land policy, and electricity generation. The results demonstrated efficient farmland and water management to support food security and mitigate global warming sustainably.

A few researchers have used IFMOO models to handle uncertainties and risks in APP problems. As noted above, investigators have applied various IFMOO techniques to suggest alternative cropping patterns for better outcomes. However, they have not effectively addressed differences among DMs, uncertainties, and risks that severely affect crop production.
For instance, in most studies, parameters are not consistently considered as IFNs, constraints are not incorporated into the solution framework, DM preferences and stakeholder interactions are overlooked, and the sustainability of objectives is inadequately addressed.

To overcome these shortcomings, the present study formulates an IFMOO model to design an OCP that maximizes sustainable net benefits for a large-scale farm (LSF) and farmers in Gefersa kebele. It also aids farmers, development agents, and extension workers in complex decision-making under multiple perspectives and scenarios for a LSF in Abeshge district.

3 IFO Method

3.1 Preliminaries

Definition 3.1.1 (Atanassov, 1986). An IFS $\tilde{A}$ in the universe X is given by $\tilde{A} = \{\langle x, \mu_{\tilde{A}}(x), \nu_{\tilde{A}}(x)\rangle : x \in X\}$, where $\mu_{\tilde{A}}(x), \nu_{\tilde{A}}(x), \pi_{\tilde{A}}(x)$: $X \to [0,1]$ such that
$0 \le \mu_{\tilde{A}}(x) + \nu_{\tilde{A}}(x) \le 1$ and $\pi_{\tilde{A}}(x) = 1 - (\mu_{\tilde{A}}(x) + \nu_{\tilde{A}}(x))$,
$\forall x \in X$. The values $\mu_{\tilde{A}}(x)$, $\nu_{\tilde{A}}(x)$ and $\pi_{\tilde{A}}(x)$ describe the degree of membership, non-membership, and indeterminacy of x being in $\tilde{A}$, respectively.
Definition 3.1.2 (Mahapatra & Roy, 2009). A triangular IFN $\tilde{A}$ is an IFS, represented as $\tilde{A} = \langle a_1, a_2, a_3; a_1', a_2, a_3'\rangle$, where $a_1' \le a_1 \le a_2 \le a_3 \le a_3'$, with

$$\mu_{\tilde{A}}(x) = \begin{cases} \frac{x-a_1}{a_2-a_1}, & \text{if } a_1 < x \le a_2 \\ \frac{a_3-x}{a_3-a_2}, & \text{if } a_2 \le x < a_3 \\ 0, & \text{otherwise,} \end{cases}$$

and

$$\nu_{\tilde{A}}(x) = \begin{cases} \frac{a_2-x}{a_2-a_1'}, & \text{if } a_1' < x \le a_2 \\ \frac{x-a_2}{a_3'-a_2}, & \text{if } a_2 \le x < a_3' \\ 1, & \text{otherwise.} \end{cases}$$

Definition 3.1.3 (S. K. Singh & Yadav, 2015a).
Let $\tilde{A} = \langle a_1, a_2, a_3; a_1', a_2, a_3'\rangle$ be a triangular IFN, the accuracy function of $\tilde{A}$ is denoted by $\Gamma(\tilde{A})$ and defined as $\Gamma(\tilde{A}) = \frac{a_1'+a_1+4a_2+a_3+a_3'}{8}$.
Accuracy function Γ is used to defuzzify IFNs.

In handling of practical problems, vagueness and uncertainty can be addressed in an IFE by considering parameters as IFNs and treating inequality and equality as intuitionistic fuzzy inequalities and equality. Based on this principle, an IFMOO problem is formulated (V. Singh & Yadav, 2018)

$$\begin{aligned} &\max\{\widetilde{f_1}(X), \widetilde{f_2}(X), ..., \widetilde{f_{k_1}}(X)\}, \\ &\min\{\widetilde{f_{k_1+1}}(X), \widetilde{f_{k_1+2}}(X), ..., \widetilde{f_k}(X)\} \\ &\qquad \text{subject to} \\ &\widetilde{g_i}(X) \precsim \widetilde{c_i},\ i = 1, 2, \ldots, m_1, \\ &\widetilde{g_i}(X) \succsim \widetilde{c_i},\ i = m_1+1, m_1+2, \ldots, m_2, \\ &\widetilde{g_i}(X) \approx \widetilde{c_i},\ i = m_2+1, m_2+2, \ldots, m, \\ &X \ge 0, \end{aligned} \tag{1}$$

where $\widetilde{f_j}(X)$ and $\widetilde{g_i}(X)$ are intuitionistic fuzzy functions, X is n-dimensional variable $\forall j = 1, 2, ..., k$ and $\forall i = 1, 2, ..., m$.

To reformulate problem (1) as an equivalent crisp MOO problem, each parameter has to be defuzzified applying the accuracy function (Rădulescu et al., 2014). Then, the degrees of acceptance and rejection of the objectives have to be described to form a single objective optimization problem. Accordingly, the solution of the IFMOO problem can be found by solving such an equivalent single objective problem (S. K. Singh & Yadav, 2015b).

The IFMOO problem (1) can be changed into the following equivalent deterministic MOO problem (V. Singh & Yadav, 2018):

$$\begin{aligned} &\max\{f_1(X), f_2(X), ..., f_{k_1}(X)\}, \\ &\min\{f_{k_1+1}(X), f_{k_1+2}(X), ..., f_k(X)\} \\ &\qquad \text{subject to} \\ &g_i(X) \le c_i,\ i = 1, 2, \ldots, m_1, \\ &g_i(X) \ge c_i,\ i = m_1+1, m_1+2, \ldots, m_2, \\ &g_i(X) = c_i,\ i = m_2+1, m_2+2, ..., m, \\ &X \ge 0, \end{aligned} \tag{2}$$

where $f_j(X)$ and $g_i(X)$ are real-valued functions and $c_i \in \mathbb{R}$, $\forall j = 1, 2, ..., k$ and $\forall i = 1, 2, ..., m$.

Definition 3.1.4 (Cristofari et al., 2024). Let $\mathbb{S}$ be the set of all feasible solutions of problem (2), and let $X, X^* \in \mathbb{S}$. Then, X^* is said to be a Pareto optimal solution (POS) for problem (2) if and only if there does not exist $X \in \mathbb{S}$ such that $f_j(X^*) \leq f_j(X)$, $\forall j = 1, 2, \ldots, k_1$, and $\exists j \in \{1, 2, \ldots, k_1\}$ such that $f_j(X^*) < f_j(X)$.

Theorem 3.1.1 (Xu & Cai, 2012; Xu & Yager, 2006).
Let $\tilde{I}_j = (\mu_{\tilde{I}_j}, \nu_{\tilde{I}_j})$, $j = 1, 2, ..., k$ be a collection of intuitionistic fuzzy values, and let $w_1, w_2, ..., w_k$ be the corresponding weights, where $w_j \in (0, 1)$ and $\sum_{j=1}^{k} w_j = 1$. Then, the aggregated value using the intuitionistic fuzzy weighted geometric (IFWG) operator is given by

$$\text{IFWG}_w(\tilde{I}_1, \tilde{I}_2, ..., \tilde{I}_k) = \left(\prod_{j=1}^{k} \mu_{\tilde{I}_j}^{w_j}, 1 - \prod_{j=1}^{k} (1 - \nu_{\tilde{I}_j})^{w_j} \right) \tag{3}$$

3.2 The Solution Method

Most existing studies consider the optimistic variant of the problem (Kis et al., 2021), paying little attention to alternative perspectives in the solution process. However, this consideration has its own limitations in addressing practical problems. Due to the inconsistent nature of human judgment, DMs may deviate from their initial standpoint after evaluating the obtained solution against the intended goals. Consequently, existing methods overlook this important aspect of DM judgment and insights. Therefore, identifying the influence of optimistic, pessimistic, and mixed perspectives is highly valuable for obtaining consistent and robust solutions to MOO problems (Chen et al., 2023; Mahajan & Gupta, 2021b). The main difference among these three perspectives arises from the choice of violation and tolerance values used to determine the non-membership degrees, while the membership function remains identical across all cases.

In an IFE, parameter values, aspiration levels, coefficients of the objectives and constraints, as well as the equalities and inequalities in the model, are flexible. Consequently, the maximum and minimum allowable values of the constraints and objectives can vary.

To incorporate flexibility in the constraints, a violation parameter ℓ_i is associated with the ith constraint, $i = 1, 2, \ldots, m_1$, as specified by the DMs. For constraints of the form $\leq$, the upper bound c_i is relaxed to $c_i + \lambda(\ell_i)$ in the solution procedure (Tsegaye et al., 2021).

The membership and non-membership functions for each objective are described based on the difference between the maximum U_j and minimum L_j achievable goals, which are identified using a table of extreme solutions. Then, the tolerance variables δ_j and ζ_j are obtained by using

$$\delta_j = \lambda(U_j - L_j) \text{ and } \zeta_j = \lambda(U_j - (L_j - \delta_j)) = \delta_j(1 + \lambda) \text{ where } L_j = \min\{f_j(X)\}, U_j = \max\{f_j(X)\}, \text{ and } \lambda \in (0, 1), j = 1, 2, ..., k.$$

The membership and non-membership functions are generally characterized by nonlinear behavior due to instantaneous variation at each solution point. Among nonlinear functions, the exponential function is preferable for the IFMOO problem because of its efficiency and flexibility in evaluating the marginal values of objectives and constraints (Ahmadini & Ahmad, 2021; Mahajan & Gupta, 2021a). Accordingly, exponential membership and non-membership functions are formulated to describe the optimistic, pessimistic, and mixed features and to obtain an efficient solution for the IFMOO problem.

3.2.1 The optimistic approach

In the optimistic approach, DM takes a liberal view of rejection (V. Singh et al., 2021). Therefore, the linear membership ($\mu_{U_j}(f_j(X))$) and non-membership ($\nu_{U_j}(f_j(X))$) functions for the jth objective function $f_j(X)$ of the maximization problem are respectively described as follows:

$$\mu_{U_j}(f_j(X)) = \begin{cases} 0, & \text{if } f_j(X) \leq L_j \\ \frac{f_j(X) - L_j}{U_j - L_j}, & \text{if } L_j < f_j(X) < U_j \\ 1, & \text{if } f_j(X) \geq U_j, \end{cases} \tag{4}$$

and

$$\nu_{U_j}(f_j(X)) = \begin{cases} 1, & \text{if } f_j(X) \leq L_j - \delta_j \\ \frac{U_j - f_j(X)}{U_j - (L_j - \delta_j)}, & \text{if } L_j - \delta_j < f_j(X) < U_j \\ 0, & \text{if } f_j(X) \geq U_j, \end{cases} \tag{5}$$

where δ_j is a tolerance value of the jth objective and defined as $\delta_j = \lambda(U_j - L_j)$ and $\lambda \in (0, 1)$, $\forall j = 1, 2, ..., k_1$. If $U_j = L_j$, then we define $\mu_{U_j}(f_j(X)) = 1$.

The respective exponential membership function ($\mu^E_{U_j}(f_j(X))$) and non-membership function ($\nu^E_{U_j}(f_j(X))$) for the jth objective respectively defined as

$$\mu^E_{U_j}(f_j(X)) = \begin{cases} 0, & \text{if } f_j(X) \leq L_j \\ \frac{e^{-d_j((U_j - f_j(X))/(U_j - L_j))} - e^{-d_j}}{1 - e^{-d_j}}, & \text{if } L_j < f_j(X) < U_j \\ 1, & \text{if } f_j(X) \geq U_j, \end{cases} \tag{6}$$

and

$$\nu^E_{U_j}(f_j(X)) = \begin{cases} 1, & \text{if } f_j(X) \leq L_j - \delta_j \\ \frac{e^{-d_j((f_j(X) + \delta_j - L_j)/(U_j + \delta_j - L_j))} - e^{-d_j}}{1 - e^{-d_j}}, & \text{if } L_j - \delta_j < f_j(X) < U_j \\ 0, & \text{if } f_j(X) \geq U_j. \end{cases} \tag{7}$$

where, d_j is the shape parameter.

The linear membership and non-membership functions for minimization objectives can be described as

$$\mu_{L_j}(f_j(X)) = \begin{cases} 1, & \text{if } f_j(X) \leq L_j \\ \frac{U_j - f_j(X)}{U_j - L_j}, & \text{if } L_j < f_j(X) < U_j \\ 0, & \text{if } f_j(X) \geq U_j, \end{cases} \tag{8}$$

and

$$\nu_{L_j}(f_j(X)) = \begin{cases} 0, & \text{if } f_j(X) \leq L_j \\ \frac{f_j(X) - L_j}{(U_j + \delta_j) - L_j}, & \text{if } L_j < f_j(X) < U_j + \delta_j \\ 1, & \text{if } f_j(X) \geq U_j + \delta_j, \end{cases} \tag{9}$$

where δ_j is a tolerance value of the jth objective and defined as $\delta_j = \lambda(U_j - L_j)$ and $\lambda \in (0, 1)$, $\forall j = k_1 + 1, k_1 + 2, ..., k$. If $U_j = L_j$, then we define $\mu_{L_j}(f_j(X)) = 1$.

The corresponding exponential non-membership function ($\mu^E_{L_j}(f_j(X))$) and non-membership function ($\nu^E_{L_j}(f_j(X))$) for the jth objective respectively defined as

$$\mu^E_{L_j}(f_j(X)) = \begin{cases} 0, & \text{if } f_j(X) \leq L_j \\ \frac{e^{-d_j((f_j(X) - L_j)/(U_j - L_j))} - e^{-d_j}}{1 - e^{-d_j}}, & \text{if } L_j < f_j(X) < U_j \\ 1, & \text{if } f_j(X) \geq U_j, \end{cases} \tag{10}$$

and

$$\nu^E_{L_j}(f_j(X)) = \begin{cases} 1, & \text{if } f_j(X) \leq L_j \\ \frac{e^{-d_j((U_j + \delta_j - f_j(X))/(U_j + \delta_j - L_j))} - e^{-d_j}}{1 - e^{-d_j}}, & \text{if } L_j < f_j(X) < U_j + \delta_j \\ 0, & \text{if } f_j(X) \geq U_j + \delta_j. \end{cases} \tag{11}$$

Their general shape is shown in Figure 1.

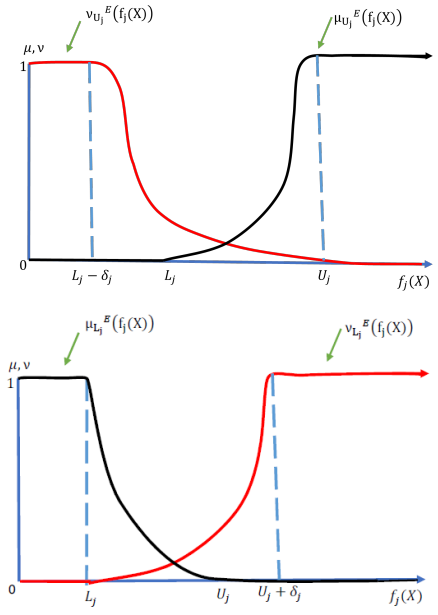

(a) (b)

Figure 1: Exponential membership and non-membership functions for maximization (a) and minimization (b) objectives under the optimistic approach.

3.2.2 The pessimistic approach

In the pessimistic approach, the DM is presumably extra cautious about acceptance (V. Singh et al., 2021). The linear non-membership function $\nu_{U_j}(f_j(X))$ of the jth objective $f_j(X)$ under a pessimistic approach to the maximization problem is expressed as

$$\nu_{U_j}(f_j(X)) = \begin{cases} 1, & \text{if } f_j(X) \le L_j \\ \frac{(L_j+\delta_j)-f_j(X)}{(L_j+\delta_j)-L_j}, & \text{if } L_j < f_j(X) < L_j + \delta_j \\ 0, & \text{if } f_j(X) \ge L_j + \delta_j, \end{cases} \tag{12}$$

$\forall j = 1, 2, \ldots, k_1$.
The corresponding exponential non-membership function $\nu^E_{U_j}(f_j(X))$ is defined as

$$\nu^E_{U_j}(f_j(X)) = \begin{cases} 1, & \text{if } f_j(X) \le L_j \\ \frac{e^{-d_j((f_j(X)-L_j)/\delta_j)}-e^{-d_j}}{1-e^{-d_j}}, & \text{if } L_j < f_j(X) < L_j + \delta_j \\ 0, & \text{if } f_j(X) \ge L_j + \delta_j. \end{cases} \tag{13}$$

The linear non-membership function $\nu_{L_j}(f_j(X))$ of the jth objective $f_j(X)$ under a pessimistic approach to the minimization problem is expressed as

$$\nu_{L_j}(f_j(X)) = \begin{cases} 0, & \text{if } f_j(X) \le U_j - \delta_j \\ \frac{f_j(X)-(U_j-\delta_j)}{U_j-(U_j-\delta_j)}, & \text{if } U_j - \delta_j < f_j(X) < U_j \\ 1, & \text{if } f_j(X) \ge U_j, \end{cases} \tag{14}$$

$\forall j = k_1 + 1, k_1 + 2, \ldots, k$.
The corresponding exponential non-membership function $\nu^E_{L_j}(f_j(X))$ is defined as

$$\nu^E_{L_j}(f_j(X)) = \begin{cases} 0, & \text{if } f_j(X) \le U_j - \delta_j \\ \frac{e^{-d_j(U_j-f_j(X))/\delta_j)}-e^{-d_j}}{1-e^{-d_j}}, & \text{if } U_j - \delta_j < f_j(X) < U_j \\ 1, & \text{if } f_j(X) \ge U_j. \end{cases} \tag{15}$$

Their possible shape is shown in Figure 2.

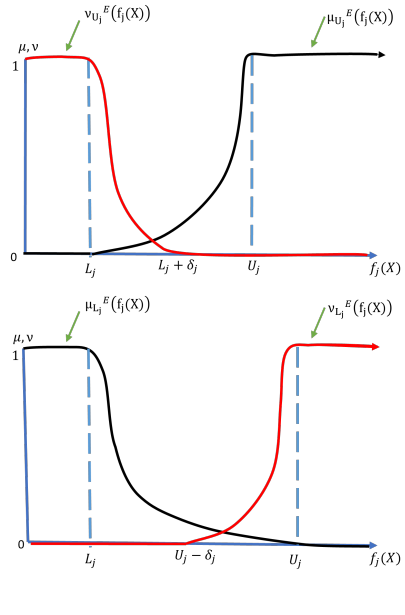

(a) (b)

Figure 2: Exponential membership and non-membership functions for maximization (a) and minimization (b) objectives under a pessimistic approach.

3.2.2 The mixed approach

In a mixed approach, the DM is not flexible in rejecting and is not capable of extra acceptance (V. Singh & Yadav, 2018). The linear non-membership function $\nu_{U_j}(f_j(X)))$ of the jth objective function $f_j(X)$ to the maximization problem is defined as

$$\nu_{U_j}(f_j(X)) = \begin{cases} 1, & \text{if } f_j(X) \le L_j - \delta_j \\ \frac{(L_j+\zeta_j)-f_j(X)}{(L_j+\zeta_j)-(L_j-\delta_j)}, & \text{if } L_j - \delta_j < f_j(X) < L_j + \zeta_j \\ 0, & \text{if } f_j(X) \ge L_j + \zeta_j, \end{cases} \tag{16}$$

where δ_j and ζ_j are the tolerance variables of the jth objective and defined as $\delta_j = \lambda(U_j - L_j)$,
$\zeta_j = \delta_j(1+\lambda)$, $\lambda \in (0,1)$, $j = 1, 2, \ldots, k_1$.
The corresponding exponential non-membership function $\nu^E_{U_j}(f_j(X))$ is constructed as

$$\nu^E_{U_j}(f_j(X)) = \begin{cases} 1, & \text{if } f_j(X) \le L_j - \delta_j \\ \frac{e^{-d_j((f_j(X)-(L_j-\delta_j))/(\zeta_j+\delta_j))}-e^{-d_j}}{1-e^{-d_j}}, & \text{if } L_j - \delta_j < f_j(X) < L_j + \zeta_j \\ 0, & \text{if } f_j(X) \ge L_j + \zeta_j. \end{cases} \tag{17}$$

The linear non-membership function $\nu_{L_j}(f_j(X)))$ of the jth objective function $f_j(X)$ to the minimization problem is defined as

$$\nu_{L_j}(f_j(X)) = \begin{cases} 1, & \text{if } f_j(X) \le U_j - \zeta_j \\ \frac{f_j(X)-(U_j-\zeta_j)}{(U_j+\delta_j)-(U_j-\zeta_j)}, & \text{if } U_j - \zeta_j < f_j(X) < U_j + \delta_j \\ 0, & \text{if } f_j(X) \ge U_j + \delta_j, \end{cases} \tag{18}$$

where δ_j and ζ_j are the tolerance variables of the jth objective and defined as $\delta_j = \lambda(U_j - L_j)$, $\zeta_j = \delta_j(1+\lambda)$, $\lambda \in (0,1)$, $j = k_1 + 1, k_1 + 2, \ldots, k$.
The corresponding exponential non-membership function $\nu^E_{L_j}(f_j(X))$ is constructed as

$$\nu^E_{L_j}(f_j(X)) = \begin{cases} 0, & \text{if } f_j(X) \le U_j - \zeta_j \\ \frac{e^{-d_j((U_j+\delta_j)-f_j(X))/(\zeta_j+\delta_j))}-e^{-d_j}}{1-e^{-d_j}}, & \text{if } U_j - \zeta_j < f_j(X) < U_j + \delta_j \\ 1, & \text{if } f_j(X) \ge U_j + \delta_j. \end{cases} \tag{19}$$

Their general shape is shown in Figure 3.

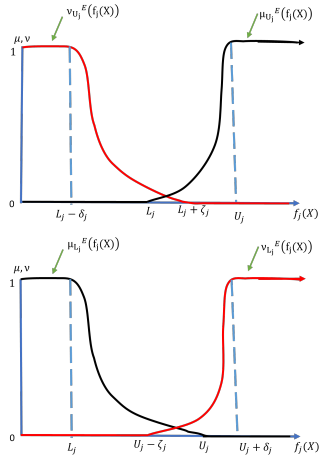

(a) (b)

Figure 3: Exponential membership and non-membership functions for maximization (a) and minimization (b) objectives under the mixed approach.

After converting an IFMOO problem into its equivalent crisp MOO problem using the accuracy function (S. K. Singh & Yadav, 2015a), the membership and non-membership functions are constructed based on the DMs' viewpoints. Accordingly, aggregation operators have been proposed (Mahajan & Gupta, 2021b; S. K. Singh & Yadav, 2015b; V. Singh & Yadav, 2018) to combine the membership and non-membership functions. However, such aggregation methods have certain limitations, as they fail to consider for both the satisfaction and dissatisfaction associated with all objectives. To address this limitation, the IFWG operator, previously applied to various multicriteria decision-making problems, is extended in this study to the MOO problem.

To formulate a single aggregation operator based on Theorem 3.1.1, a multiplicative combination is employed to integrate the independently defined degrees of acceptance and rejection. This approach helps to emphasize the interaction between the two degrees. Accordingly, the aggregation operator can be expressed as

$$\begin{aligned} Z(\mu,\nu) &= \left(\prod_{j=1}^{k}\mu_j^{w_j}\right)\times\left(1-(1-\prod_{j=1}^{k}(1-\nu_j)^{w_j})\right) \\ &= \left(\prod_{j=1}^{k}\mu_j^{w_j}\right)\times\left(\prod_{j=1}^{k}(1-\nu_j)^{w_j}\right) \end{aligned} \tag{20}$$

Therefore, the IFMOO problem (1) can be solved using an equivalent crisp model by employing the aggregation operator (20) as follows:

$$\begin{aligned} &\max \left(\prod_{j=1}^{k}\alpha_{o_j}^{w_j}\right)\times\left(\prod_{j=1}^{k}(1-\beta_{o_j})^{w_j}\right) \\ &\text{subject to} \\ &\mu_{U_j}^{E}(f_j(X)) \geq \alpha_{o_j},\ j=1,2,\ldots,k_1 \\ &\mu_{L_j}^{E}(f_j(X)) \geq \alpha_{o_j},\ j=k_1+1,k_1+2,\ldots,k \\ &\nu_{U_j}^{E}(f_j(X)) \leq \beta_{o_j},\ j=1,2,\ldots,k_1 \\ &\nu_{L_j}^{E}(f_j(X)) \leq \beta_{o_j},\ j=k_1+1,k_1+2,\ldots,k \\ &0 \leq \alpha_{o_j}+\beta_{o_j} \leq 1,\ j=1,2,\ldots,k_1,k_1+1,k_1+2,\ldots,k \\ &0 \leq \beta_{o_j} \leq \alpha_{o_j},\ j=1,2,\ldots,k_1,k_1+1,k_1+2,\ldots,k \\ &g_i(X) \leq c_i+\lambda(\ell_i),\ i=1,2,\ldots,m_1 \\ &X \geq 0, \end{aligned} \tag{21}$$

where w_j is the weight assigned to the jth objective such that $w_j \in (0,1)$ and $\sum_{j=1}^{k} w_j = 1$.

Problem (21) can be expressed based on the DM's perspectives, using the membership and non-membership functions constructed from Sections 3.2.1 to 3.2.3, as presented below.

From an optimistic viewpoint, problem (21) can be expressed as

$$\begin{aligned} &\max \left(\prod_{j=1}^{k}\alpha_{o_j}^{w_j}\right)\times\left(\prod_{j=1}^{k}(1-\beta_{o_j})^{w_j}\right) \\ &\text{subject to} \\ &e^{d_j(1-((U_j-f_j(X))/(U_j-L_j)))}+\alpha_{o_j}(1-e^{d_j}) \geq 1,\ j=1,2,\ldots,k_1 \\ &e^{d_j(1-((f_j(X)-L_j)/(U_j-L_j)))}+\alpha_{o_j}(1-e^{d_j}) \geq 1,\ j=k_1+1,k_1+2,\ldots,k \\ &e^{d_j(1-((f_j(X)-(L_j-\delta_j))/(U_j-(L_j-\delta_j))))}+\beta_{o_j}(1-e^{d_j}) \leq 1,\ j=1,2,\ldots,k_1 \\ &e^{d_j(1-(((U_j+\delta_j)-f_j(X))/((U_j+\delta_j)-L_j)))}+\beta_{o_j}(1-e^{d_j}) \leq 1,\ j=k_1+1,k_1+2,\ldots,k \\ &0 \leq \alpha_{o_j}+\beta_{o_j} \leq 1,\ j=1,2,\ldots,k_1,k_1+1,k_1+2,\ldots,k \\ &0 \leq \beta_{o_j} \leq \alpha_{o_j},\ j=1,2,\ldots,k_1,k_1+1,k_1+2,\ldots,k \\ &g_i(X) \leq c_i+\lambda(\ell_i),\ i=1,2,\ldots,m_1 \\ &X \geq 0. \end{aligned} \tag{22}$$

The pessimistic variant of problem (21) described as

$$\begin{aligned} &\max \left(\prod_{j=1}^{k}\alpha_{o_j}^{w_j}\right)\times\left(\prod_{j=1}^{k}(1-\beta_{o_j})^{w_j}\right) \\ &\text{subject to} \\ &e^{d_j(1-((U_j-f_j(X))/(U_j-L_j)))}+\alpha_{o_j}(1-e^{d_j}) \geq 1,\ j=1,2,\ldots,k_1 \\ &e^{d_j(1-((f_j(X)-L_j)/(U_j-L_j)))}+\alpha_{o_j}(1-e^{d_j}) \geq 1,\ j=k_1+1,k_1+2,\ldots,k \\ &e^{d_j(1-((f_j(X)-L_j)/\delta_j))}+\beta_{o_j}(1-e^{d_j}) \leq 1,\ j=1,2,\ldots,k_1 \\ &e^{d_j(1-((U_j-f_j(X))/\delta_j))}+\beta_{o_j}(1-e^{d_j}) \leq 1,\ j=k_1+1,k_1+2,\ldots,k \\ &0 \leq \alpha_{o_j}+\beta_{o_j} \leq 1,\ j=1,2,\ldots,k_1,k_1+1,k_1+2,\ldots,k \\ &0 \leq \beta_{o_j} \leq \alpha_{o_j},\ j=1,2,\ldots,k_1,k_1+1,k_1+2,\ldots,k \\ &g_i(X) \leq c_i+\lambda(\ell_i),\ i=1,2,\ldots,m_1 \\ &X \geq 0. \end{aligned} \tag{23}$$

For the mixed approach, problem (21) is expressed as

$$\begin{aligned} &\max \left(\prod_{j=1}^{k}\alpha_{o_j}^{w_j}\right)\times\left(\prod_{j=1}^{k}(1-\beta_{o_j})^{w_j}\right) \\ &\text{subject to} \\ &e^{d_j(1-((U_j-f_j(X))/(U_j-L_j)))}+\alpha_{o_j}(1-e^{d_j}) \geq 1,\ j=1,2,\ldots,k_1 \\ &e^{d_j(1-((f_j(X)-L_j)/(U_j-L_j)))}+\alpha_{o_j}(1-e^{d_j}) \geq 1,\ j=k_1+1,k_1+2,\ldots,k \\ &e^{d_j(1-((f_j(X)-(L_j-\delta_j))/(\delta_j+\zeta_j)))}+\beta_{o_j}(1-e^{d_j}) \leq 1,\ j=1,2,\ldots,k_1 \\ &e^{d_j(1-(((U_j+\delta_j)-f_j(X))/(\delta_j+\zeta_j)))}+\beta_{o_j}(1-e^{d_j}) \leq 1,\ j=k_1+1,k_1+2,\ldots,k \\ &0 \leq \alpha_{o_j}+\beta_{o_j} \leq 1,\ j=1,2,\ldots,k_1,k_1+1,k_1+2,\ldots,k \\ &0 \leq \beta_{o_j} \leq \alpha_{o_j},\ j=1,2,\ldots,k_1,k_1+1,k_1+2,\ldots,k \\ &g_i(X) \leq c_i+\lambda(\ell_i),\ i=1,2,\ldots,m_1 \\ &X \geq 0. \end{aligned} \tag{24}$$

Theorem 3.2.1. A unique optimal solution (X^*, α^*, β^*) of problem (22) corresponds to a POS X^* of problem (2), where $\alpha^* = (\alpha_{o1}^*, \alpha_{o2}^*, \ldots, \alpha_{ok_1}^*)$

and $\beta^* = (\beta^*_{o1}, \beta^*_{o2}, ..., \beta^*_{ok_1})$.

Proof. Since

$$Z(\alpha, \beta) = \left(\prod_{j=1}^{k_1} \alpha_{o_j}^{w_j}\right) \times \left(\prod_{j=1}^{k_1} (1 - \beta_{o_j})^{w_j}\right)$$

Let (X^*, α^*, β^*) be a unique solution of problem (22). Then

$$Z(\alpha^*, \beta^*) > Z(\alpha, \beta), \quad \forall (X, \alpha, \beta) \text{ in the feasible space of (22).}$$

Suppose X^* is not a POS of problem (2). Then, by Definition 3.1.4, $\exists\, \hat{X}$ in the feasible space of (2) such that

$$f_j(\hat{X}) \geq f_j(X^*), \forall j = 1, 2, \ldots, k_1 \text{ and } f_j(\hat{X}) > f_j(X^*), \text{for at least one} j \in \{1, 2, ..., k_1\} \ (i)$$

Thus,

$$\frac{f_j(\hat{X}) - L_j}{U_j - L_j} \geq \frac{f_j(X^*) - L_j}{U_j - L_j}, \quad \forall j = 1, 2, ..., k_1,$$

and

$$\frac{f_j(\hat{X}) - L_j}{U_j - L_j} > \frac{f_j(X^*) - L_j}{U_j - L_j} \quad \text{for at least one } j \in \{1, 2, ..., k_1\}.$$

Since $d_j > 0$,

$$\Longrightarrow \frac{e^{-d_j((U_j - f_j(\hat{X}))/(U_j - L_j))} - e^{-d_j}}{1 - e^{-d_j}} \geq \frac{e^{-d_j((U_j - f_j(X^*))/(U_j - L_j))} - e^{-d_j}}{1 - e^{-d_j}}, \quad \forall j \in \{1, 2, ..., k_1\},$$

and

$$\frac{e^{-d_j((U_j - f_j(\hat{X}))/(U_j - L_j))} - e^{-d_j}}{1 - e^{-d_j}} > \frac{e^{-d_j((U_j - f_j(X^*))/(U_j - L_j))} - e^{-d_j}}{1 - e^{-d_j}},$$

for at least one $j \in \{1, 2, ..., k_1\}$. (ii)

Similarly, for non-membership functions:

$$\frac{U_j - f_j(\hat{X})}{U_j - (L_j - \delta_j)} \leq \frac{U_j - f_j(X^*)}{U_j - (L_j - \delta_j)}, \forall j \in \{1, 2, ..., k_1\},$$

and

$$\frac{U_j - f_j(\hat{X})}{U_j - (L_j - \delta_j)} < \frac{U_j - f_j(X^*)}{U_j - (L_j - \delta_j)}, \quad \text{for at least one } j \in \{1, 2, ..., k_1\},$$

$$\Longrightarrow \frac{e^{-d_j((f_j(\hat{X}) + \delta_j - L_j)/(U_j + \delta_j - L_j))} - e^{-d_j}}{1 - e^{-d_j}} \leq \frac{e^{-d_j((f_j(X^*) + \delta_j - L_j)/(U_j + \delta_j - L_j))} - e^{-d_j}}{1 - e^{-d_j}},$$

$\forall j \in \{1, 2, ..., k_1\}$, and

$$\frac{e^{-d_j((f_j(\hat{X}) + \delta_j - L_j)/(U_j + \delta_j - L_j))} - e^{-d_j}}{1 - e^{-d_j}} < \frac{e^{-d_j((f_j(X^*) + \delta_j - L_j)/(U_j + \delta_j - L_j))} - e^{-d_j}}{1 - e^{-d_j}},$$

for at least one $j \in \{1, 2, ..., k_1\}$. (iii)

Define

$$\hat{\alpha}_{o_j} = \frac{e^{-d_j\left(\frac{U_j - f_j(\hat{X})}{U_j - L_j}\right)} - e^{-d_j}}{1 - e^{-d_j}},$$

$$\alpha^*_{o_j} = \frac{e^{-d_j\left(\frac{U_j - f_j(X^*)}{U_j - L_j}\right)} - e^{-d_j}}{1 - e^{-d_j}},$$

$$\hat{\beta}_{o_j} = \frac{e^{-d_j\left(\frac{f_j(\hat{X}) + \delta_j - L_j}{U_j + \delta_j - L_j}\right)} - e^{-d_j}}{1 - e^{-d_j}},$$

$$\beta^*_{o_j} = \frac{e^{-d_j\left(\frac{f_j(X^*) + \delta_j - L_j}{U_j + \delta_j - L_j}\right)} - e^{-d_j}}{1 - e^{-d_j}}.$$

Then, using (ii) and (iii), we get

$$\hat{\alpha}_{o_j} \geq \alpha^*_{o_j}, \ \forall j \in \{1, 2, ..., k_1\} \quad \text{and} \quad \hat{\alpha}_{o_j} > \alpha^*_{o_j} \text{ for at least one } j \in \{1, 2, ..., k_1\}. \tag{iv}$$

$$\begin{aligned} &\hat{\beta}_{o_j} \leq \beta^*_{o_j} \Rightarrow 1 - \hat{\beta}_{o_j} \geq 1 - \beta^*_{o_j}, \ \forall j \in \{1, 2, ..., k_1\}, \\ &\hat{\beta}_{o_j} < \beta^*_{o_j} \Rightarrow 1 - \hat{\beta}_{o_j} > 1 - \beta^*_{o_j}, \text{ for at least one } \ j \in \{1, 2, ..., k_1\}. \end{aligned} \tag{v}$$

Now, using (iv), we get

$$\prod_{j=1}^{k_1} \hat{\alpha}_{o_j}^{w_j} > \prod_{j=1}^{k_1} (\alpha^*_{o_j})^{w_j}. \tag{vi}$$

Using (v), we obtain

$$\prod_{j=1}^{k_1} (1 - \hat{\beta}_{o_j})^{w_j} > \prod_{j=1}^{k_1} (1 - \beta^*_{o_j})^{w_j}. \tag{vii}$$

Finally, from (vi) and (vii), we conclude:

$$\prod_{j=1}^{k_1} \hat{\alpha}_{o_j}^{w_j} \prod_{j=1}^{k_1} (1 - \hat{\beta}_{o_j})^{w_j} > \prod_{j=1}^{k_1} (\alpha^*_{o_j})^{w_j} \prod_{j=1}^{k_1} (1 - \beta^*_{o_j})^{w_j}$$

$$\Rightarrow Z(\hat{\alpha}, \hat{\beta}) > Z(\alpha^*, \beta^*),$$

which contradicts the optimality of (X^*, α^*, β^*) for problem (22). Hence, no such $\hat{X}$ exists, and therefore X^* is a POS of problem (2). □

The theorem can be proved similarly for the remaining two perspectives of the DMs and for minimization objectives.

The overall solution procedure of the proposed method for solving an IFMOO problem can be summarized as follows:

Step 1. Formulate the IFMOO problem (1).

Step 2. Transform the IFMOO problem into the equivalent crisp MOOP (2) by employing the accuracy function.

Step 3. Solve each objective function independently and construct the pay-off table to determine the lower and upper bounds, denoted by L_j and U_j, respectively, for each objective function $f_j(X)$, where $j = 1, 2, ..., k$.

Step 4. Construct the exponential membership and non-membership functions corresponding to each objective function under the optimistic, pessimistic, and mixed approaches using the tolerance parameters δ_j and ζ_j, where $j = 1, 2, ..., k$.

Step 5. Relax or reduce the $\leq$ type and $\geq$ type constraints by employing the assigned violation parameter l_i in the forms $c_i + \lambda(l_i)$ and $c_i - \lambda(l_i)$, respectively, where $\lambda \in (0, 1)$ and $i = 1, 2, ..., m$.

Step 6. Develop and solve the problem according to the DM's preference under the optimistic (22) or pessimistic (23) or mixed (24) model.

Step 7. If the obtained solution satisfies the DM, then terminate the solution procedure. Otherwise, reformulate the problem and repeat the process until a satisfactory solution is obtained.

4 Comparative Analysis

To verify the effectiveness of the proposed method, a comparative analysis was conducted using the approach proposed by V. Singh and Yadav (2018). The manufacturing problem presented in their study was employed for this purpose. Accordingly, the transformed equivalent crisp problem is

$$\begin{aligned}
&\max\ f_1(X) = 7.5x_1 + 10.125x_2 + 8x_3,\\
&\min\ f_2(X) = 2.9375x_1 + 3.8750x_2 + 5.1250x_3\\
&\qquad\text{subject to}\\
&2.9375x_1 + 2.0625x_2 + 2.9375x_3 \le 328.125,\\
&3.875x_1 + 2.9375x_2 + 2.0625x_3 \le 355.625,\\
&2.0625x_1 + 2.9375x_2 + 2.9375x_3 \ge 355,\\
&X = (x_1, x_2, x_3) \ge 0.
\end{aligned} \tag{25}$$

By solving each objective independently, subject to the constraints, the ideal solutions and the extreme values of the objectives are identified. Accordingly, $X_1 = (0, 84.09, 52.66)$ and $X_2 = (0, 120.85, 0)$ which give $L_1 = 1223.62, U_1 = 1272.69$, and $L_2 = 468.30, U_2 = 595.73$.
For an optimistic DM, problem (25) is transformed into a single-objective problem of the form (26) using model (22), by assigning equal weights to the objectives and considering violation parameters of 25 and 20 units for the first and second constraints, respectively.

$$\begin{aligned}
&\max Z = \alpha_1^{0.5}\alpha_2^{0.5}(1-\beta_1)^{0.5}(1-\beta_2)^{0.5}\\
&\qquad\text{subject to}\\
&e^{0.2(1-((1272.69-(7.5x_1+10.125x_2+8x_3))/(1272.69-1223.62)))} + \alpha_1(1-e^{0.2}) \ge 1,\\
&e^{0.2(1-((2.9375x_1+3.8750x_2+5.1250x_3-468.30)/(595.73-468.30)))} + \alpha_2(1-e^{0.2}) \ge 1,\\
&e^{0.2(1-((7.5x_1+10.125x_2+8x_3-(1223.62-(\lambda(1272.69-1223.62))))/(1272.69-(1223.62-(\lambda(1272.69-1223.62))))))}+\\
&\beta_1(1-e^{0.2}) \le 1,\\
&e^{0.2(1-(((595.73+(\lambda(595.73-468.30)))-(2.9375x_1+3.8750x_2+5.1250x_3))/((595.73+(\lambda(595.73-468.30)))-468.30)))}+\\
&\beta_2(1-e^{0.2}) \le 1,\\
&2.0625x_1 + 3.8750x_2 + 2.9375x_3 \le 333.125 + \lambda(25),\\
&3.8750x_1 + 2.0625x_2 + 2.0625x_3 \le 365.625 + \lambda(20),\\
&2.9375x_1 + 2.0625x_2 + 2.9375x_3 \ge 360,\\
&0 \le \alpha_j + \beta_j \le 1, \quad j = 1, 2\\
&0 \le \alpha_j \le 1, \quad j = 1, 2\\
&0 \le \beta_j \le 1, \quad j = 1, 2\\
&x_1, x_2, x_3 \ge 0.
\end{aligned} \tag{26}$$

Solving this problem, using LINGO (LINDO Systems Inc., 2017) version 21, the solution is presented in Table 1.

Table 1: Solutions of problem (26) under different λ values.

λ	X	$f_1(X)$	$f_2(X)$	$g_1(X)$	$g_2(X)$	$g_3(X)$
0.3	(0.00, 121.49, 3.30)	1248.50	482.56	257.33	361.63	363.63
0.4	(0.00, 123.79, 0.00)	1253.35	479.68	255.31	363.62	363.62
0.5	(0.00, 124.46, 0.00)	1260.24	482.31	256.72	365.62	365.62
0.6	(0.00, 125.14, 0.00)	1267.13	484.95	258.12	367.62	367.62
0.7	(0.00, 125.70, 0.00)	1272.69	487.08	259.25	369.24	369.24
0.8	(0.00, 125.70, 0.00)	1272.69	487.08	259.25	369.24	369.24

As λ increases, $f_1(X)$ improves while $f_2(X)$ reaches its lowest value around $\lambda = 0.4$ and then slightly worsens for larger values of λ. This shows a trade-off, where increasing emphasis shifts from minimizing $f_2(X)$ toward maximizing $f_1(X)$. The solution becomes stable for larger λ.

Similarly, by reformulating problem (25) for pessimistic and mixed DM perspectives using models (23) and (24), respectively, we obtain the following solutions presented in Tables 2 and 3, respectively.

Table 2: Solutions of Problem (25) under the pessimistic perspective.

λ	X	$f_1(X)$	$f_2(X)$	$g_1(X)$	$g_2(X)$	$g_3(X)$
0.3	(0.00, 114.81, 11.82)	1256.98	505.45	271.51	361.62	371.97
0.4	(0.00, 118.60, 7.39)	1259.93	497.44	266.32	363.62	370.09
0.5	(0.00, 122.39, 2.96)	1262.88	489.44	261.13	365.63	368.22
0.6	(2.02, 118.03, 6.35)	1260.97	495.83	268.01	367.62	369.52
0.7	(2.91, 118.91, 4.40)	1260.91	491.84	266.70	369.62	409.67
0.8	(3.47, 118.96, 4.23)	1264.38	492.86	267.98	371.62	369.04

For the pessimistic variants of the problem, as λ increases, $f_1(X)$ improves while $f_2(X)$ remains relatively stable in the mid-range of λ, with only minor fluctuations in both objectives.

Table 3: Solutions of Problem (25) under the mixed perspective.

λ	X	$f_1(X)$	$f_2(X)$	$g_1(X)$	$g_2(X)$	$g_3(X)$
0.3	(0.00, 114.81, 11.82)	1256.98	505.45	271.51	361.62	371.97
0.4	(0.00, 118.60, 7.39)	1259.93	497.44	266.32	363.62	370.09
0.5	(0.00, 119.26, 7.42)	1262.88	500.15	267.76	365.62	372.12
0.6	(0.00, 125.15, 0.00)	1267.13	484.95	258.12	367.62	367.62
0.7	(0.00, 125.49, 0.00)	1270.58	486.27	258.82	368.62	368.62
0.8	(0.00, 125.56, 0.00)	1271.13	486.54	258.96	368.82	368.82

For the mixed variants of the problem, as λ increases, the solution steadily improves $f_1(X)$, while $f_2(X)$ stabilizes after an initial fluctuation. Around $\lambda = 0.6$, the solution minimizes $f_2(X)$.

Table 4: Comparison of the proposed method with existing approach.

Variant	Proposed method (λ = 0.3 to 0.8)	Existing method (from t = 1 to 5, under two reference conditions)
Optimistic	$f_1(X)$ maximized within the range 1248.50 to 1272.69, $f_2(X)$ minimized within the range 487.08 to 479.68	$f_1(X)$ maximized within the range 1244.91 to 1248.62, $f_2(X)$ minimized within the range 530.80 to 520.33
Pessimistic	$f_1(X)$ maximized within the range 1256.98 to 1264.38, $f_2(X)$ minimized within the range 505.45 to 489.44	$f_1(X)$ maximized within the range 1248.63 to 1251.92, $f_2(X)$ minimized within the range 539.37 to 530.7
Mixed	$f_1(X)$ maximized within the range 1256.98 to 1271.13, $f_2(X)$ minimized within the range 505.45 to 484.95	$f_1(X)$ = 1248.77 (maximized), $f_2(X)$ = 530.66 (minimized)

The proposed method dominates the existing approaches across all decision-making variants by achieving higher values of $f_1(X)$ and lower values of $f_2(X)$ under different values of $\lambda \in (0, 1)$. It shows a significant reduction in $f_2(X)$, indicating improved minimization performance. Generally, the results demonstrate that the proposed model provides more efficient and balanced trade-off between the two conflicting objectives.

5 Model Application

5.1 Description of the Study Area

The farming site is in Abeshge district, Gurage Zone, central Ethiopia, between 8°19′–8°45′ N latitude and 37°45′–38°7′ E longitude (Nasir & Hundie, 2014). Mean annual temperatures range from 18°C to 28.3°C, with rainfall of 801–1400 mm, mostly during the Kiremt season (Dessie et al., 2017). The soil is sandy loam, with a pH of 6.40–6.92.
Farming is mainly rainfed due to limited irrigation, though a few seasonal rivers support perennial crops like mangoes and bananas along their banks. *Teff* (Eragrostis tef), maize (Zea mays), pepper (Capsicum annuum), chickpea (Cicer arietinum), bean (Phaseolus vulgaris), and sorghum (Sorghum bicolor) are the most widely cultivated crops in the area. These crops dominate the farming pattern, accounting for about 85% of the cropped area in the district.

The study area was chosen due to its high crop production potential and the availability of accessible agricultural data. The considered LSF has detailed information on existing cropping patterns, which makes the farming site suitable for empirical analysis. Furthermore, the study area represents the dominant farming system of the area, allowing the findings to be relevant to smallholder farmers in the area. This LSF practices rainfed farming on 1,033ha of land in Gefersa kebele. The location map of the study area is shown in Figure 4.

The existing farming pattern mainly targeted on the achievement of maximum production. The required input allocation to the crops are mainly determined by experience, even though they rarely apply the advice and paradigm of the developmental agents and extension workers in the district.

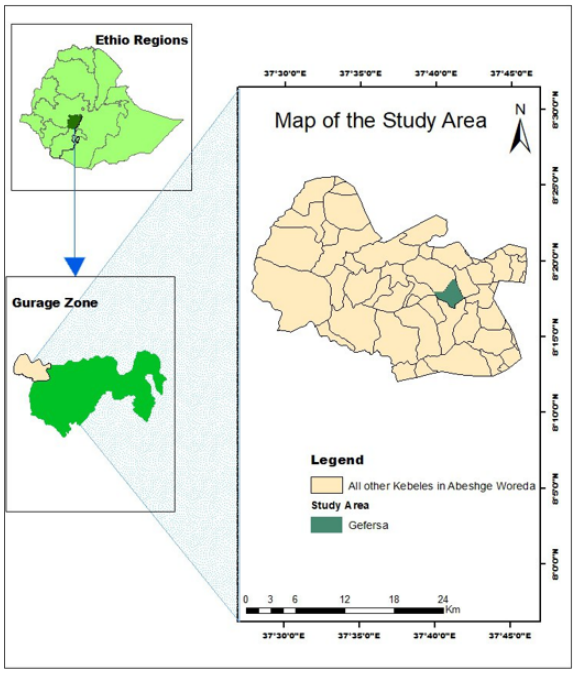

Figure 4: Map of the study area.

5.2 Methods of Data Collection and Analysis

A stratified purposive sampling method was employed to intentionally select the large-scale farm (LSF) site based on its suitability for the study. The selection criteria included the availability of reliable and accessible data, representative farming practices, adequate capital investment, and sufficient manpower. These characteristics enabled the farm to effectively represent the target study population and provide meaningful insights into the research objectives.

The data were collected from farmers, managers, and workers of the LSF, extension experts, development agents, the zonal rural development office, meteorological stations, and marketing agencies through surveys, questionnaires, and key informant interviews.

The dataset incorporates environmental, climatic, hydrological, agricultural, and socio-economic factors. Hydrological data cover effective rainfall and crop water demand. Effective rainfall was calculated using the dependable rain (FAO/AGLW formula) method Allen et al., 1998, while crop water demand was estimated with the Penman-Monteith equation (Allen et al., 1998; Smith, 1992) using crop evapotranspiration.

Crop data such as rooting depth, crop coefficient, critical depletion, yield response, crop height, and crop calendar were obtained from FAO Manual 56 (Allen et al., 1998) and related literature.
Socio-economic data include crop market prices, labor and machinery costs, fertilizer, herbicide, and pesticide dosages and prices, and land resource information.

The gathered data from different sources for a specific parameter are arranged into five groups, viz., the extreme minimum, minimum, median, maximum, and extreme maximum values, based on the level of their deviation from the median value. The values less than the median value are arranged into the extreme minimum and minimum values. Specifically, the average of the highly deviated values from the median value is taken as the extreme minimum value, while the average of the relatively less deviated values from the median is considered as the minimum value. In the same manner, the values greater than the median value are arranged into the maximum and extreme maximum values in the agricultural production problem. The average of the median values of a parameter is taken as the mean value.
Using this principle, the aggregated values are used to construct triangular IFNs to represent the APP problem more realistically.

In this study, the last twelve years climatic data from 2013 to 2024 were gathered from Emdbir meteorological station, with an altitude of $2082m$, latitude $8.13°$N and longitude $37.93°$E.
In order to handle the current extreme variation in the cost of input resources for crop cultivation and crop prices in the country, we have employed closely related data for the proposed study. Accordingly, the average data from 2022 to 2024 of the existing cropping schemes, crop yield (FAO, 2022, 2023), labor force, crop prices, cost of seeds, and other related expenditures for cultivation and agricultural input resources are presented in Tables 5 to 9.

Crop data are presented in Supplementary Materials S.7 and S.8. These, along with the soil data in Supplementary Material S.9, are used to calculate crop water requirements.
The considered crops are denoted as c_1 for maize, c_2 for *teff*,c_3 for sorghum, c_4 for pepper, c_5 for chickpea, c_6 for bean.

In Table 5, F_{1c_n} and F_{2c_n} represent the fertilizers required for crop c_n, where $n = 1, 2, 3, 4, 5, 6$, in the first and second rounds, respectively. Accordingly, F_{1c_n} denotes NPS, while F_{2c_n} represents Urea. Similarly, H_{1c_n} and H_{2c_n} represent the required herbicides for crop c_n in the first and second rounds, respectively. The pesticide required for crop c_n is denoted by P_{c_n}. Thus, the following symbols are used to denote different herbicides and pesticides: H_{2c_1} and H_{2c_3} for Atrazine, H_{1c_2} for 2,4-D, H_{2c_2} for Pallas 45 OD, H_{1c_4} for Glyphosate, H_{1c_5} and H_{2c_6} for Pendimethalin, H_{c_6} for S-metolachlor, P_{c_1} for Diazinon 60 EC, P_{c_2} for Dimethoate, P_{c_3} for Karate 5 EC, P_{c_4} for Ethiozinon 60 EC, P_{c_5} for Highway 50 EC, and P_{c_6} for Profit.

Table 5: Usage of fertilizer, herbicide and pesticide.

Crop	F_{1c_n} (kg/ha)	F_{2c_n} (kg/ha)	H_{1c_n} (L/ha)	H_{2c_n} (L/ha)	P_{c_n} (L/ha)
maize (c_1)	$\widetilde{100}$	$\widetilde{125}$	-	$\widetilde{1}$	$\widetilde{1}$
teff (c_2)	$\widetilde{100}$	$\widetilde{100}$	$\widetilde{1}$	$\widetilde{0.5}$	$\widetilde{1}$
sorghum (c_3)	$\widetilde{100}$	$\widetilde{100}$	-	$\widetilde{1}$	$\widetilde{1}$
pepper (c_4)	$\widetilde{100}$	$\widetilde{200}$	$\widetilde{1.5}$	-	$\widetilde{1.5}$
chickpea (c_5)	$\widetilde{100}$	-	$\widetilde{1}$	-	$\widetilde{1}$
bean (c_6)	$\widetilde{100}$	-	$\widetilde{1}$	$\widetilde{0.75}$	$\widetilde{1}$

The IFN in Table 5 describe the following numbers.
$\widetilde{200} = \langle 196, 198, 208;\ 194, 198, 210\rangle$,
$\widetilde{125} = \langle 123, 125, 127;\ 122, 125, 128\rangle$,
$\widetilde{100} = \langle 97, 99, 105;\ 95.5, 99, 106.5\rangle$,
$\widetilde{2.5} = \langle 2, 2.6, 2.8;\ 1.9, 2.8, 2.9\rangle$,
$\widetilde{0.5} = \langle 0.2, 0.5, 0.7;\ 0.1, 0.5, 1\rangle$.
$\widetilde{1.5} = \langle 1.1, 1.6, 1.7;\ 1, 1.6, 1.8\rangle$,
$\widetilde{1} = \langle 0.75, 1, 1.25;\ 0.5, 1, 1.5\rangle$,
$\widetilde{0.75} = \langle 0.6, 0.7, 1;\ 0.3, 0.7, 1.3\rangle$,
$\widetilde{2} = \langle 1.9, 2, 2.1;\ 1.5, 2, 2.5\rangle$

The costs of cultivation, including plowing, threshing, land rent, seed, labor, herbicides and pesticides, and fertilizers, are provided in Supplementary Materials S.2, S.3, S.4, S.11, and S.12, respectively.
The overall cost of the cultivation of each crop is presented in Table 6.

Table 6: Cost of cultivation (I_{c_n}) and crop yield (Y_{c_n}).

Crop	I_{c_n} (ETB/ha)	Y_{c_n} (qtl/ha)
maize (c_1)	$\langle 35623, 35627, 35628; 35620, 35627, 35629\rangle$	$\langle 50, 54, 62; 47, 54, 65\rangle$
teff (c_2)	$\langle 35698, 35705, 35714; 35689, 35705, 35719\rangle$	$\langle 12.5, 13.5, 16.5; 12, 13.5, 17\rangle$
sorghum (c_3)	$\langle 26838, 26845, 26854; 26829, 26845, 26859\rangle$	$\langle 23, 24.5, 27.5; 22.5, 24.5, 29\rangle$
pepper (c_4)	$\langle 41113, 41120, 41129; 41104, 41120, 41134\rangle$	$\langle 11, 13.5, 14; 10, 13.5, 16\rangle$
chickpea (c_5)	$\langle 20655, 20659, 20666; 20649, 20659, 20674\rangle$	$\langle 16.5, 17.5, 20; 15.5, 17.5, 22\rangle$
bean (c_6)	$\langle 25124, 25131, 25140; 25115, 25131, 25145\rangle$	$\langle 21, 23.5, 24; 20, 23.5, 25\rangle$

The climatic data are used to calculate the crop water requirements, which are presented in Supplementary Material S.10.

Table 7: Seed (E_{c_n}), labor (B_{c_n}) and water requirement (W_{c_n}).

Crop	E_{c_n} (kg/ha)	B_{c_n} (md/ha)	W_{c_n} (m^3/ha)
maize (c_1)	$\langle 22, 26, 25; 17, 26, 27\rangle$	$\langle 80, 86, 89; 75, 86, 92\rangle$	$\langle 3570, 3610, 3625; 3565, 3610, 3648\rangle$
teff (c_2)	$\langle 29, 30, 30.5; 28.5, 30, 32\rangle$	$\langle 70, 76, 80; 64, 76, 82\rangle$	$\langle 2580, 2625, 2640; 2564, 2625, 2660\rangle$
sorghum (c_3)	$\langle 14, 14.5, 16.5; 13.5, 14.5, 18\rangle$	$\langle 35, 41, 45; 30, 41, 46\rangle$	$\langle 3240, 3249, 3252; 3225, 3249, 3255\rangle$
pepper (c_4)	$\langle 15, 15.5, 17.5; 14.5, 15.5, 19\rangle$	$\langle 97, 99, 105; 94, 99, 108\rangle$	$\langle 4750, 4766, 4770; 4705, 4766, 4783\rangle$
chickpea (c_5)	$\langle 26, 28, 30; 25, 28, 31\rangle$	$\langle 25, 31, 35; 20, 31, 36\rangle$	$\langle 2515, 2540, 2560; 2505, 2540, 2572\rangle$
bean (c_6)	$\langle 19, 21, 23; 18, 21, 24\rangle$	$\langle 47, 51, 52; 45, 51, 55\rangle$	$\langle 2355, 2360, 2386; 2347, 2360, 2400\rangle$

The farming machines used in the area are a tractor and a combine harvester. Machine hours for plowing are considered until the land is ready for sowing; details are in Supplementary Material S.1. The required total machine hours for each crop are shown in Table 8.

Table 8: Machine hours requirement (M_{c_n}) and profit (N_{c_n}).

Crop	M_{c_n} (hr/ha)	N_{c_n} (ETB/ha)
maize (c_1)	$\langle 1.83, 2.167, 2.33; 1.42, 2.167, 2.42\rangle$	$\langle 33117, 33123, 33136; 33109, 33123, 33138\rangle$
teff (c_2)	$\langle 1.83, 2.167, 2.33; 1.42, 2.167, 2.42\rangle$	$\langle 13293, 13295, 13297; 13290, 13295, 13300\rangle$
sorghum (c_3)	$\langle 1.75, 2, 2.42; 1.5, 2, 2.5\rangle$	$\langle 18148, 18154, 18165; 18141, 18154, 18170\rangle$
pepper (c_4)	$\langle 1.75, 2, 2.42; 1.5, 2, 2.5\rangle$	$\langle 192873, 192881, 192888; 192862, 192881, 192893\rangle$
chickpea (c_5)	$\langle 1.83, 2.167, 2.33; 1.42, 2.167, 2.42\rangle$	$\langle 25830, 25842, 25849; 25820, 25842, 25853\rangle$
bean (c_6)	$\langle 1.75, 2, 2.42; 1.5, 2, 2.5\rangle$	$\langle 16262, 16269, 16278; 16253, 16269, 16283\rangle$

The cropland allocation in the existing situation during 2020 - 2024 is given in the Supplementary Material S.5. Accordingly, the average land allocation of the existing system and the attainability and non-attainability degrees of the intended objectives are depicted in Table 9. Where x_1, x_2, x_3, x_4, x_5, and x_6 denote the land area allocated to maize, *teff*, sorghum, pepper, chickpea, and beans, respectively. The functions $f_1(X)$, $f_2(X)$, $f_3(X)$, and $f_4(X)$, respectively, represent the yield, profit, cost, and labor objectives.

Table 9: Existing farm pattern.

$X = (x_1, x_2, x_3, x_4, x_5, x_6)$		$f_1(X)$	$f_2(X)$	$f_3(X)$	$f_4(X)$
(221.02, 141.41, 401.32, 106.42, 62.29, 121.57)		29470.15	41510180	31413470	64160
	μ	0.81	0.20	0.17	0.20
	ν	0.19	0.28	0.30	0.28

Some mathematical software is employed to solve the considered APP problem and assist in analyzing the results of the study. CROPWAT 8.0 software (Smith, 1992) is used to generate and analyze the water requirement of crops, and LINGO (LINDO Systems Inc., 2017) is used to solve complex mathematical problems.

5.3 Problem Formulation

As a result of the inconsistent nature and imprecision of the pertained agricultural data, crop planning rests under the influence of risk and uncertainty (Luo et al., 2023). So the parameters in the APP problem are described as IFN. Thus, the objectives and constraints of the intended problem are expressed as intuitionistic fuzzy functions. Accordingly, IFMOO model is employed for comprehensive and efficacious investigation.

The *Kiremt* season is the widely practiced cropping season in the study area. Crops such as maize, pepper, and sorghum are sown during the *Belg* season and harvested by the end of *Kiremt*. *Teff* and beans are sown in the *Kiremt* season and harvested during the *Bega* season, while chickpea is planted in the last days of *Kiremt* and harvested in the *Bega* season. Thus, all six crops considered in this study are generally cultivated within a single cropping season.

Table 10: Decision variable and parameters.

Parameters	Description
TL	Total farmland for crop cultivation (ha)
TL_r	Minimum land area required for cultivation (ha)
Y_c	Average yield per unit area of crop c (qtl/ha)
N_c	Average net profit of crop c per hectare (ETB/ha)
I_c	Average investment per unit area of crop c (ETB/ha)
M_c	Average machine-hours required per unit area of crop c (hr/ha)
B_c	Average labor required per unit area of crop c (md/ha)
W_c	Average water requirement per unit area of crop c (m^3/ha)
E_c	Seed required per unit area of crop c (kg/ha)
F_{lc}	l^{th} type of fertilizer required per unit area for crop c (kg/ha)
P_{lc}	l^{th} type of pesticide required per unit area for crop c (L/ha)
H_{lc}	l^{th} type of herbicide required per unit area for crop c (L/ha)
TM	Total available machine-hours (hr)
TW	Total available water (m^3)
TE_c	Total available seed for crop c (kg)
TF_l	Total available l^{th} fertilizer (kg)
TP_l	Total available l^{th} pesticide (L)
TH_l	Total available l^{th} herbicide (L)
Decision variable	Description
X_c	Land area allocated to crop c (ha)

Note: md denotes man-days.

Objective functions

Based on their accessibility and regional importance, the following four objectives are considered in this study.

(i) Crop yield achievement

The estimated yield of a crop is equal to the product of the cultivable area of land and the average yield produced per unit area of land.

Thus, the maximization of the total yield of the considered six crops can be expressed as

$$\max \widetilde{f_1}(X) \approx \sum_{c=1}^{6} \widetilde{Y_c} X_c. \tag{27}$$

(ii) Net profit goal

The net profit of various crops, is the product of the net profit of each crop per unit area of land and its respective utilized land, which is described as

$$\max \widetilde{f_2}(X) \approx \sum_{c=1}^{6} \widetilde{N_c} X_c. \tag{28}$$

(iii) Cost of cultivation goal

To get the optimum production, farmers should invest a certain amount of money for land rent, fertilizers, seeds, herbicides, pesticides, rental machines, labor force, etc. Minimizing this working capital is another important objective of farmers and mathematically given by

$$\min \widetilde{f_3}(X) \approx \sum_{c=1}^{6} \widetilde{I_c} X_c. \tag{29}$$

(vi) Labor requirement

The labor objective is described as

$$\min \widetilde{f_4}(X) \approx \sum_{c=1}^{n} \widetilde{B_c} X_c. \tag{30}$$

Constraints

The above four objectives are subject to the following eight constraints.

(ii) Water requirement

Additional water through irrigation is required to meet the crop's evapotranspiration needs and optimize yield. The constraint for water supply can be described as

$$\sum_{c=1}^{6} \widetilde{W_c} X_c \precsim \widetilde{TW}. \tag{31}$$

For sustainable optimal crop yield and maximum profit, agricultural input resources should not be used at the expense of the environment (Li et al., 2020). Therefore, to reduce the adverse effects of fertilizers, pesticides, and herbicides on the environment, the optimum amounts of these inputs must be considered alongside the utilization of other favorable resources.

(iii) Dosage of fertilizer

To maintain and improve the productivity of the soil, different types of fertilizers have to be used optimally according to the characteristics of the crops, soil type and climate of the region. This constraint is expressed as

$$\sum_{c=1}^{6} \widetilde{F_{lc}} X_c \precsim \widetilde{TF_l},\ l = 1, 2. \tag{32}$$

(iv) Amount of Herbicide

DM requires a certain level of herbicides for several crops during growth stage for better yield taking the availability and environmental aspects into account. Mathematically described as

$$\sum_{c=1}^{6} \widetilde{H_{l_c}} X_c \precsim \widetilde{TH_l},\ l = 1, 2, ..., L. \tag{33}$$

(v) Dosage of pesticide

Pesticide is another essential input resource of agriculture to protect crops during growth stage from different pests and insects. This constraint is formulated as

$$\sum_{c=1}^{6} \widetilde{P_{lc}} X_c \precsim \widetilde{TP_l},\ l = 1, 2, ..., L. \tag{34}$$

(vi) Machine hours

Different types of machines are needed for various tasks of agriculture, such as tilling, plowing, sowing, cultivating, harvesting, threshing, etc. The sum of the machine hours allocated to each season should not exceed the machine hours required in a year. That means,

$$\sum_{c=1}^{6} \widetilde{M_c} X_c \precsim \widetilde{TM}. \tag{35}$$

(vii) Cultivable land availability

The sum of cultivable land for all crops must not exceed the total available land. Furthermore, the total cultivable land should be less than the entire arable land available in the study area. This is formulated as

$$\sum_{c=1}^{6} X_c \precsim \widetilde{TL}. \tag{36}$$

On the other hand, a minimum cultivable land area should be allocated to crop production to maintain a minimum level of agricultural output and profit while ensuring efficient utilization of available land resources. This constraint is mathematically expressed as

$$\sum_{c=1}^{6} X_c \succsim \widetilde{TL_r}. \tag{37}$$

(i) Seed requirement

Seed availability constraints were incorporated into the model to describe the limitations in accessing selected seed for each crop. The maximum seed availability for each crop was determined based on the recommended seed requirement per hectare (Table 7), the maximum feasible cultivable area for each crop, and crop suitability conditions under local agro-ecological settings (Semu et al., 2022). This constraint mathematically expressed as

$$\widetilde{E_c} X_c \precsim \widetilde{TE_c}, \quad c = 1, 2, ..., 6. \tag{38}$$

(viii) Non-negativity

In the modelling APP problem, all decision variables should be non-negative.

$$X_c \geq 0 \qquad c = 1, 2, ..., 6. \tag{39}$$

The stated objectives and constraints align with economic, environmental, and social goals, with aims to boost net benefits, use resources wisely to limit environmental harm, and increase local jobs (Li et al., 2020; Zhang & Georgescu, 2022).

In this study, the three variants of the problem are considered independently to address the interference of uncontrolled conditions and associated risks, and individual differences in the DM process. This assists farmers and managers from different perspectives by proposing various possible alternative management schemes.

In the optimistic assumption, a farmer considers using farming resources with varying degrees of acceptance and flexibility to accommodate other possible alternative operations, presuming that it offers certain benefits. Conversely, a pessimist DM tends to be skeptical about implementing all possible alternative farming tasks and partially considers those with a lower degree of acceptance. From a mixed perspective, the farmer's assumption lies between the optimistic and pessimistic viewpoints.

As a result, the solution of the APP problem varies according to each perspective (Kis et al., 2021), which leads to differences in the determination of the OCP. Each viewpoint has its advantages and disadvantages. Therefore, this study considers the optimistic, pessimistic, and mixed aspects of DM for efficient management of agricultural resources.

In this study, from $1,033ha$ land of the LSF, nearly $1,017ha$ of farmland is considered for crop cultivation, and $6ha$ to $7ha$ of land is supposed to be left permanently for forestation to maintain the ecological balance of the environment. In the existing system, $5ha$ of cropland is occupied by perennial crops. About $1.50ha$ of land of the LSF is permanently left over as a residential place for workers and roads. Moreover, $2.5ha$ of land is not suitable for farming and is currently used for animal grazing.
The land management of the LSF is a traditional approach based on the weather conditions. They interchangeably use plots of land for different crops, and there is no reasonable pattern of operation on cropland.
In this work, three scenarios of crop cultivation are designed based on the conventional cultivation pattern and suitability of the devised farming system in the study area.

The first scenario considers the case when chickpeas are planted on the land leftover in the first season of crop cultivation. Thus, in this scenario, chickpea faces the same land rent as other crops. This system is mainly adopted to fertilize unplowed land and to make use of fields left uncultivated in the first season due to factors like irregular rainfall, labor shortages, limited seed varieties, and lack of capital or fertilizers.

In the second scenario, farmers plant chickpeas on land right after harvesting maize. This common practice helps to use the fertile soil left by maize and saves farmers from the additional cost of renting extra land for smallholder farmers with limited fields to cultivate multiple crops. Based on the existing farming system in the study area, at least 33% of the land allocated to maize is subsequently used for chickpea cultivation after maize harvest.

In the third scenario, chickpeas are planted after harvesting maize, sorghum, and beans. Like the second scenario, the most important reason for farmers to use this cropping plan is to increase the yield from fertile land and minimize additional cultivation expenses. In order to effectively utilize the land for chickpea after harvesting maize, sorghum, and bean, the land allocated to chickpea should not be less than the combined land allocated to *teff* and pepper. Furthermore, the land allocated to bean should be at least equal to that allocated to sorghum. However, according to the farmers, this scenario is rarely practiced as land preparation for the succeeding crop after harvesting sorghum is a relatively challenging activity.

As chickpea is cultivated as a second crop after harvesting other crops within the same cropping season, the land rent for chickpea under the second and third scenarios decreases significantly by 65% relative to the annual land lease cost. Thus, to effectively utilize the available land in this production cycle, the upper limits of some constraints in the second and third scenarios are relaxed based on resource availability.

In the problem formulation of the three scenarios, the upper and lower limits of the constraints, the value of violations, and tolerances are mainly based on the availability of agricultural resources. For the second and third scenarios, the land constraint attributed to chickpeas is expressed in terms of the remaining crops.
The weights assigned to the objectives and constraints are estimated based on the preferences rated by managers of the LSF, farmers, and developmental agents of the study area.

6 Results and Discussions

We denote the land areas allocated to crop c by x_c, where $c = 1, 2, ..., 6$, representing the land areas of maize, *teff*, sorghum, pepper, chickpea, and bean, respectively.

The functions $f_j(X)$, where $j = 1, 2, 3, 4$, denote the objectives of production, profit, expenditure, and manpower, respectively. The constraints are denoted by $g_i(X)$, where $i = 1, 2, ..., 8$, corresponding respectively to water, first-round fertilizer, second-round fertilizer, first-round herbicide, second-round herbicide, pesticide, machine hours, and the maximum available land area. In addition, minimum land area cultivation requirements are imposed to secure the minimum profit and yield, while seed constraints are included to account for limitations in seed availability.

Based on the available agricultural resources, the violation parameters of the constraints are assigned as $\ell_1 = 5235$, $\ell_2 = 935$, $\ell_3 = 940$, $\ell_4 = 96$, $\ell_5 = 88$, $\ell_6 = 78$, $\ell_7 = 104$, and $\ell_8 = 4$. The violation parameters for the seed constraints of maize, *teff*, sorghum, pepper, chickpea, and bean are assigned as 66, 40, 10, 10, 44, and 38, respectively, based on their availabilities.

The weights assigned to the production, profit, cost, and labor force objectives are 30%, 28%, 28%, and 14%, respectively. Utilizing all these values, the formulated problem is solved under optimistic, pessimistic, and mixed viewpoints by employing models (22), (23), and (24), respectively. The problem is defined using tolerance values expressed as multiples of λ, with violations evaluated under the three approaches. To explore different solutions, several values of $\lambda \in (0, 1)$, specifically $0.30, 0.40, 0.50, 0.60, 0.70$, and 0.80, are considered in the solution process. Accordingly, the APP problem is solved for the three scenarios based on the objectives and constraints outlined in Section 5.3 and the data presented in Tables 5 to 8.

Scenario 1: When chickpea is planted on the fallow land.

The mathematical expression of this problem has the following form:

$$
\begin{aligned}
&\max \widetilde{f}_1(X) = \widetilde{56}x_1 \oplus \widetilde{14.5}x_2 \oplus \widetilde{25}x_3 \oplus \widetilde{13.5}x_4 \oplus \widetilde{18}x_5 \oplus \widetilde{23.5}x_6,\\
&\max \widetilde{f}_2(X) = \widetilde{33125}x_1 \oplus \widetilde{13295}x_2 \oplus \widetilde{18154}x_3 \oplus \widetilde{192881}x_4 \oplus \widetilde{24342}x_5 \oplus \widetilde{16269}x_6,\\
&\min \widetilde{f}_3(X) = \widetilde{35625}x_1 \oplus \widetilde{3705}x_2 \oplus \widetilde{26845}x_3 \oplus \widetilde{41119}x_4 \oplus \widetilde{20659}x_5 \oplus \widetilde{25132}x_6,\\
&\min \widetilde{f}_4(X) = \widetilde{84}x_1 \oplus \widetilde{74}x_2 \oplus \widetilde{41}x_3 \oplus \widetilde{100}x_4 \oplus \widetilde{31}x_5 \oplus \widetilde{50}x_6\\
&\qquad\qquad \text{subject to}\\
&\widetilde{3610}x_1 \oplus \widetilde{2620}x_2 \oplus \widetilde{3245}x_3 \oplus \widetilde{4765}x_4 \oplus \widetilde{2540}x_5 \oplus \widetilde{2365}x_6 \precsim \widetilde{3410610},\\
&\widetilde{100}x_1 \oplus \widetilde{100}x_2 \oplus \widetilde{100}x_3 \oplus \widetilde{100}x_4 \oplus \widetilde{100}x_5 \oplus \widetilde{100}x_6 \precsim \widetilde{101700},\\
&\widetilde{125}x_1 \oplus \widetilde{100}x_2 \oplus \widetilde{100}x_3 \oplus \widetilde{200}x_4 \precsim \widetilde{108055},\\
&\widetilde{1}x_2 \oplus \widetilde{1.5}x_4 \oplus \widetilde{1}x_5 \oplus \widetilde{1}x_6 \precsim \widetilde{1145},\\
&\widetilde{1}x_1 \oplus \widetilde{0.5}x_2 \oplus \widetilde{1}x_3 \oplus \widetilde{0.75}x_6 \precsim \widetilde{1017},\\
&\widetilde{1}x_1 \oplus \widetilde{1}x_2 \oplus \widetilde{1}x_3 \oplus \widetilde{1.5}x_4 \oplus \widetilde{1}x_5 \oplus \widetilde{1}x_6 \precsim \widetilde{1100},\\
&\widetilde{2.67}x_1 \oplus \widetilde{2.67}x_2 \oplus \widetilde{2}x_3 \oplus \widetilde{2}x_4 \oplus \widetilde{2.67}x_5 \oplus \widetilde{2}x_6 \precsim \widetilde{2205},\\
&\widetilde{1}x_1 \oplus \widetilde{1}x_2 \oplus \widetilde{1}x_3 \oplus \widetilde{1}x_4 \oplus \widetilde{1}x_5 \oplus \widetilde{1}x_6 \precsim \widetilde{1017},\\
&\widetilde{1}x_1 \oplus \widetilde{1}x_2 \oplus \widetilde{1}x_3 \oplus \widetilde{1}x_4 \oplus \widetilde{1}x_5 \oplus \widetilde{1}x_6 \succsim \widetilde{1015},\\
&\widetilde{26}x_1 \precsim \widetilde{21611},\ \widetilde{30}x_2 \precsim \widetilde{15255},\ \widetilde{14.5}x_3 \precsim \widetilde{99156},\\
&\widetilde{15.5}x_4 \precsim \widetilde{6509},\ \widetilde{28}x_5 \precsim \widetilde{15662},\ \widetilde{20}x_6 \precsim \widetilde{12204},\\
&X = (x_1, x_2, x_3, x_4, x_5, x_6) \geq 0,
\end{aligned}
\tag{40}
$$

where,

$\widetilde{1145} = \langle 1140, 1145, 1146;\ 1139, 1145, 1147\rangle$,
$\widetilde{1015} = \langle 1014, 1015, 1016;\ 1013, 1015, 1017\rangle$,
$\widetilde{2205} = \langle 2200, 2205, 2207;\ 2197, 2205, 2208\rangle$,
$\widetilde{3410610} = \langle 3410609, 3410610, 3410615;\ 3410607, 3410610, 3410617\rangle$,
$\widetilde{101700} = \langle 101697, 101699, 101705;\ 101695, 101699, 101707\rangle$,
$\widetilde{108055} = \langle 108052, 108057, 108058;\ 108050, 108057, 108060\rangle$,
$\widetilde{21611} = \langle 21605, 21610, 21611; 21604, 21610, 21612\rangle$,
$\widetilde{15255} = \langle 15250, 15255, 15256;\ 15249, 15255, 15257\rangle$,
$\widetilde{99156} = \langle 99151, 99156, 99157;\ 99150, 99156, 99158\rangle$,
$\widetilde{15662} = \langle 15657, 15662, 15663;\ 15656, 15662, 15664\rangle$,

$\widetilde{1017} = \langle 1016, 1017, 1018;\ 1015, 1017, 1019\rangle$,
$\widetilde{1100} = \langle 1099, 1101, 1107;\ 1098, 1101, 1108\rangle$,
$\widetilde{1} = \langle 0.95, 0.99, 1;\ 0.94, 0.99, 1.15\rangle$,

$\widetilde{12204} = \langle 12199, 12204, 12205;\ 12198, 12204, 12206\rangle$,
$\widetilde{28138} = \langle 28132, 28138, 28140;\ 28130, 28138, 28142\rangle$,
$\widetilde{6509} = \langle 6504, 6509, 6510;\ 6503, 6509, 6511\rangle$.

The remaining values of the coefficients of the variables are presented in Tables 5 to 8.

The solutions of problem (40) obtained using the proposed optimistic approach for different $\lambda \in (0, 1)$ are presented in Table 11.

Table 11: Solutions of problem (40) under an optimistic perspective.

λ	X	$f_1(X)$	$f_2(X)$	$f_3(X)$	$f_4(X)$	Z
0.3	(153.44, 0, 314.97, 78.79, 152.82, 314.97)	27333.18	34842180	28234760	54150	0.2651
0.4	(162.93, 0, 305.66, 81.88, 158.86, 305.66)	27557.00	35579290	28340800	54630	0.2811
0.5	(171.96, 0, 296.48, 84.73, 165.36, 296.48)	27766.47	36269800	28436290	55064	0.2949
0.6	(180.58, 0, 287.40, 87.37, 172.26, 287.40)	27963.23	36919230	28522470	55464	0.3070
0.7	(187.95, 0, 278.65, 89.34, 180.41, 278.65)	28121.20	37441020	28579940	55761	0.3176
0.8	(191.60, 0, 270.90, 89.31, 192.28, 270.90)	28163.46	37578060	28551380	55751	0.3274

From the above solutions, Table 11, the better compromised solution is obtained when $\lambda = 0.8$. So, the compromised solution for the first scenario is $X = (191.60, 0, 270.90, 89.31, 192.28, 270.90)$ and its detail is depicted in Table 12.

Table 12: Compromise solution of problem (40).

$X=(x_1,x_2,x_3,x_4,x_5,x_6)$		$f_1(X)$	$f_2(X)$	$f_3(X)$	$f_4(X)$
(191.60, 0, 270.90, 89.31, 192.28, 270.90)		28163.46	37578060	28551380	55751
	μ	0.48	0.50	0.37	0.31
	ν	0.20	0.20	0.26	0.29
$X=(x_1,x_2,x_3,x_4,x_5,x_6)$		$g_1(X)$	$g_2(X)$	$g_3(X)$	$g_4(X)$
(191.60, 0, 270.90, 89.31, 192.28, 270.90)		3124448	101500	68902	597.15
$X=(x_1,x_2,x_3,x_4,x_5,x_6)$		$g_5(X)$	$g_6(X)$	$g_7(X)$	$g_8(X)$
(191.60, 0, 270.90, 89.31, 192.28, 270.90)		665.68	1059.65	2287	1015

Based on the results given in Table 12, the required input resources to cultivate the crops under the allocated cropland are presented in Table 13.

Table 13: Input resource requirements for allocated crops under scenario one.

Crop	Seed (kg)	F_{1c_n} (kg)	F_{2c_n} (kg)	H_{1c_n} (L)	H_{2c_n} (L)	P_{c_n} (L)
maize (c_1)	4789.95	15344	23949.79	-	153.44	153.44
sorghum (c_3)	4063.58	31497	27090.56	-	314.97	314.97
pepper (c_4)	1428.93	7879	17861.63	133.96	-	133.96
chickpea (c_5)	5383.90	15282	-	192.28	-	152.82
bean (c_6)	5418.11	31497	-	270.90	203.17	314.97

Scenario 2: Chickpea is planted after harvesting maize.
The mathematical expression of this problem has the following form:

$$
\begin{aligned}
&\max \widetilde{f}_1(X) = \widetilde{56}x_1 \oplus \widetilde{14.5}x_2 \oplus \widetilde{25}x_3 \oplus \widetilde{13.5}x_4 \oplus \widetilde{18}x_5 \oplus \widetilde{23.5}x_6,\\
&\max \widetilde{f}_2(X) = \widetilde{36100}x_1 \oplus \widetilde{13295}x_2 \oplus \widetilde{18154}x_3 \oplus \widetilde{192881}x_4 \oplus \widetilde{29865}x_5 \oplus \widetilde{16269}x_6,\\
&\min \widetilde{f}_3(X) = \widetilde{32650}x_1 \oplus \widetilde{3705}x_2 \oplus \widetilde{26845}x_3 \oplus \widetilde{41119}x_4 \oplus \widetilde{15135}x_5 \oplus \widetilde{25132}x_6,\\
&\min \widetilde{f}_4(X) = \widetilde{84}x_1 \oplus \widetilde{74}x_2 \oplus \widetilde{41}x_3 \oplus \widetilde{100}x_4 \oplus \widetilde{31}x_5 \oplus \widetilde{50}x_6\\
&\qquad\qquad \text{subject to}\\
&\widetilde{3610}x_1 \oplus \widetilde{2620}x_2 \oplus \widetilde{3245}x_3 \oplus \widetilde{4765}x_4 \oplus \widetilde{2540}x_5 \oplus \widetilde{2365}x_6 \precsim \widetilde{3667300},\\
&\widetilde{100}x_1 \oplus \widetilde{100}x_2 \oplus \widetilde{100}x_3 \oplus \widetilde{100}x_4 \oplus \widetilde{100}x_5 \oplus \widetilde{100}x_6 \precsim \widetilde{105900},\\
&\widetilde{125}x_1 \oplus \widetilde{100}x_2 \oplus \widetilde{100}x_3 \oplus \widetilde{200}x_4 \precsim \widetilde{127125},\\
&\widetilde{1}x_2 \oplus \widetilde{1.5}x_4 \oplus \widetilde{1}x_5 \oplus \widetilde{1}x_6 \precsim \widetilde{1145},\\
&\widetilde{1}x_1 \oplus \widetilde{0.5}x_2 \oplus \widetilde{1}x_3 \oplus \widetilde{0.75}x_6 \precsim \widetilde{1017},\\
&\widetilde{1}x_1 \oplus \widetilde{1}x_2 \oplus \widetilde{1}x_3 \oplus \widetilde{1.5}x_4 \oplus \widetilde{1}x_5 \oplus \widetilde{1}x_6 \precsim \widetilde{1525},\\
&\widetilde{2.167}x_1 \oplus \widetilde{2.167}x_2 \oplus \widetilde{2}x_3 \oplus \widetilde{2}x_4 \oplus \widetilde{2.167}x_5 \oplus \widetilde{2}x_6 \precsim \widetilde{2715},\\
&\widetilde{1}x_1 \oplus \widetilde{1}x_2 \oplus \widetilde{1}x_3 \oplus \widetilde{1}x_4 \oplus \widetilde{1}x_6 \precsim \widetilde{1017},\\
&\widetilde{1}x_1 \oplus \widetilde{1}x_2 \oplus \widetilde{1}x_3 \oplus \widetilde{1}x_4 \oplus \widetilde{1}x_6 \succsim \widetilde{1015},\\
&\widetilde{1}x_1 \succsim \widetilde{1}x_5,\ \widetilde{1}x_5 \succsim \widetilde{0.33}x_1,\\
&\widetilde{26}x_1 \precsim \widetilde{21611},\ \widetilde{30}x_2 \precsim \widetilde{15255},\ \widetilde{14.5}x_3 \precsim \widetilde{99156},\\
&\widetilde{15.5}x_4 \precsim \widetilde{6509},\ \widetilde{28}x_5 \precsim \widetilde{15662},\ \widetilde{20}x_6 \precsim \widetilde{12204},\\
&X=(x_1,x_2,x_3,x_4,x_5,x_6) \geq 0,
\end{aligned}
\tag{41}
$$

where

$$
\begin{aligned}
\widetilde{3667300} &= \langle 3667293, 3667304, 3667307; 3667290, 3667304, 3667310\rangle,\\
\widetilde{2715} = \langle 2712, 2715, 2718; 2710, 2715, 2720\rangle,\ \widetilde{0.33} &= \langle 0.31, 0.33, 0.35; 0.30, 0.33, 0.36\rangle,\\
\widetilde{105900} &= \langle 105895, 105900, 105905; 105890, 105900, 105910\rangle,\\
\widetilde{127125} &= \langle 127122, 127125, 127128; 127120, 127125, 127130\rangle,\\
\widetilde{29490} &= \langle 29491, 29492, 29498; 29488, 29492, 29499\rangle,\\
\widetilde{36100} &= \langle 36096, 36098, 36104; 36095, 36098, 36105\rangle,\\
\widetilde{15135} &= \langle 15132, 15134, 15140; 15130, 15134, 15142\rangle,\\
\widetilde{29865} &= \langle 29862, 29865, 29868; 29860, 29865, 29870\rangle,\\
\widetilde{32650} &= \langle 32648, 32650, 32655; 32645, 32650, 32660\rangle,\\
\widetilde{1525} &= \langle 1522, 1525, 1528; 1520, 1525, 1530\rangle.
\end{aligned}
$$

By solving problem (41) using the proposed method for the optimistic variants of the problem, a better compromise solution is obtained for $\lambda = 0.8$. The resulting compromised optimal solution for the second scenario is $X = (156.00, 0.00, 661.58, 122.85, 51.48, 74.57)$, with details presented in Table 14.

Table 14: Compromise solution of problem (41).

$X = (x_1, x_2, x_3, x_4, x_5, x_6)$		$f_1(X)$	$f_2(X)$	$f_3(X)$	$f_4(X)$
(156.00, 0.00, 661.58, 122.85, 51.48, 74.57)		29358.32	44088180	30558420	57384
	μ	0.92	0.30	0.36	0.54
	ν	0.03	0.30	0.26	0.18
$X = (x_1, x_2, x_3, x_4, x_5, x_6)$		$g_1(X)$	$g_2(X)$	$g_3(X)$	$g_4(X)$
(156.00, 0.00, 661.58, 122.85, 51.48, 74.57)		3601808	106648	110228	310.32
$X = (x_1, x_2, x_3, x_4, x_5, x_6)$		$g_5(X)$	$g_6(X)$	$g_7(X)$	$g_8(X)$
(156.00, 0.00, 661.58, 122.85, 51.48, 74.57)		873.51	1127.90	2271.97	1015

The required input resources to cultivate the crops under the allocated cropland are presented in Table 15.

Table 15: Input resource requirements for allocated crops under scenario two.

Crop	Seed (kg)	F_{1c_n} (kg)	F_{2c_n} (kg)	H_{1c_n} (L)	H_{2c_n} (L)	P_{c_n} (L)
maize (c_1)	3900.00	15600	19500	-	156.00	156.00
sorghum (c_3)	9923.75	66158	66158	-	661.58	661.58
pepper (c_4)	1965.58	12285	24570	184.27	-	184.27
chickpea (c_5)	1441.44	5148	-	51.48	-	51.48
bean (c_6)	1491.36	7457	-	74.57	55.93	74.57

Scenario 3: Chickpea is planted after harvesting maize, sorghum and beans.
The mathematical expression of this scenario has the following form:

$$
\begin{aligned}
&\max \widetilde{f}_1(X) = \widetilde{56}x_1 \oplus \widetilde{14.5}x_2 \oplus \widetilde{25}x_3 \oplus \widetilde{13.5}x_4 \oplus \widetilde{18}x_5 \oplus \widetilde{23.5}x_6,\\
&\max \widetilde{f}_2(X) = \widetilde{36100}x_1 \oplus \widetilde{13295}x_2 \oplus \widetilde{21130}x_3 \oplus \widetilde{192881}x_4 \oplus \widetilde{29865}x_5 \oplus \widetilde{19245}x_6,\\
&\min \widetilde{f}_3(X) = \widetilde{32650}x_1 \oplus \widetilde{3705}x_2 \oplus \widetilde{23870}x_3 \oplus \widetilde{41119}x_4 \oplus \widetilde{15135}x_5 \oplus \widetilde{22155}x_6,\\
&\min \widetilde{f}_4(X) = \widetilde{84}x_1 \oplus \widetilde{74}x_2 \oplus \widetilde{41}x_3 \oplus \widetilde{100}x_4 \oplus \widetilde{31}x_5 \oplus \widetilde{50}x_6\\
&\qquad\qquad \text{subject to}\\
&\widetilde{3610}x_1 \oplus \widetilde{2620}x_2 \oplus \widetilde{3245}x_3 \oplus \widetilde{4765}x_4 \oplus \widetilde{2540}x_5 \oplus \widetilde{2365}x_6 \precsim \widetilde{3667300},\\
&\widetilde{100}x_1 \oplus \widetilde{100}x_2 \oplus \widetilde{100}x_3 \oplus \widetilde{100}x_4 \oplus \widetilde{100}x_5 \oplus \widetilde{100}x_6 \precsim \widetilde{105900},\\
&\widetilde{125}x_1 \oplus \widetilde{100}x_2 \oplus \widetilde{100}x_3 \oplus \widetilde{200}x_4 \precsim \widetilde{127125},\\
&\widetilde{1}x_2 \oplus \widetilde{1.5}x_4 \oplus \widetilde{1}x_5 \oplus \widetilde{1}x_6 \precsim \widetilde{1145},\\
&\widetilde{1}x_1 \oplus \widetilde{0.5}x_2 \oplus \widetilde{1}x_3 \oplus \widetilde{0.75}x_6 \precsim \widetilde{1017},\\
&\widetilde{1}x_1 \oplus \widetilde{1}x_2 \oplus \widetilde{1}x_3 \oplus \widetilde{1.5}x_4 \oplus \widetilde{1}x_5 \oplus \widetilde{1}x_6 \precsim \widetilde{1525},\\
&\widetilde{2.167}x_1 \oplus \widetilde{2.167}x_2 \oplus \widetilde{2}x_3 \oplus \widetilde{2}x_4 \oplus \widetilde{2.167}x_5 \oplus \widetilde{2}x_6 \precsim \widetilde{2715},\\
&\widetilde{1}x_1 \oplus \widetilde{1}x_2 \oplus \widetilde{1}x_3 \oplus \widetilde{1}x_4 \oplus \widetilde{1}x_6 \precsim 1017,\\
&\widetilde{1}x_1 \oplus \widetilde{1}x_2 \oplus \widetilde{1}x_3 \oplus \widetilde{1}x_4 \oplus \widetilde{1}x_6 \succsim 1015,\\
&\widetilde{1}x_5 \precsim \widetilde{1}x_1 \oplus \widetilde{1}x_3 \oplus \widetilde{1}x_6,\ \widetilde{1}x_5 \succsim \widetilde{1}x_2 \oplus \widetilde{1}x_4,\ \widetilde{1}x_6 \succsim \widetilde{1}x_3.\\
&\widetilde{26}x_1 \precsim \widetilde{21611},\ \widetilde{30}x_2 \precsim \widetilde{15255},\ \widetilde{14.5}x_3 \precsim \widetilde{99156},\\
&\widetilde{15.5}x_4 \precsim \widetilde{6509},\ \widetilde{28}x_5 \precsim \widetilde{15662},\ \widetilde{20}x_6 \precsim \widetilde{12204},\\
&X = (x_1, x_2, x_3, x_4, x_5, x_6) \geq 0,
\end{aligned}
\tag{42}
$$

$$
\begin{aligned}
\text{where } \widetilde{21130} &= \langle 21126, 21130, 21134; 21124, 21130, 21136\rangle,\\
\widetilde{23870} &= \langle 23864, 23870, 23876; 23862, 23870, 23878\rangle,\\
\widetilde{19245} &= \langle 19240, 19245, 19247; 19237, 19245, 19248\rangle,\\
\widetilde{22155} &= \langle 22153, 22155, 22160; 22152, 22155, 22163\rangle.
\end{aligned}
$$

By solving problem (42) using the proposed method for the optimistic variants of the problem, a compromise solution is obtained for $\lambda = 0.8$. The resulting compromised optimal solution for the third scenario is $X = (409.19, 0.00, 277.16, 51.48, 51.48, 277.16)$, with details presented in Table 16.

Table 16: Compromise solution of problem (42).

$X = (x_1, x_2, x_3, x_4, x_5, x_6)$		$f_1(X)$	$f_2(X)$	$f_3(X)$	$f_4(X)$
(409.19, 0.00, 277.16, 51.48, 51.48, 277.16)		37405.40	37428600	29013310	66522
	μ	0.41	0.72	0.33	0.38
	ν	0.24	0.10	0.28	0.26
$X = (x_1, x_2, x_3, x_4, x_5, x_6)$		$g_1(X)$	$g_2(X)$	$g_3(X)$	$g_4(X)$
(409.19, 0.00, 277.16, 51.48, 51.48, 277.16)		3406694	106648	89162	405.86
$X = (x_1, x_2, x_3, x_4, x_5, x_6)$		$g_5(X)$	$g_6(X)$	$g_7(X)$	$g_8(X)$
(409.19, 0.00, 277.16, 51.48, 51.48, 277.16)		894.23	1092.22	2441.61	1015

The required input resources to cultivate the crops under the allocated cropland are presented in Table 17.

Table 17: Input resource requirements for allocated crops under scenario three.

Crop	Seed (kg)	F_{1c_n} (kg)	F_{2c_n} (kg)	H_{1c_n} (L)	H_{2c_n} (L)	P_{c_n} (L)
maize (c_1)	10229.87	40919	51149.35	-	409.19	409.19
sorghum (c_3)	4157.44	27716	27716.26	-	277.16	277.16
pepper (c_4)	823.68	5148	10296.00	77.22	-	77.22
chickpea (c_5)	1441.44	5148	-	51.48	-	51.48
bean (c_6)	5543.25	27716	-	277.16	207.87	277.16

Similarly, the considered problem under the three scenarios can also be solved for pessimistic and mixed DMs. The compromise solutions for each scenario under pessimistic and mixed viewpoints are presented in the upper and lower parts of Table 18, respectively.

Table 18: Solutions under pessimistic and mixed perspectives.

Scenario	λ	X	Z
1	0.40	(168.27, 0.00, 304.30, 84.61, 153.51, 304.30)	0.4132
2	0.40	(144.67, 0.00, 661.32, 141.05, 47.74, 67.97)	0.4626
3	0.40	(412.14, 0.00, 277.56, 47.74, 47.74, 277.56)	0.4495
1	0.30	(189.12, 0.00, 317.99, 72.76, 117.14, 317.99)	0.4067
2	0.40	(144.67, 0.00, 661.32, 104.06, 47.74, 104.95)	0.4352
3	0.30	(414.56, 0.00, 276.82, 46.80, 46.80, 276.81)	0.4491

Based on the obtained results, the arable land allocated to the six crops under the three approaches regarding the conventional pattern and the three scenarios is presented in Figure 5.

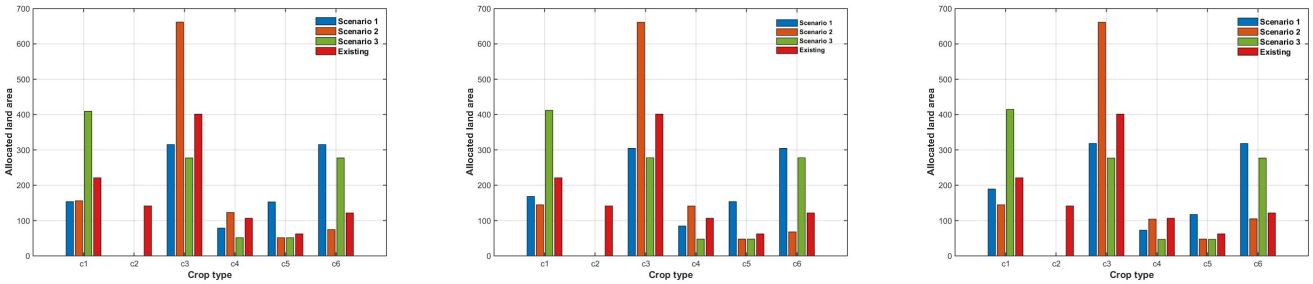

(a) (b) (c)

Figure 5: Allocated land area to the six crops under the optimistic (a), pessimistic (b) and mixed (c) perspectives relative to the existing pattern.

Let X_1, X_2, and X_3 denote the compromised solutions for the first, second, and third scenarios, respectively, under pessimistic and mixed views (Table 18). The objective values, along with the membership and non-membership degrees of the objectives for the pessimistic and mixed variants of the problem, are presented in Table 19.

Table 19: Goal achievement under pessimistic and mixed perspectives.

	Pessimistic perspective				Mixed perspective			
	$f_1(X_1)$	$f_2(X_1)$	$f_3(X_1)$	$f_4(X_1)$	$f_1(X_1)$	$f_2(X_1)$	$f_3(X_1)$	$f_4(X_1)$
$f(X_1)$	27724.77	36105370	28462070	55064	28719.63	34095870	28677430	55719
μ	0.44	0.45	0.38	0.34	0.54	0.40	0.35	0.31
ν	0.00	0.00	0.00	0.00	0.00	0.00	0.00	0.02
	$f_1(X_2)$	$f_2(X_2)$	$f_3(X_2)$	$f_4(X_2)$	$f_1(X_2)$	$f_2(X_2)$	$f_3(X_2)$	$f_4(X_2)$
$f(X_2)$	28745.80	46965540	30707130	57780	29115.66	40433450	30115760	55931
μ	0.78	0.34	0.34	0.52	0.86	0.25	0.41	0.58
ν	0.00	0.00	0.00	0.00	0.00	0.21	0.06	0.00
	$f_1(X_3)$	$f_2(X_3)$	$f_3(X_3)$	$f_4(X_3)$	$f_1(X_3)$	$f_2(X_3)$	$f_3(X_3)$	$f_4(X_3)$
$f(X_3)$	37470.45	36717860	28917350	66314	37538.86	36566940	28909570	66329
μ	0.42	0.68	0.35	0.38	0.42	0.67	0.35	0.38
ν	0.00	0.00	0.00	0.00	0.00	0.00	0.00	0.00

Based on the obtained solutions using the pessimistic and mixed approaches (Table 18), the agricultural resource consumptions for the three scenarios under each perspective, in order, are presented in Tables 20 and 21.

Table 20: Resource consumption under the pessimistic viewpoint.

$g_1(X_1)$	$g_2(X_1)$	$g_3(X_1)$	$g_4(X_1)$	$g_5(X_1)$	$g_6(X_1)$	$g_7(X_1)$	$g_8(X_1)$
3106967	101500	68386.55	584.73	700.80	1057.30	2245.60	1015.00
$g_1(X_2)$	$g_2(X_2)$	$g_3(X_2)$	$g_4(X_2)$	$g_5(X_2)$	$g_6(X_2)$	$g_7(X_2)$	$g_8(X_2)$
3621577	106274	112424.80	327.28	856.96	1133.26	2254.39	1015
$g_1(X_3)$	$g_2(X_3)$	$g_3(X_3)$	$g_4(X_3)$	$g_5(X_3)$	$g_6(X_3)$	$g_7(X_3)$	$g_8(X_3)$
3392248	106274	88821.33	396.91	897.87	1086.61	2433.60	1015

Table 21: Resource consumption under the mixed viewpoint.

$g_1(X_1)$	$g_2(X_1)$	$g_3(X_1)$	$g_4(X_1)$	$g_5(X_1)$	$g_6(X_1)$	$g_7(X_1)$	$g_8(X_1)$
3110209	101500	69990.82	544.27	745.60	1051.38	2235.20	1015
$g_1(X_2)$	$g_2(X_2)$	$g_3(X_2)$	$g_4(X_2)$	$g_5(X_2)$	$g_6(X_2)$	$g_7(X_2)$	$g_8(X_2)$
3533070	106274	105027.60	308.79	884.70	1114.77	2254.39	1015
$g_1(X_3)$	$g_2(X_3)$	$g_3(X_3)$	$g_4(X_3)$	$g_5(X_3)$	$g_6(X_3)$	$g_7(X_3)$	$g_8(X_3)$
3389983	106180.50	88862.42	393.83	898.99	1085.21	2432.72	1015

The OCP obtained using the proposed optimization method was compared with existing patterns. Since the second scenario represents a commonly practiced farming system in the district, a comparison was made between the existing cropping pattern and the optimized plan under the optimistic approach for this scenario.

As shown in Table 9, the area of land allocated to maize, *teff*, chickpea and bean in the existing situation was $221.03ha$, $141.41ha$, $62.29ha$, and 121.57, respectively, while in the proposed pattern, as presented in Table 14, the land area allocated to these crops respectively decreased to $156ha$, $0.00ha$, $51.45ha$, and 74.57. The area of land allocated to sorghum and pepper in the existing situation was $401.33ha$ and $106.42ha$, respectively, while in the proposed pattern, the land area allocated to these crops respectively increased to $661.58ha$ and 122.85.

In the conventional farming pattern, $991.76ha$ (96.00%) of $1,033ha$ of land is allocated to five crops in the first round of farming, and $62.29ha$ (28.18%) of $221.03ha$ of land is allocated to chickpea in the second round farming. In the proposed cropping pattern, $1,015ha$ (98.26%) of $1,033ha$ of land is allocated to four crops in the first season of farming and $51.48ha$ (33%) of $156ha$ of land is allocated to chickpea in the second round of farming.

The results of the study showed that, including in the remaining scenarios and DM approaches, *teff* should not be included in the farming patterns in favour of increasing the land area for other crops to attain better results regarding all objectives and constraints.

From the allocated arable land in the existing farm patterns, a total of $29,470.15qtl$ of yield was obtained under the existing cropping pattern, but this is slightly reduced to $29,358.32qtl$ in the proposed approach. If we consider the remaining objectives, the total gain was $41,510,180ETB$ in the existing pattern, but it can be increased to $44,088,180ETB$ applying the proposed farming pattern. On the other hand, the cost of cultivation and labor force were $31,413,470ETB$ and $64,160md$, respectively, in the existing farm plan, and these can be minimized to $30,558,420ETB$ and $57,384md$, respectively, by employing the suggested farming pattern.

Employing the proposed cropping pattern, the objectives are achieved with higher degrees of membership and lower degrees of non-membership compared to the existing cropping plan, except for the maximization of the yield target. However, in the existing situation, the production objective is accomplished at the cost of agrarian assets and the remaining goals.

There are notable differences between the conventional farming system and the suggested farming plan in the usage of manpower, fertilizers, and agricultural machines; whereas there are slight differences in the usage of herbicides and pesticides. If we consider the fertilizer constraint, $208,591.20kg$ of fertilizer was required to cultivate $1,054ha$ of farmland in the existing farming pattern, while the suggested farming plan requires $216,876kg$ of fertilizer to cultivate $1,066.48ha$ of farmland within the two production cycles. To cultivate the allocated crops on the respective areas of land, $2,392hrs$ (machine hrs.) were required using the existing plan, whereas the suggested plan require $2,272hrs$.

Comparing the obtained results of optimistic approach under the first, second, and third scenarios, Tables 12, 14, and 16, respectively, the following assessments have been made.
A comparatively wide area of land is allocated to sorghum and maize, under

the second and third scenarios, respectively, while pepper and bean are allocated in a wide area of farmland under the second and third scenarios, respectively. In contrast, Chickpeas share the largest area of land under the first scenario. Considering the resource constraints, water and fertilizer consumption can be minimized by applying the first farming scenario, while herbicide and pesticide consumption can be reduced by applying the second scenario. Whereas seed utilization can be minimized in the second scenario. In the achievement of the considered objectives, enhanced overall production and minimum expenditure are attained under the third scenario. While the total gain is significantly improved under the second scenario and the number of manpower is sufficiently minimized by applying the first farming scenario.

Based on the results of the three variants of the problem, as presented in Tables 12, 14, 16, 18, 19, 20, and 21 there is significant variation in the land allocation to the six crops under each scenario. This proves the solution of APP problem is contingent upon the DM's perspective. For example, in the first scenario, the land allocated to maize under the optimistic approach is reduced by $23.33ha$ and $2.48ha$, respectively, in the pessimistic and mixed approaches. Whereas the cropland allocated to bean in the mixed approach, respectively, decreased by $13.69ha$ and $47.09ha$ in the pessimistic and optimistic approaches.

The total cost of cultivation and manpower goals are better minimized under a pessimistic approach, while total crop production and profit are better achieved under the mixed and optimistic approaches, respectively.In the second scenario, a relatively equal large land area is allocated to sorghum under the three approaches, whereas for beans, a wide area is allocated under the mixed approach, but this is reduced by 30.38ha and 36.98ha under the optimistic and pessimistic approaches, respectively. The farmland allocated to maize and chickpea remains the same under the pessimistic and mixed approaches and differs by 11.33ha for maize and 3.74ha for chickpea under the optimistic approach. In this scenario, the yield maximization target is improved under the optimistic approach, while the profit maximization target is better achieved under the pessimistic approach. In contrast, the cost and manpower minimization targets are enhanced under the mixed approach.

In the third scenario, sorghum and beans share almost equal land areas under the three approaches. Moreover, a wide area of land is allocated to maize, with slight variations under the three approaches. The production and cost of cultivation goals are improved under the mixed approach, while the profit target is significantly maximized under the optimistic approach.

Water and fertilizer are fairly utilized under the pessimistic approach for the first scenario, whereas herbicide and pesticide consumption are minimized under the mixed approach.In the second scenario, water and herbicide usage are reduced under the mixed approach, while pesticide consumption is minimized under the pessimistic approach. In the third scenario, water consumption is significantly reduced under the pessimistic approach, while fertilizer and herbicide utilization are minimized under the pessimistic and mixed approaches, respectively.

7 Conclusion and Recommendations

In this paper, the APP problem is addressed using the IFMOO method from different perspectives, considering three common cropping scenarios in the study area. The resulting farming plans offer practical solutions aimed at reducing the overall vulnerability of six main crops in Abeshge district to various agricultural challenges.

The comparison assessment made between the previous farming system and the proposed cropping patterns verified that the proposed farming patterns have several advantages for better achievement of the stated objectives and efficient utilization of agricultural resources.

The existing farming system in the district relies heavily on capital and labor, often causing harm to the environment. If this continues, the area will face soil degradation unless resources are managed properly. All stakeholders need to take action, especially in reducing fertilizer use. For example, using manure and compost can help protect soil fertility, and practices like crop rotation can lower the need for herbicides.

The study has numerous benefits in assisting the managers of LSF and farmers of the district for optimal management of agricultural resources. It also indicates the advantages of OCP to overcome the potential disaster of crops due to climate change and soil infertility. Furthermore, the study can be used to predict promising cropping plans from a long-term perspective as well.

A proficient IFMOO model is proposed to address uncertainties and associated risks of agriculture, aiming to achieve sustainable crop production goals. Incorporating the risk management analysis model into the IFMOO model can increase the efficiency and applicability of the proposed approach to APP problems. Moreover, higher-order extensions of IFO techniques, such as hesitant IFO (Teferi et al., 2025), are also helpful in capturing the hesitation among DMs.

Data availability

The detailed experimental data used to support the findings of this study are included in the supplementary information file(s).

Acknowledgements

The author gratefully acknowledges the Editor-in-Chief and the anonymous reviewers for their careful evaluation, insightful comments, and constructive suggestions. Their contributions have substantially improved the presentation, clarity, and scientific rigor of this manuscript.

Conflict of Interest

The author declares that he has no competing financial interests or personal relationships that could have influenced the work reported in this paper.

Funding

The author did not receive any funding for this research.

References

Ahmadini, A. A. H., & Ahmad, F. (2021). A novel intuitionistic fuzzy preference relations for multiobjective goal programming problems. *Journal of Intelligent and Fuzzy Systems*, *40*(3), 4761–4777.

Allen, R. G., Pereira, L. S., Raes, D., & Smith, M. (1998). *Crop evapotranspiration: Guidelines for computing crop water requirements*. FAO.

Amini, A. (2015). Application of fuzzy multi-objective programming in optimization of crop production planning. *Asian Journal of Agricultural Research*, *9*(5), 208–222.

Andrews, D. J., & Kassam, A. H. (1976). The importance of multiple cropping in increasing world food supplies. *Multiple Cropping*, *27*, 1–10.

Angelov, P. (1995). Intuitionistic fuzzy optimisation. *Notes on Intuitionistic Fuzzy Sets*, *1*(1), 27–33.

Atanassov, K. T. (1986). Intuitionistic fuzzy sets. *Fuzzy Sets and Systems*, *20*(1), 87–96.

Awulachew, S. B., & Ayana, M. (2011). Performance of irrigation: An assessment at different scales in ethiopia. *Experimental Agriculture*, *47*(S1), 57–69.

Bairwa, S. L., Kushwaha, S., & Bairwa, S. (2013). *Managing risk and uncertainty in agriculture: A review*. Poddar Publication.

Biswas, A., & Pal, B. B. (2005). Application of fuzzy goal programming technique to land use planning in agricultural system. *Omega*, *33*(5), 391–398.

Carravilla, M. A., & Oliveira, J. F. (2013). Operations research in agriculture: Better decisions for a scarce and uncertain world. *Annals of Operations Research*, *219*(1), 1–22. https://doi.org/10.1007/s10479-013-1456-4

Chen, Y., Fu, Q., Singh, V. P., Ji, Y., Li, M., & Wang, Y. (2023). Optimization of agricultural soil and water resources under fuzzy and random uncertainties. *Agricultural Water Management*, *281*, 108264.

Cristofari, A., De Santis, M., & Lucidi, S. (2024). On necessary optimality conditions for sets of points in multiobjective optimization. *Journal of Optimization Theory and Applications*, *203*, 126–145.

Dessie, M., Woldeamanuel, T., & Mekonnen, G. (2017). Value chain analysis of red pepper: The case of abeshge district, gurage zone, south ethiopia. *International Journal of Environmental Science and Natural Resources*, *2*(3), 1–8.

Duan, S. X., Wibowo, S., & Chong, J. (2021). A multicriteria analysis approach for evaluating the performance of agriculture decision support systems for sustainable agribusiness. *Mathematics*, *9*(8), 884.

FAO. (2017). *The state of food and agriculture: Leveraging food systems for inclusive rural transformation*.

FAO. (2022). Yield, production quantity, and producer prices annual [FAOSTAT]. https://www.fao.org/faostat/en

FAO. (2023). Faostat statistical database [Accessed 2023]. https://www.fao.org/faostat/en/

Gebremichael, A., Quraishi, S., & Mamo, G. (2014). Analysis of seasonal rainfall variability for agricultural water resource management in southern region, ethiopia. *Journal of Natural Sciences Research*, *4*(11), 56–79.

Guo, R., Qiu, X., & He, Y. (2021). Research on agricultural cooperation potential between china and cee countries based on resource complementarity. *Mathematics*, *9*(5), 503.

Gupta, A. P., Harboe, R., & Tabucanon, M. T. (2000). Fuzzy multiple-criteria decision making for crop area planning in narmada river basin. *Agricultural Systems*, *63*(1), 1–18.

Haile, G. G., & Kasa, A. K. (2015). Irrigation in ethiopia: A review. *Academia Journal of Agricultural Research*, *3*(10), 264–269.

Kelbore, Z. G. (2014). *Essays on the ethiopian agriculture* [Doctoral dissertation]. University of Trento.

Kis, T., Kovács, A., & Mészáros, C. (2021). On optimistic and pessimistic bilevel optimization models for demand response management. *Energies*, *14*(8), 2095.

Kousar, S., Zafar, A., Kausar, N., Pamucar, D., & Kattel, P. (2022). Fruit production planning in semiarid zones: A novel triangular intuitionistic fuzzy linear programming approach. *Mathematical Problems in Engineering*, *2022*(Article ID 3705244), 1–13.

Li, M., Fu, Q., Singh, V. P., Ji, Y., Liu, D., Zhang, C., & Li, T. (2019). An optimal modelling approach for managing agricultural water-energy-food nexus under uncertainty. *Science of the Total Environment*, *651*, 1416–1434.

Li, M., Fu, Q., Singh, V. P., Liu, D., Li, T., & Zhou, Y. (2020). Managing agricultural water and land resources with tradeoff between economic, environmental, and social considerations. *Agricultural Systems*, *178*, 102685.

Li, M., Fu, Q., Singh, V. P., Ma, M., & Liu, X. (2017). An intuitionistic fuzzy multi-objective non-linear programming model for sustainable irrigation water allocation. *Journal of Hydrology*, *555*, 80–94.

LINDO Systems Inc. (2017). *Lingo 17.0 user manual*.

Luo, J., Chang, Y. P., & Kaliyaperumal, K. (2023). A novel optimization approach for rural development based on sustainable agriculture planning. *Energy Exploration and Exploitation*, *41*(5), 1724–1745.

Mahajan, S., & Gupta, S. K. (2021a). On fully intuitionistic fuzzy multiobjective transportation problems using different membership functions. *Annals of Operations Research*, *296*, 211–241.

Mahajan, S., & Gupta, S. K. (2021b). On optimistic, pessimistic and mixed approaches for fully intuitionistic fuzzy multiobjective nonlinear programming problems. *Expert Systems with Applications*, *168*, 114309.

Mahapatra, G. S., & Roy, T. K. (2009). Reliability evaluation using triangular intuitionistic fuzzy numbers arithmetic operations. *International Journal of Mathematical and Computational Sciences*, *3*(6), 574–581.

Mirajkar, A. B., & Patel, P. L. (2012). Optimal irrigation planning using multi-objective fuzzy linear programming models. *ISH Journal of Hydraulic Engineering*, *18*(3), 232–240.

Mirkarimi, S. H., Joolaie, R., Eshraghi, F., & Abadi, F. S. B. (2013). Application of fuzzy goal programming in cropping pattern management. *International Journal of Agriculture and Crop Sciences*, *6*(15), 1062–1067.

Nasir, M., & Hundie, B. (2014). The effect of off-farm employment on agricultural production and productivity. *Journal of Economics and Sustainable Development*, *5*(23), 85–98.

Nishad, A. K., & Singh, S. R. (2015). Solving multi-objective decision making problem in intuitionistic fuzzy environment. *International Journal of System Assurance Engineering and Management*, *6*(2), 206–215.

Ouda, S. A., Zohry, A. E. H., & Morsy, M. (2017). *Cropping pattern modification to overcome abiotic stresses: Water, salinity and climate*. Springer.

Paudel, M. N. (2016). Multiple cropping for raising productivity and farm income of small farmers. *Journal of Nepal Agricultural Research Council*, *2*, 37–45.

Pawar, S. V., Patel, P. L., & Mirajkar, A. B. (2022). Intuitionistic fuzzy approach in multi-objective optimization for krbmc irrigation system, india. *ISH Journal of Hydraulic Engineering*, *28*(1), 463–470.

Pawar, S. V., Patel, P. L., & Mirajkar, A. B. (2026). Multi-objective optimization of the krbmc irrigation system using intuitionistic fuzzy approach with non-linear membership functions. *ISH Journal of Hydraulic Engineering*, 1–14.

Rădulescu, M., Rădulescu, C. Z., & Zbăganu, G. (2014). A portfolio theory approach to crop planning under environmental constraints. *Annals of Operations Research*, *219*, 243–264.

Rasikh, Z. U. R., Joolaie, R., Keramatzadeh, A., & Mirkarimi, S. (2024). Optimizing the cropping pattern in nangarhar province based on the perspective of sustainable agricultural development: Fuzzy goal programming approach. *Process Integration and Optimization for Sustainability*, *8*(4), 1119–1129.

Roszkowska, E., Jefmański, B., Dudek, A., & Kusterka-Jefmańska, M. (2024). IFMCDM: An R package for intuitionistic fuzzy multi-criteria decision making methods. *SoftwareX*, *26*, 101721.

Semu, M., Regassa, A., & Yitbarek, T. (2022). Characterization and classification of soils and land suitability evaluation for the production of major crops at anzecha watershed, gurage zone, ethiopia. *Applied and Environmental Soil Science*, *2022*, 1–22.

Sen, D. K., Datta, S., & Mahapatra, S. S. (2018). Sustainable supplier selection in intuitionistic fuzzy environment. *Benchmarking: An International Journal*, *25*(2), 545–574.

Singh, G. (2012). Factors influencing cropping pattern in bulandshahr district-with special reference to the size of land holding. *International Journal of Scientific Research Publications*, *2*(5), 1–10.

Singh, S. K., & Yadav, S. P. (2015a). Efficient approach for solving type-1 intuitionistic fuzzy transportation problem. *International Journal of System Assurance Engineering and Management*, *6*(3), 259–267.

Singh, S. K., & Yadav, S. P. (2015b). Modeling and optimization of multi-objective non-linear programming problem. *Applied Mathematical Modelling*, *39*(16), 4617–4629.

Singh, V., & Yadav, S. P. (2018). Modeling and optimization of multi-objective programming problems in intuitionistic fuzzy environment: Optimistic, pessimistic and mixed approaches. *Expert Systems with Applications*, *102*, 143–157.

Singh, V., Yadav, S. P., & Singh, S. K. (2021). Duality theory in atanassov's intuitionistic fuzzy mathematical programming problems: Optimistic, pessimistic and mixed approaches. *Annals of Operations Research*, *296*(1), 667–706.

Smith, M. (1992). *Cropwat: A computer program for irrigation planning and management* (tech. rep. No. 46). Food and Agriculture Organization of the United Nations.

Teferi, H. T., Feyissa, Y. K., & Aemro, Y. G. (2025). An effective solution approach for multi-objective optimization problems in a hesitant intuitionistic fuzzy environment. *Journal of Fuzzy Extension and Applications*, e236548.

Tsegaye, H., Thillaigovindan, N., & Alemayehu, G. (2021). An efficient method for solving intuitionistic fuzzy multi-objective optimization problems. *Punjab University Journal of Mathematics*, *53*(9), 631–664.

Wang, Y. (2022). Application of fuzzy linear programming model in agricultural economic management. *Journal of Mathematics*, *2022*, 1–13.

Weintraub, A., & Romero, C. (2006). Operations research models and the management of agricultural and forestry resources. *Interfaces*, *36*(5), 446–457.

Xu, Z., & Cai, X. (2012). *Intuitionistic fuzzy information aggregation*. Springer. https://doi.org/10.1007/978-3-642-29584-3

Xu, Z., & Yager, R. R. (2006). Some geometric aggregation operators based on intuitionistic fuzzy sets. *International Journal of General Systems*, *35*(4), 417–433.

Zeng, L., Li, J., Zhou, Z., & Yu, Y. (2020). Optimizing land use patterns for the grain for green project. *Ecological Indicators*, *114*, 106347.

Zeng, X., Kang, S., Li, F., Zhang, L., & Guo, P. (2010). Fuzzy multi-objective linear programming applying to crop area planning. *Agricultural Water Management*, *98*(1), 134–142.

Zerssa, G., Feyssa, D., Kim, D. G., & Eichler-Löbermann, B. (2021). Challenges of smallholder farming in ethiopia. *Agriculture*, *11*(3), 192.

Zhang, H., & Georgescu, P. (2022). Sustainable organic farming, food safety and pest management: An evolutionary game analysis. *Mathematics*, *10*(13), 2269.

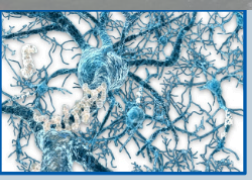

East African Journal of Biophysical and Computational Sciences

(EAJBCS)

ISSN (Online): 2789-3618 | ISSN (Print): 2789-360X

Author Guidelines

East African Journal of Biophysical and Computational Sciences (EAJBCS)

2026 | HU- CNCS

Table of Contents

1. About the Journal 1

2. Editorial Policies and Journal Governance 2

3. Open Access Policy and Licensing 2

4. Manuscript Types and Structure 3

5. Manuscript Preparation and Formatting 5

6. Authorship and Contributor Roles 8

7. Ethical Standards and Research Integrity 9

8. Peer Review Process 10

9. Data, Code, and Materials Sharing 11

10. Equity, Diversity, and Inclusion (EDI) 11

11. Discoverability, Metadata, and Indexing 12

12. Submission Process 12

13. Post-Acceptance and Publication 12

14. Contact Information 13

Author Guidelines

1. About the Journal

The East African Journal of Biophysical and Computational Sciences (EAJBCS) (ISSN Online: 2789-3618; Print: 2789-360X) is a double-blind, peer-reviewed, open-access journal published by the College of Natural and Computational Sciences, Hawassa University.

EAJBCS publishes high-quality original research, reviews, and short communications in biophysical, computational, and interdisciplinary natural sciences. The journal promotes rigorous, innovative, and impactful research that contributes to scientific advancement at both regional and global levels.

Published biannually in English, EAJBCS operates under a CC BY NC 4.0 license and does not charge publication fees, ensuring equitable access for authors. The journal is indexed in AJOL, DOAJ, CABI Abstracts, and FAO AGRIS, and holds a national accreditation.

Aims and Scope

EAJBCS aims to publish high-quality, original research that advances knowledge in biophysical, computational, and related interdisciplinary sciences. The journal promotes innovative, data-driven, and applied research addressing regional and global challenges.

The Journal invites publications from different disciplines to advance the depths of knowledge related to physics, chemistry, geology, biology, & veterinary medicine. The manuscript originated from other sciences such as biotechnology, sport science, statistics, and mathematics can also be accepted based on their adjunct nature from both regional and international researchers.

Special Issues

The peer review process for special issues follows the same rigorous standards applied to regular submissions. In these cases, a guest editor may coordinate the review by selecting reviewers and providing recommendations; however, the Editor-in-Chief or designated section editor maintains full oversight to ensure that publishing ethics, transparency, and responsiveness are upheld. While guest editors may suggest decisions, the final responsibility for accepting or rejecting manuscripts rests with the journal editor. This approach guarantees that all special issues and article collections meet the same high standards of quality, integrity, and consistency as regular submissions.

2. Editorial Policies and Journal Governance

2.1 Editorial Board

- The editorial board comprises recognized experts with diverse geographic and institutional affiliations, reflecting the journal's commitment to inclusivity and international standards.
- Full names, affiliations, and contact information for all editorial board members are published on the journal website.
- The Editor-in-Chief and section editors are responsible for upholding editorial independence and ensuring the integrity of the peer review process.

Editorial Board Diversity:

EAJBCS is committed to promoting equity, diversity, and inclusion (EDI) in its editorial leadership, reviewer pool, and published content. The board is periodically reviewed to ensure representation across gender, ethnicity, career stage, and geographic region, in line with best practices recommended by the COPE.

2.2 Ownership and Management

- EAJBCS is owned and managed by the College of Natural and Computational Sciences, Hawassa University.
- The journal's governance structure, including the roles of the publisher, editorial board, and advisory committees, is transparently described on the journal website.

3. Open Access Policy and Licensing

3.1 Open Access Statement

EAJBCS is an open-access journal. All articles are freely available online immediately upon publication, ensuring the widest possible dissemination and accessibility of research findings.

3.2 Licensing

- Articles are published under the **Creative Commons Attribution-Noncommercial (CC BY-NC 4.0)** license. This permits the sharing, distribution, and reproduction of the work in any medium for non-commercial purposes only, provided the original work is properly cited and any changes made are clearly indicated.
- Licensing terms are clearly indicated on the full text of all published articles (PDF).
- Authors retain copyright of their work and grant EAJBCS the right to publish and distribute the article, as stated in the Manuscript Submission and Copyright Transfer Form.

3.3 Article Processing Charges (APCs)

- EAJBCS **does not charge** submission or publication fees (APCs).

4. Manuscript Types and Structure

4.1 Article Types

EAJBCS accepts the following types of submissions:

- **Original Research Articles:** Full-length reports of novel research findings (a maximum of 6,000 words).
- **Review Articles:** Comprehensive syntheses of research topics (a maximum of 6,000 words).
- **Short Communications:** Brief reports of significant findings or methodological advances (a maximum of 1,500 words).
- **Book Reviews:** Critical evaluations of recent publications in relevant fields (a maximum of 1,500 words).
- **Editorials and Commentaries:** Invited or submitted perspectives on topical issues.

4.2 Manuscript Structure

All manuscripts should adhere to the following structure, unless otherwise specified for particular article types:

Title Page

- Article title (concise and informative)
- Author names and affiliations
- Corresponding author's contact information (email, postal address)
- ORCID iDs for all authors
- Suggested running head (max 50 characters)

Abstract

- Structured or unstructured (as appropriate), not exceeding 300 words
- Clearly state the purpose, methods, key results, and conclusions
- Avoid abbreviations and references

Keywords

- 3 to 7 keywords and separated by semicolons
- Select terms not present in the title to enhance discoverability

Main Text

- **Introduction:** Background, rationale, research gap, and objectives
- **Materials and Methods**: Detailed methodology, ethical approvals, data sources, statistical analysis, and reproducibility measures
- **Results:** Clear presentation of findings, supported by tables and figures as appropriate
- **Discussion**: Interpretation of results, comparison with existing literature, limitations, and implications
- **Conclusion**: Summary of main findings and recommendations

Acknowledgments

- Recognition of funding sources, technical assistance, and non-author contributions

Conflict of Interest Statement

- Disclosure of any financial or non-financial conflicts for all authors

Funding Statement

- Details of all funding sources supporting the work

Data Availability Statement

- Description of where and how supporting data can be accessed

Ethics Statement

- Confirmation of ethical approvals and informed consent, as applicable

Author Contributions

- Specification of each author's role using the CRediT taxonomy

References

- Complete and consistently formatted list, following the APA (author-year) style

Tables and Figures

- Numbered sequentially, with descriptive titles and legends

Supplementary Materials

- Additional data, code, or materials, as appropriate

5. Manuscript Preparation and Formatting

5.1 Language and Style

- Manuscripts must be written in clear, concise English.
- Authors whose first language is not English are strongly encouraged to use professional English editing services before submission.

5.2 Formatting Requirements

- File formats: Microsoft Word (.docx, .doc, .rtf) or LaTeX (with accompanying PDF and source files).
- Font: Times New Roman, 12-point size
- Line spacing: 1.5
- Margins: 2.5 cm on all sides
- Page numbers: Automatic numbering on all pages
- SI units: Use the International System of Units throughout
- Abbreviations: Define at first use and avoid excessive use

5.3 Tables and Figures

5.3.1 Tables

- Prepare tables using the Word Table Editor or LaTeX tabular environment; avoid embedding tables as images.
- Tables should be numbered consecutively (Arabic numerals) and cited in the order of appearance in the text. Each table must have a concise title (maximum 20 words) placed above, and a detailed legend (maximum 300 words) below.
- Tables should be simple, self-explanatory, and not duplicate information presented in the text or figures. Experimental details may be included in the table legend where appropriate.
- All tables must be submitted on separate pages. Authors should indicate the approximate placement of each table within the text.
- The use of color and shading is not permitted. Emphasis may be indicated using superscripts, symbols, or bold text, which must be clearly explained in the legend

5.3.1 Figure

- Figures should be numbered consecutively (Arabic numerals) and cited in order. Each figure must include a concise title and a descriptive legend.
- Figures should be submitted in high-resolution formats (JPEG, GIF, PNG or embedded in PowerPoint/Word). Recommended resolution: 900 dpi (line art), 600 dpi (combined), and 300 dpi (photographs). Standard figure sizes should fit either single-column (~8 cm width) or full-page (~17 cm width). For images a landscape orientation is recommended (9:16).
- Use uppercase letters for figure parts (e.g., Figure 1A). All keys and symbols must be included within the figure. Avoid duplication of data and minimize unnecessary white space.

- Indicate figure placement in the text. Permission must be obtained for previously published material and acknowledged in the legend.

5.4 Supplementary Materials

- Authors may submit supplementary files (datasets, code, multimedia) to enhance the transparency and reproducibility of their work.
- Supplementary materials are subject to peer review and will be published alongside the article.

5.5. Citations and References

- All manuscripts must cite relevant and appropriate literature to support statements. Authors should ensure that citations are accurate, original, and directly support the claims made. Citation manipulation or inappropriate referencing may lead to rejection.
- Authors should:
    - Cite original sources where possible and avoid unnecessary or excessive citations
    - Ensure all cited works have been read and are properly represented
    - Avoid bias (e.g., excessive self-citation or citing from a single source or region)
    - Prefer peer-reviewed sources
- Only published, in-press, or publicly available preprints may be included in the reference list. Unpublished data and personal communications should be cited only within the text with permission.
- References must be formatted consistently using standard journal abbreviations (Index Medicus/MEDLINE) and listed in alphabetical order

5.5.1 In-text citations

- Use the author–year (APA 7th) style for in-text citations. Cite the author's surname followed by the year (e.g., Blanco, 2024).
- For two authors, include both names (Nevo and Chen, 2024); for three or more, use the first author followed by et al. (e.g., Dave et al., 2024). Use lowercase letters (e.g., 2024a, 2024b) to distinguish multiple works by the same author in the same year.
- Multiple citations should be listed alphabetically and separated by semicolons. In narrative citations, include the author's name in the sentence; in parenthetical citations, include both author and year in parentheses.
- Ethiopian names should follow the same format (e.g., Dereje, 2024; Dereje and Bantewalu, 2024; Dereje et al., 2024).

5.5.2 In reference list

Journal article

- Szilard, R. (2004). Theories and applications of plate analysis: Classical, numerical and engineering methods. *Appl.Mech. Rev.*,57(6), B32–B33
- Kitterød, N.-O., & Leblois, É. (2021). Estimation of sediment thickness by solving poisson's equation with bedrock outcrops as boundary conditions. *Hydrology Research*, 52(3), 597–619.
- Beirão da Veiga, L., Brezzi, F., Cangiani, A., Manzini, G., Marini, L. D., & Russo, A. (2013). Basic principles of virtual element methods. *Mathematical Models and Methods in Applied Sciences*, 23(01), 199–214.
- Bastian, P., Blatt, M., Dedner, A., Dreier, N.-A., Engwer, C., Fritze, R., Gräser, C., Grüninger, C., Kempf, D., Klöfkorn, R., et al. (2021). The dune framework: Basic concepts and recent developments. *Computers & Mathematics with Applications*, 81, 75–112.

Books

- de Boor, C. (2001). *A practical guide to splines*(3rd). Springer-Verlag
- Hoffman, J. D., & Frankel, S. (2018). *Numerical methods for engineers and scientists*. CRC Press.

Book chapter

- Smith, J. R., & Taylor, S. D. (2022). Digital literacy in the classroom. In M. L. Anderson (Ed.), *Modern educational strategies* (pp. 45–67). Academic Press.

Conference /workshop/seminar proceedings

- Roberts, L. (2024, June 12–14). *The ethics of artificial intelligence in healthcare [Paper presentation]*. Global Health Summit, Berlin, Germany.
- Nguyen, T. (2025). Neural networks for urban planning. In K. Schmidt (Ed.), *Proceedings of the 12th International Workshop on AI & City Design* (pp. 112–125). Springer

Publications of organizations

- WHO (World Health Organization). (2023). *World health statistics 2023: Monitoring health for the SDGs.* WHO, Geneva, Switzerland.
- CSA (Central Statistical Authority). (1991). *Agricultural Statistics. 1991*. Addis Ababa, CTA Publications. 250 pp.

Dissertation or Thesis

- Kaufman, J. L. (2024). *The impact of remote work on middle management communication [Doctoral dissertation, Stanford University]*. ProQuest Dissertations and Theses Global

- Moreno, G. (2025). *Urban heat islands and public health in coastal cities [Master's thesis, University of Miami]*. Scholarly Repository. https://scholarship.miami.edu/theses/1234

Publications from websites (URLs)

- National Institute of Mental Health. (2022, May 10). Anxiety disorders. https://www.nimh.nih.gov/health/topics/anxiety-disorders
- FAO (Food and Agriculture Organization) (2000). Crop and Food Supply Assessment Mission to Ethiopia. FAOIWFP. Rome. (http://www.fao.org~/GIEWS). (Accessed on 21 July 2000).

6. Authorship and Contributor Roles

6.1 Authorship Criteria

EAJBCS adheres to the ICMJE recommendations for authorship:

- Substantial contributions to the conception or design of the work; or the acquisition, analysis, or interpretation of data
- Drafting the work or revising it critically for important intellectual content
- Final approval of the version to be published
- Agreement to be accountable for all aspects of the work

To qualify as an author, an individual (including any co-author) must have made a substantial contribution to at least one of the above criteria. Individuals who do not meet this requirement should be acknowledged rather than listed as authors.

6.2 Contributor Roles (CRediT Taxonomy)

Authors must specify their individual contributions using the CRediT taxonomy (e.g., conceptualization, methodology, data curation, writing – original draft, writing – review & editing, supervision, funding acquisition).

6.3 Corresponding Author Responsibilities

- Ensures all authors have reviewed and approved the manuscript
- Manages all communications with the journal
- Handles post-publication queries and corrections

6.4 Changes to Authorship

- Any changes to the author list after submission require written consent from all authors, with a clear explanation for the change.

7. Ethical Standards and Research Integrity

7.1 Publication Ethics

EAJBCS upholds the highest standards of publication ethics, guided by COPE and ICMJE principles.

- Plagiarism, data fabrication, image manipulation, and other forms of misconduct are strictly prohibited.
- All submissions are screened using Turnitin software.
- Manuscripts with a similarity index >20% (excluding references) may be rejected

7.2 Human and Animal Research

- Studies involving human participants must include a statement of ethical approval from an appropriate institutional review board (IRB) and confirmation of informed consent.
- Animal studies must comply with international, national, and institutional guidelines for humane treatment and include a statement of ethical approval.

7.3 Clinical Trials and Reporting Guidelines

- Authors must adhere to relevant reporting guidelines and submit completed checklists as supplementary files.

7.4 Data Availability and Transparency

- Authors must provide a Data Availability Statement describing where and how the data supporting the findings can be accessed, or explain any restrictions.
- Where possible, datasets should be deposited in recognized repositories with persistent identifiers (e.g., DOI).

7.5 Conflict of Interest and Funding Disclosure

- All authors must disclose any financial or non-financial conflicts of interest, or state explicitly if none exist.
- Funding sources must be clearly identified, including grant numbers and the role of funders in the research.

7.6 Declaration on Use of Generative AI and AI-Assisted Technologies

- Authors must disclose any use of generative AI or AI-assisted technologies during manuscript preparation at the time of submission. While such tools can support efficiency by helping synthesize literature, identify research gaps, generate ideas, or improve language and readability, they must never replace human expertise, critical thinking, or scholarly judgment. All AI-generated content must be carefully

reviewed, verified, and edited to ensure accuracy, originality, and alignment with the author's own analysis and insights.
- Authors remain fully responsible and accountable for the content of their work, including safeguarding data privacy, intellectual property, and compliance with ethical standards. The use of AI tools must be transparent to readers, and a disclosure statement should be added in a dedicated section before the references list.
- AI tools must not be listed or cited as authors or co-authors, as authorship implies responsibilities that only humans can fulfill. Basic tools for grammar, spelling, or reference checking do not require disclosure.

Declaration statement on Generative AI and AI-Assisted Technologies

- During the preparation of this work, the author(s) used [NAME OF TOOL/SERVICE] to [REASON]. After using this tool/service, the author(s) reviewed and edited the content as needed and take(s) full responsibility for the content of the published article.

7.7 Corrections, Retractions, and Expressions of Concern

- EAJBCS follows COPE guidelines for handling corrections, retractions, and expressions of concern.
- Authors are responsible for notifying the journal promptly if errors are identified post-publication.

8. Peer Review Process

8.1 Peer Review Model

- **EAJBCS operates a double-blind peer review process:** both authors and reviewers remain anonymous to each other, minimizing bias and ensuring objective evaluation.
- In exceptional cases, open peer review or post-publication review may be considered, with appropriate disclosure.

8.2 Reviewer Selection and Recognition

- Reviewers are selected based on subject expertise, publication record, and absence of conflicts of interest.
- The journal maintains a diverse reviewer pool, reflecting geographic, institutional, and demographic diversity.
- Reviewers receive formal recognition, including certificates and eligibility for annual reviewer awards.

8.3 Peer Review Workflow

1. **Initial Editorial Screening:** Manuscripts are assessed for scope, originality, and compliance with submission guidelines.
2. **Assignment to Section Editor:** Suitable manuscripts are assigned to a section editor for oversight.
3. **Reviewer Invitation**: At least two independent reviewers are invited.
4. **Review and Decision:** Reviewers evaluate the manuscript for scientific rigor, originality, clarity, and ethical compliance, providing detailed reports and recommendations.
5. **Editorial Decision:** Based on reviewer feedback, the editor decides to accept, request revisions, or reject the manuscript.
6. **Revision and Re-Review:** Authors respond to reviewer comments and submit revised manuscripts, which may undergo further review.
7. **Final Decision and Acceptance:** Upon satisfactory revision, the manuscript is accepted for publication.

9. Data, Code, and Materials Sharing

- EAJBCS encourages the sharing of data, code, and materials to promote transparency and reproducibility.
- Authors should deposit datasets and code in recognized repositories and provide persistent identifiers.
- If data cannot be shared due to ethical, legal, or privacy constraints, authors must provide a clear explanation in the Data Availability Statement.

10. Equity, Diversity, and Inclusion (EDI)

- EAJBCS is committed to promoting equity, diversity, and inclusion in its editorial practices, reviewer selection, and published content.
- Authors are encouraged to:
    - Use inclusive language and avoid bias in reporting
    - Provide detailed demographic descriptions of study populations
    - Justify sample selection and discuss generalizability constraints
    - Include positionality or reflexivity statements where relevant
    - Cite a diverse range of sources, including underrepresented scholars
- The journal periodically reviews its policies and practices to ensure alignment with evolving EDI standards.

11. Discoverability, Metadata, and Indexing

- All articles are assigned Digital Object Identifiers (DOIs) and registered with CrossRef for persistent citation and discoverability.
- Metadata, including abstracts, keywords, author affiliations, and funding information, are provided in machine-readable formats to facilitate indexing in major databases such as AJOL, DOAJ, CABI Abstracts, and FAO AGRIS.
- The journal maintains up-to-date ISSN registration for both print and electronic versions.

12. Submission Process

12.1 Online Submission System

- Manuscripts must be submitted via the journal's online submission platform by clicking https://journals.hu.edu.et/hu-journals/index.php/eajbcs/submission
- Authors are required to complete all metadata fields, upload the main manuscript and supplementary files, and provide signed author agreements and ethical declarations.

12.2 Submission Checklist

Authors must ensure that:

- The manuscript adheres to the journal's formatting and structure requirements
- All authors meet the authorship criteria and have approved the submission
- Ethical approvals and informed consent statements are included, as applicable
- Data availability, conflict of interest, and funding statements are provided
- Relevant reporting checklists are completed and uploaded
- Figures and tables are submitted in the correct format and resolution

12.3 Copyright Transfer and Author Agreement

- Upon acceptance, authors are required to sign a copyright transfer or license agreement, specifying the terms of publication and reuse.
- The agreement template is available on the journal website.

13. Post-Acceptance and Publication

13.1 Proofs and Corrections

- Authors will receive proofs for review before publication.
- Only minor corrections (e.g., typographical errors) are permitted at this stage.
- Substantive changes require editorial approval.

13.2 Publication Frequency and Timeliness

- EAJBCS publishes articles on a **biannual basis**, with continuous online publication to ensure timely dissemination
- The journal adheres to its stated publication schedule and promptly communicates any delays to authors.

13.3 Post-Publication Updates

- Corrections, retractions, and expressions of concern are published in accordance with COPE and ICMJE guidelines, with clear linkage to the original article.

14. Contact Information

For inquiries regarding submissions, editorial policies, or technical support, please contact:

Editorial Office

East African Journal of Biophysical and Computational Sciences

Phone: +251-913-267054

Email: eajbcs@hu.edu.et

Principal Contact

Dr. Admasu Tadesse

Editor in chief, EAJBCS

College of Natural and Computational Sciences, Hawassa University

Phone +251-913267054

Email: admasut@hu.edu.et

Support Contact

Dr. Abnet Woldesenbet

Editorial Manager, EAJBCS

Phone +251- 911811819

Email: abnetm@hu.edu.et